Interactome of the β2b subunit of L-type voltage-gated calcium channels in cardiomyocytes

Dissertation zur Erlangung des
naturwissenschaftlichen Doktorgrades
der Julius-Maximilians-Universität Würzburg

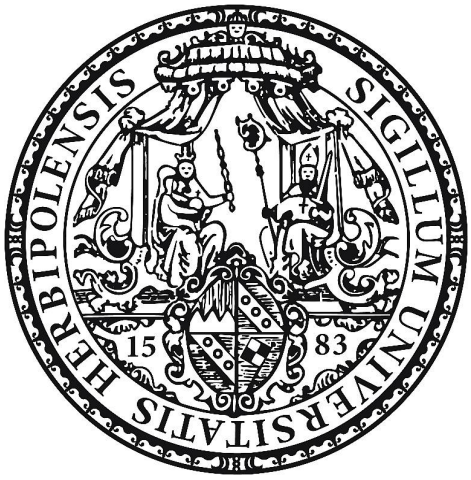

vorgelegt von

Yiliam Cruz García

aus Havanna

Würzburg, 2020

Eingereicht am: ……..……..

Mitglieder der Promotionskommission:

Vorsitzender: ……..

Gutachter: Prof. Dr. Michaela Kuhn

Gutachter: Prof. Dr. Thomas Dandekar

Tag des Promotionskolloquiums: ……..…

Doktorurkunde ausgehändigt am: …….…….

TABLE OF CONTENTS

LIST OF ABBREVIATIONS

AID	α-interaction domain
APEX	ascorbate peroxidase
ARC	adult rat cardiomyocytes
CAMKII	calcium/calmodulin-dependent protein kinase II
Cavα1	voltage-gated calcium channel α1 subunit
Cavα2δ	voltage-gated calcium channel α2δ subunit
Cavβ	voltage-gated calcium channel β subunit
Cavγ	voltage-gated calcium channel γ subunit
CICR	Ca^{2+}-induced Ca^{2+} release
CSD	chromo shadow domain
CT	C-terminus
DHP	dihydropyridine
DMEM	Dulbecco's Modified Eagle Medium
EC	excitation-contraction
EDTA	ethylenediaminetetraacetic acid
FFR	force-frequency relationship
GK	guanylate kinase
GST	glutathione S-transferase
HP1	heterochromatin protein 1
IPTG	isopropyl-β-D-thiogalactopyranosid
JPH2	junctophilin 2
LC-MS/MS	liquid chromatography-tandem mass spectrometry
LFQ	label-free quantification
LTCC	L-type voltage-gated calcium channel
MS	mass spectrometry

NT	N-terminus
PBS	phosphate-buffered saline
PKA	cAMP-dependent protein kinase
PP2A	phosphatase 2A
RT	room temperature
RyR	ryanodine receptor
SDS	sodium dodecyl sulfate
SERCA2a	sarcoplasmic/endoplasmic reticulum Ca^{2+} ATPase 2a
SR	sarcoplasmic reticulum
T-tubules	transverse tubules
VDAC1	voltage-dependent anion-selective channel protein 1
VGCC	voltage-gated calcium channel

LIST OF FIGURES

LIST OF TABLES

ABSTRACT

L-type voltage-gated calcium channels (LTCC) are heteromultimeric membrane proteins that allow Ca^{2+} entry into the cell upon plasma membrane depolarization. The β subunit of voltage-dependent calcium channels (Cavβ) binds to the α-interaction domain in the pore-forming α1 subunit and regulates the trafficking and biophysical properties of these channels. Of the four Cavβ isoforms, Cavβ2 is predominantly expressed in cardiomyocytes. This subunit associates with diverse proteins besides LTCC, but the molecular composition of the Cavβ2 nanoenvironments in cardiomyocytes is yet unresolved. Here, we used a protein-labeling technique in living cells based on an engineered ascorbate peroxidase 2 (APEX2). In this strategy, Cavβ2b was fused to APEX2 and expressed in adult rat cardiomyocytes using an adenovirus system. Nearby proteins covalently labeled with biotin-phenol were purified using streptavidin-coated beads and identified by mass spectrometry (MS). Analysis of the *in situ* APEX2-based biotin labeling by MS revealed 61 proteins located in the nanoenvironments of Cavβ2b, with a high specificity and consistency in all the replicates. These proteins are involved in diverse cellular functions such as cellular trafficking, sarcomere organization and excitation-contraction coupling. Among these proteins, we demonstrated an interaction between the ryanodine receptor 2 (RyR2) and Cavβ2b, probably coupling LTCC and the RyR2 into a supramolecular complex at the dyads. This interaction is mediated by the Src homology 3 (SH3) domain of Cavβ2b and is necessary for an effective pacing frequency-dependent increase in Ca^{2+}-induced Ca^{2+} release in cardiomyocytes.

ZUSAMMENFASSUNG

Die spannungabhängigen L-Typ Kalziumkanäle (LTCC) sind heteromultimere Membranproteine, die den Einstrom von Kalzium (Ca^{2+}) in die Zelle nach Depolarisation der Plasmamembran vermitteln. Die β-Untereinheit von spannungsabhängigen Kalziumkanälen (Cavβ2) bindet an die α-Interaktionsdomäne in der porenformenden α1-Untereinheit und reguliert den Transport und die biophysikalischen Eigenschaften dieser Kanäle. Es gibt vier Isoformen der β-Untereinheiten, die als Cavβ bezeichnet werden, von denen die Cavβ2 Isoform hauptsächlich in Kardiomyozyten exprimiert wird. Diese Untereinheit assoziiert neben dem LTCC mit einer Vielzahl an weiteren Proteinen. Die molekulare Zusammensetzung der Cavβ2 Nanoumgebung, bzw. die Interaktionspartner der Cavβ2 Untereinheit, in Kardiomyozyten ist jedoch immer noch nicht bekannt. In dieser Arbeit verwendeten wir eine Proteinmarkierungstechnik in lebenden Zellen auf Basis einer modifizierten Ascorbatperoxidase 2 (APEX2) um die Cavβ2 Nanoumgebung genauer zu charakterisieren. Dafür wurde Cavβ2b mit APEX2 fusioniert und adenoviral vermittelt in adulten Ratten-Kardiomyozyten exprimiert. APEX2 katalysiert die kovalente Markierung von möglichen Interaktionspartnern in unmittelbarer Nähe der APEX markierten Cavβ2 Untereinheit mit Biotin-Phenol. Markierte Proteine wurden mit Streptavidin beschichteten Beads isoliert und mittels Massenspektrometrie (MS) identifiziert. Die Analyse der MS ergab 61 Proteine in der Nanoumgebung von Cavβ2b. Die Analyse zeichnete sich durch eine hohe Spezifität und Beständigkeit in allen Replikaten aus. Diese identifizierten Proteine haben diverse Funktionen wie zelluläre Transportsteuerung, den Aufbau von Sarkomeren und elektromechanischen Kopplung. Eines dieser Proteinen war der Ryanodinrezeptor 2 (RyR2) und damit konnten wir eine Interaktion von RyR2 und Cavβ2b nachweisen, welche wahrscheinlich die LTCCs und RyR2 zu einem supramolekularen Komplex in den Dyaden verbindet. Diese Interaktion wird durch die Src homology 3 (SH3) Domäne von Cavβ2b vermittelt und ist für einen effektive Stimulationsfrequenz-abhängigen Anstieg der Calcium-induzierten Calciumfreisetzung in Kardiomyozyten notwendig.

1. INTRODUCTION

This section provides the background necessary for understanding the scope of the work presented hereby. It outlines fundamental information regarding the structure, function and tissue distribution of voltage-gated calcium channels (VGCC) and their individual subunits, and introduces the proteins known so far to interact with the β subunit of the VGCC (Cavβ), the main focus of this study. Additionally, it delineates the strategies used for the identification of protein interaction partners, specifically focusing on the method employed to achieve the central goal of our study, namely, to characterize the nanoenvironments of Cavβ in cardiomyocytes. Moreover, this section describes the excitation-contraction coupling in skeletal and cardiac muscle, a mechanism where we suggest Cavβ could play an important role.

1.1 Voltage-gated calcium channels

VGCC mediate the selective passage of Ca^{2+} ions through cellular membranes in response to membrane depolarization, playing a major role in cellular processes including muscle contraction, secretion, neurotransmitter release, gene regulation, and neuronal development (Catterall WA, 2009; Zamponi GW *et al.*, 2015; Kamijo S *et al.*, 2018). VGCC are heteromultimeric membrane proteins composed of a pore-forming α1 subunit (Cavα1), a cytoplasmic Cavβ, and an extracellular α2 subunit linked to a transmembrane δ subunit (Cavα2δ) through disulfide bridges, with an additional γ subunit (Cavγ) in some tissues (Campiglio M and Flucher BE, 2015).

Based on the membrane voltage required for their activation, VGCC are grouped in two classes (Figure 1). The first class includes high-voltage-activated (HVA) calcium channels, which are activated by strong depolarization. These are further classified according to their electrophysiological and pharmacological properties into the L, P/Q, N and R types. The second class are the low-voltage-activated (LVA) calcium channels, also known as T-type calcium channels (Alexander SP *et al.*, 2017).

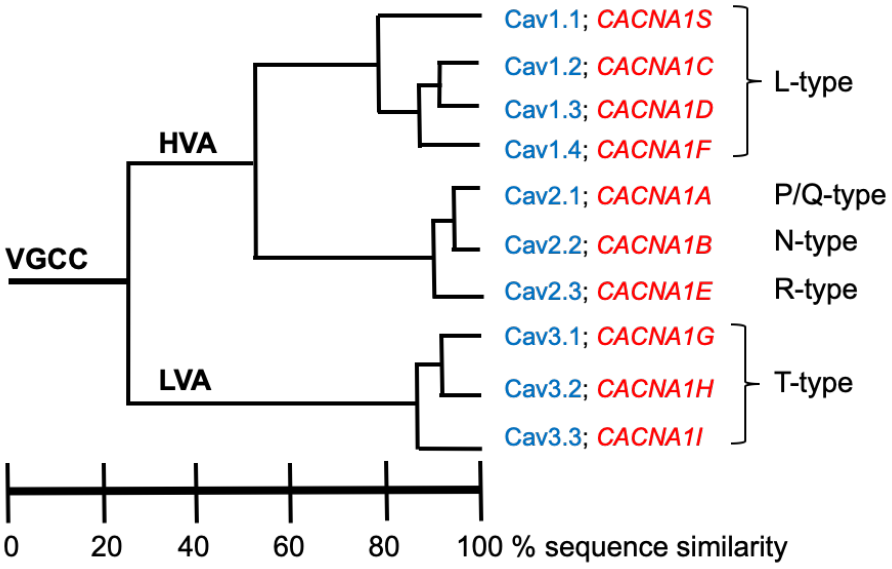

Figure 1. Sequence homology of voltage-gated calcium channel α1 subunits. The calcium channel α1 subunits can be divided into three subclasses according to their amino acid sequence identity: Cav1, Cav2 and Cav3. The Cav1 and Cav2 subclasses are loosely termed high-voltage-activated (HVA) channels whereas Cav3 comprises low-voltage-activated (LVA) channels. According to their electrophysiological and pharmacological properties they can be also classified as L, P/Q, N, R and T types. Protein nomenclature (blue), gene names (red).

1.1.1 The Cavα1 subunit

The Cavα1 subunit consists of four homologous motifs (I-IV), each composed of six membrane-spanning α-helices (S1-S6) linked by intra and extracellular variable loops (Figure 2A). The S4 segments function as the voltage sensor and the four pore loops between segments S5 and S6 determine ion selectivity and conductance (Yu FH *et al.*, 2005). The accessory subunits (Cavβ and Cavα2δ) are tightly but not covalently bound to the Cavα1 subunit and modulate its biophysical properties and trafficking to the membrane (Cantí C *et al.*, 2005; Tran-Van-Minh A and Dolphin AC, 2010; Cassidy JS *et al.*, 2014; Neely A and Hidalgo P, 2014).

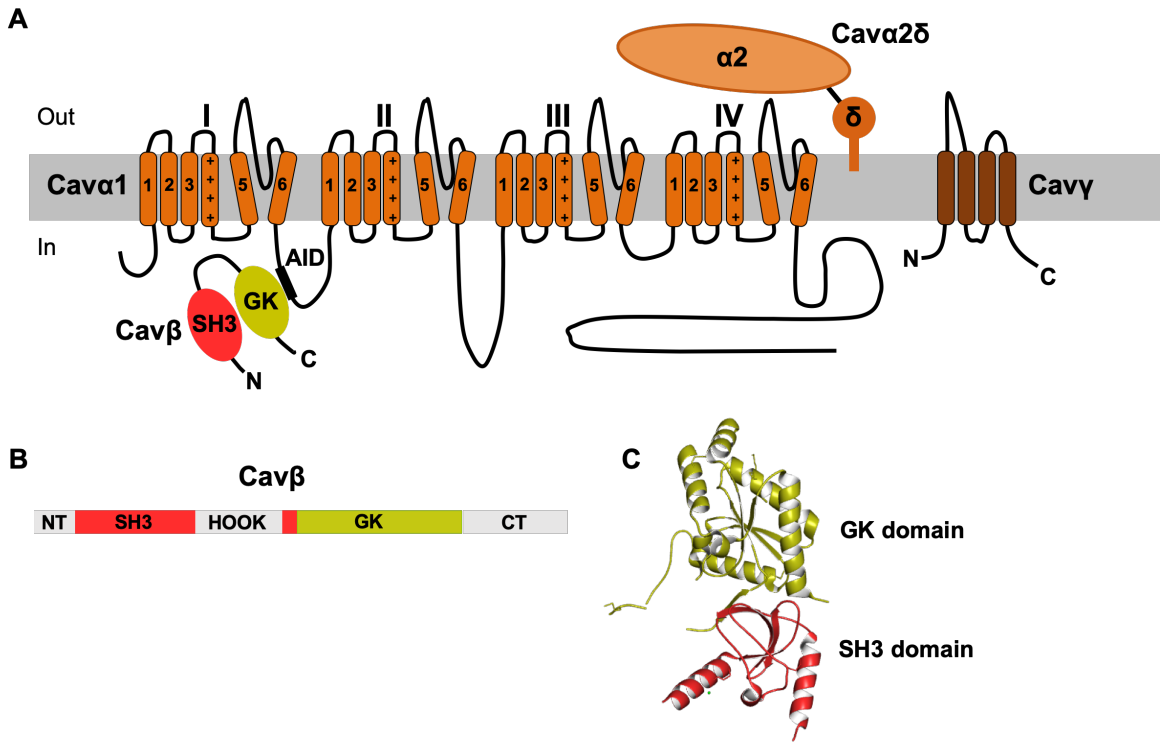

Figure 2. Subunit topology of the voltage-gated calcium channel. The Cavα1 subunit consists of four homologous domains (I to IV), each containing six transmembrane segments (S1-S6) (orange cylinders). Segment S4 (with multiple positively charged amino acids) forms the voltage sensor. The membrane-anchored Cavα2δ subunit is mostly extracellular. It consists of the extracellular Cavα2 subunit and the membrane-associated Cavδ subunit, held together through disulfide bonds. The Cavγ subunit has four transmembrane domains and intracellular N- and C-termini. The intracellular Cavβ subunit consists of an Src homology 3 (SH3) and a guanylate kinase (GK) domains, linked by a variable HOOK region and flanked by variable N-terminus (NT) and C-terminus (CT). Through its GK domain, Cavβ interacts with the α-interaction domain (AID) on the intracellular loop connecting the domains I-II of Cavα1. The domain organization of the Cavβ subunit is shown in (B). (C) Crystal structure of Cavβ (Protein Data Bank: 1T0H). The GK and SH3 domains are represented in green and red, respectively.

Genes encoding 10 different mammalian Cavα1 subunits have been identified. Based on sequence homology of the Cavα1 subunits, VGCC are divided into three major families: Cav1, Cav2 and Cav3 (Figure 1). The Cav1 family, also known as L-type voltage-gated calcium channels (LTCC), consists of four members. All members of this family are activated by strong depolarization, mediate L-type Ca^{2+} currents and are sensitive to dihydropyridines (DHP). The Cav1.1 channels are expressed in skeletal muscle and are essential for skeletal muscle contraction (Zamponi GW *et al.*, 2015). Cav1.2 and/or Cav1.3 are expressed and often coexpressed in most electrically excitable cells, such as in neurons (Olson PA *et al.*, 2005; Dragicevic E *et al.*, 2014), adrenal chromaffin cells (Marcantoni A *et al.*, 2010), and sinoatrial node (SAN) and atrial cardiomyocytes (Mangoni ME *et al.*, 2003). In cardiomyocytes, Cav1.2 predominates and is involved in cardiac excitation-contraction (EC) coupling. By contrast, in the SAN and atrioventricular node,

Cav1.3 is the predominant LTCC isoform and is involved in pacemaker activity (Mangoni ME *et al.*, 2003). On the other hand, Cav1.4 is mainly restricted to the retina and is required for normal visual function (Zamponi GW *et al.*, 2015).

The family of Cav2 proteins is primarily responsible for the initiation of synaptic transmission at fast synapses in the nervous system. They have a larger intracellular loop connecting domains II and III, which contains a synaptic protein interaction site that binds SNARE proteins involved in exocytosis (He R *et al.*, 2018).

Cav3 channels conduct T-type Ca^{2+} currents, which are important for repetitive firing of action potentials in rhythmically firing cells such as cardiac myocytes and thalamic neurons. Unlike members of the high-voltage-activated channel Cav1 and Cav2 families, Cav3 does not require coassembly with auxiliary subunits (Campiglio M and Flucher BE, 2015). In the heart, T-type channels are abundant in sinoatrial pacemaker cells and Purkinje fibers of many species (Mesirca P *et al*., 2014, 2015). The T-type Ca^{2+} channels present in peripheral and central synapses play a key role in dendritic integration and neurotransmitter release (Lambert RC *et al.*, 2014).

1.1.2 The Cavα2δ subunit

The Cav1 and Cav2 channel families contain the Cavα2δ accessory subunit (Figure 2A). To date, there are four known mammalian Cavα2δ isoforms: Cavα2δ-1, Cavα2δ-2, Cavα2δ-3, Cavα2δ-4. Each Cavα2δ subunit gene encodes a single precursor protein that is post-translationally proteolytically processed into the α2 and δ polypeptides. (Dolphin AC, 2013, 2018). The folding of Cavα2δ involves the formation of disulfide bonds between α2 and δ that keep the polypeptides together despite the cleavage of the precursor protein (De Jongh KS *et al*., 1990; Jay SD *et al.*, 1991). Isoforms Cavα2δ-1, Cavα2δ-2 and Cavα2δ-3 are widely expressed in both the peripheral and central nervous system (Cole RL *et al.*, 2005; Margas W *et al.*, 2016). The Cavα2δ-3 transcript is also present in the auditory system (Pirone A *et al.*, 2014) and in the retina (Perez de Sevilla Müller L *et al.*, 2015). Protein Cavα2δ-4 is found in certain endocrine tissues (Qin N *et al.*, 2002) and also plays a key role in the retina (De Sevilla Müller LP *et al.*, 2013).

Cavα2δ augments the calcium current density of the Cav1 and Cav2 channels (Cantí C *et al.*, 2005; Tran-Van-Minh A and Dolphin AC, 2010). This effect can be partially explained by an increase in the trafficking of the channels that augments their cell surface expression (Cassidy JS *et al.*, 2014). However, the exact mechanism whereby Cavα2δ increases the density of VGCC in the plasma membrane is still unclear.

1.1.3 The Cavγ subunit

With 35 kDa, Cavγ is the smallest of the VGCC auxiliary subunits. There are eight different Cavγ subunit-encoding genes, all yielding proteins with four transmembrane domains and intracellular N- and C-termini (Figure 2A). Cavγ1, the first Cavγ subunit cloned from skeletal muscle (Jay SD *et al.*, 1990), is the best characterized isoform in terms of functional role and interaction with the calcium channel. Transient coexpression with the cardiac calcium channel complex demonstrated that the Cavγ subunit shifts the inactivation curve to negative potentials and accelerates current inactivation (Eberst R *et al.*, 1997). Cavγ4, 6, 7 and 8 are known to be expressed in the human heart (Yang L *et al.*, 2011). These Cavγ subunits differentially modulate the inactivation properties of the cardiac Cav1.2 channel heterologously expressed in HEK-293 cells (Yang L *et al.*, 2011). Cavγ4 was recently reported to participate in the control of Cav1.2 and Cav1.3 gene expression in human pancreatic islets, where it is essential for Ca^{2+} signaling and the regulation of insulin secretion by β cells. Accordingly, the reduction of Cavγ4 expression leads to the downregulation of Cav1.2 and Cav1.3 expression, which in turn prevents voltage-gated Ca^{2+} entry and glucose-induced insulin exocytosis (Luan C *et al.*, 2019).

1.1.4 The Cavβ subunit

The Cavβ subunit is a cytosolic protein that binds with high affinity to the α-interaction domain (AID) (Pragnell M *et al.*, 1994; De Waard M *et al.*, 1995), a highly conserved intracellular motif made up of 18 amino acids and located in the intracellular loop connecting domains I and II of the Cavα1 subunit (Figure 2A).

Cavβ proteins are encoded by four different genes, *Cacnb1-4*, with multiple alternative splice variants (Ruth P *et al.*, 1989; Pragnell M *et al.*, 1991; Perez-Reyes E *et al.*, 1992; Castellano A *et al.*, 1993a, 1993b). These variants share the same core structure in which two highly conserved regions, homologous to the Src homology 3 (SH3) and guanylate kinase (GK) domains, are linked by a variable HOOK region and flanked by variable N- and C-termini (Figure 2B and C).

The highly conserved domains place Cavβ among the membrane-associated guanylate kinase (MAGUK) proteins (McGee AW *et al.*, 2004). MAGUKs are scaffold molecules crucially involved in the organization of multiprotein complexes at synapses and other functionally specialized regions (Funke L *et al.*, 2005; Elias GM and Nicoll RA, 2007). The GK domain of Cavβ retains the overall structural characteristics of the yeast guanylate kinase, but it does not have catalytic activity (Olsen O and Bredt DS, 2003). This domain

tightly binds to Cavα1 through its high-affinity interaction with the AID (Chen YH *et al.*, 2004; Opatowsky Y *et al.*, 2004; Van Petegem F *et al.*, 2004).

SH3 domains participate in protein-protein interactions by binding to proline-rich motifs (PxxP) in target proteins (Mayer BJ, 2001). The PxxP-binding site in the SH3 domain of Cavβ is occluded by the HOOK region and a loop linking two consecutive β-sheets in SH3, as revealed by crystallography studies (Chen YH *et al.*, 2004; Opatowsky Y *et al.*, 2004; Van Petegem F *et al.*, 2004; Findeisen F *et al.*, 2017). However, it is known to bind to the PxxP motif of dynamin (Gonzalez-Gutierrez G *et al.*, 2007; Miranda-Laferte E *et al.*, 2011), which suggests that a structural rearrangement likely exposes this site to mediate the binding of Cavβ to other proteins.

Many Cavβ variants result from the alternative splicing of the exons coding for the variable N-terminus (NT), HOOK and C-terminus (CT) regions of each Cavβ subunit. The genes coding for Cavβ1 and Cavβ2 (*Cacnb1* and *Cacnb2*, respectively) undergo alternative splicing in exon 7, producing diverse HOOK regions (Buraei Z and Yang J, 2010). In *Cacnb1*, alternative splicing of the C-terminus can include or exclude exon 14. Moreover, at least five Cavβ2 variants (Cavβ2a-e) differing in their N-terminus result from the splicing of *Cacnb2*. Alternative splicing of the exons coding for the N-terminal regions of Cavβ4 creates the Cavβ4a, Cavβ4b, Cavβ4e subunits (Helton TD and Horne WA, 2002; Etemad S *et al.*, 2014), while elimination of exon 9 from Cavβ4a results in the truncated variant Cavβ4c (Hibino H *et al.*, 2003; Xu X *et al.*, 2011). Finally, *Cacnb3* is not alternatively spliced, but gives rise to a truncated isoform. Truncated products have also been reported for Cavβ1 and Cavβ2 (Buraei Z and Yang J, 2010).

1.1.4.1 Tissue distribution of the Cavβ subunit

The Cavβ1 subunit is expressed in the brain, heart, skeletal muscle, spleen, T cells and other tissues (Buraei Z and Yang J, 2010). Cavβ1a seems to be the only Cavβ subunit expressed in skeletal muscle, where it binds to Cav1.1. Cavβ2 is detected in heart, brain, lung, nerve endings at the neuro-muscular junction, T cells, osteoblasts and other tissues (Buraei Z and Yang J, 2010). This protein is also the most abundant Cavβ isoform in cardiomyocytes (Ludwig A *et al*., 1997), where the predominantly expressed Cavβ2b splice variant (Link S *et al.*, 2009) localizes mainly at the dyadic junction, associated with the Cav1.2 along the transverse tubules (T-tubules) (Gao T *et al.*, 1997). The Cavβ3 subunit is primarily expressed in smooth muscle and brain (Buraei Z and Yang J, 2010; Ferrándiz-Huertas C *et al*., 2012). The Cavβ4a, Cavβ4b, Cavβ4c splice variants are highly expressed in the brain and can also be detected in the spinal cord, eye, and heart (Hibino

H *et al.*, 2003). The truncated Cavβ4c isoform is also expressed in chicken cochlea sensory epithelia, being the only Cavβ4 isoform expressed in this tissue (Hibino H *et al.*, 2003). Cavβ4e, a recently identified splice variant, is highly expressed in mouse cerebellum and cultured cerebellar granule cells. Compared with Cavβ4a and Cavβ4b, the other two known full-length Cavβ4 variants, Cavβ4e is most abundantly expressed in the distal axon (Etemad S *et al.*, 2014).

1.1.4.2 Functions of the Cavβ subunit

The impact of Cavβ on the electrophysiological properties of the Cavα1 subunit is complex. In general, Cavβ induces an increase in Ca^{2+} current density accompanied by a shift in the activation threshold to more negative membrane potentials, which is reflected in an augmented open probability of individual channels. Among the Cavβ subunits, Cavβ2a produces the highest increase in channel open probability (Colecraft HM *et al.*, 2002; Dzhura I and Neely A, 2003). Cavβ subunits also modulate channel inactivation by shifting the voltage-dependent inactivation by around 10-20 mV to more hyperpolarized voltages (Neely A and Hidalgo P, 2014). For instance, the disruption of the interaction between Cavβ3 and Cav2.2 by small molecule inhibitors results in a decrease in the trafficking of Cav2.2 to the plasma membrane and shifts the half-activation potential for Cav2.2 toward a more positive voltage, making it harder for Cav2.2 to be activated at moderate depolarizing voltages (Chen X *et al.*, 2018).

Cavβ is also involved in VGCC surface expression and has been suggested to promote the export of Cavα1 from the endoplasmic reticulum over its retention in this organelle. Accordingly, the binding of Cavβ to the Cavα1 I-II loop could induce a conformational rearrangement that would alter the balance between export signals on the I-II loop and retention signals elsewhere on Cav1.2, thus leading to the transport of this protein to the plasma membrane (Fang K and Colecraft HM, 2011).

The widely accepted relevance of Cavβ for the traffic of the Cavα1 subunit to the plasma membrane was recently contradicted by Yang L *et al.* (2019). These authors generated transgenic mice where three mutations in the AID rendered Cavα1 unable to bind Cavβ. In these animals, AID-mutant and wild-type Cavα1 subunits were similarly localized on the plasma membrane and T-tubules. In addition, the authors inserted the T1066Y/Q1070M mutations, which confer DHP resistance (He M *et al.*, 1997; Hockerman GH *et al.*, 1997), in AID-mutant Cavα1 subunits and inhibited Ca^{2+} currents from endogenous DHP-sensitive Cav1.2 using nisoldipine. Field stimulation of cardiomyocytes isolated from transgenic mice with DHP-resistant AID-mutant Cavα1 induced sarcomere length

contraction even in the presence of 300 nM nisoldipine. Therefrom, the authors concluded that Cavβ is not required for the Cavα1 channels to traffic to the sarcolemma and trigger EC coupling (Yang L *et al.*, 2019).

It has also been suggested that Cavβ increases the plasma membrane expression of Cavα1 by protecting the channel from programmed proteasomal degradation. In one study, Cavβ-deficient Cav1.2 channels underwent ubiquitination in tsA-201 cells, while MG132-mediated inhibition of proteasomal degradation was sufficient to restore the cell surface expression of Cav1.2 in the absence of Cavβ (Altier C *et al.*, 2011). By contrast, proteasome inhibition in the same cell line did not enhance the cell surface expression of Cav2.2 in the absence of Cavβ, but was accompanied by increased ubiquitination (Waithe D *et al.*, 2011). More recently, Page KM *et al*. (2016) reported that the degradation of the ubiquitinated I-II loop of Cav2.2, but not its oligoubiquitination, is prevented when Cavβ binds to the channel.

1.2 Interaction of Cavβ with other proteins

There is abundant evidence showing that the Cavβ subunit interacts not only with Cavα1, but also with other proteins that either regulate its ability to interact with Cavα1 or have channel-independent functions. The partners of Cavβ include protein kinases, ryanodine receptor, actin and some transcription factors (Figure 3).

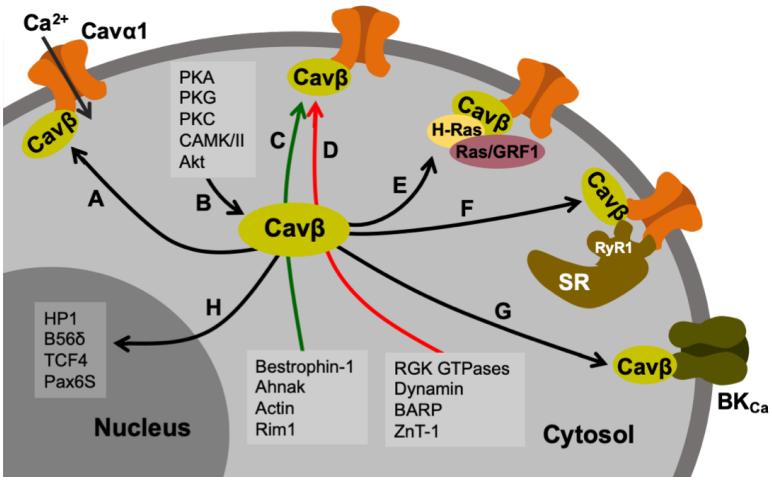

Figure 3. Interacting partners of Cavβ. (A) Cavβ regulates the gating properties of Cavα1. (B) The phosphorylation of Cavβ can regulate Cavα1-mediated currents or its interaction with other proteins. Cavβ interacts with other proteins to activate (C, green arrow) or inhibit (D, red arrow) Cavα1. (E) The interaction of Cavβ with H-Ras and Ras-specific guanine nucleotide exchange factor (Ras/GRF1) is crucial for depolarization-induced gene activation. (F) In skeletal muscle, the interaction of Cavβ with the ryanodine receptor 1 (RyR1) is essential for excitation-contraction coupling. (G) Cavβ interacts with the large-conductance Ca^{2+}-activated K^+ channels (BK_{Ca}), modulating their gating and their sensitivity to Ca^{2+}. (H) Cavβ can also translocate to the nucleus and interact with regulators of gene transcription. SR: sarcoplasmic reticulum. Adapted from Rima M *et al.* (2016).

1.2.1 Protein kinases

PKA

Cardiac L-type Ca^{2+} currents can be upregulated by the β-adrenergic receptor pathway through a non-fully elucidated molecular mechanism that involves the production of cyclic adenosine monophosphate (cAMP) and activation of the cAMP-dependent protein kinase (PKA) (Weiss S *et al.*, 2013). Mutations on amino acids S478 and S479 of Cavβ2 completely abolished the PKA-induced increase in L-type Ca^{2+} currents in a heterologous expression system, which suggests that at least these two serines could be phosphorylated by PKA in the heart (Haase H *et al.*, 1996; Bünemann M *et al.*, 1999). However, additional experiments in transgenic animal models and cardiomyocytes contradicted this finding and called into question the phosphorylation of Cavβ by PKA. Ganesan AN *et al.* (2006) observed a normal β-adrenergic response in adenovirally-transduced cardiomyocytes expressing the mutant Cavβ2 subunit (S478A and S479A), which indicates that Cavβ subunit phosphorylation is not essential for PKA regulation. Another group generated a mouse line with a stop codon in the *Cacnb2* gene that resulted in a truncated Cavβ2 protein lacking the potential PKA phosphorylation sites. The basal properties of cardiac Cav1.2 currents were unaffected in these animals (Brandmayr J *et al.*, 2012). In line with these results, a recently published study demonstrated that Cavβ2b does not contain the PKA target sites required for the β-adrenergic agonist-induced stimulation of Cav1.2 (Liu G *et al.*, 2020). In this study, the authors mutated to alanine all 37 conserved and nonconserved serine and threonine residues within 28 PKA-consensus phosphorylation sites of the human Cavβ2b (GFP-tagged 28-mutant Cavβ2b) and then generated transgenic mice with inducible cardiomyocyte-specific expression of either GFP-tagged wild-type or 28-mutant Cavβ2b subunits. The cardiomyocytes expressing GFP-tagged 28-mutant Cavβ2b underwent an isoprenaline- or forskolin-induced increase in the amplitude of Ca^{2+} currents through Cav1.2 and a hyperpolarizing shift in the voltage dependence of activation, similar to what was detected in cardiomyocytes expressing GFP-tagged wild-type Cavβ2b (Liu G *et al.*, 2020).

CAMKII

The calcium/calmodulin-dependent protein kinase II (CaMKII) directly interacts with Cavβ1 and Cavβ2, but not with Cavβ3 or Cavβ4 (Grueter CE *et al.*, 2008; Abiria SA and Colbran RJ, 2010). Mutations of the CAMKII binding (L493A) and phosphorylation (T498A) sites on Cavβ2 reduce the Ca^{2+} entry through Cav1.2 (Koval OM et al., 2010), demonstrating that both sites are required for Cav1.2 activation by CAMKII in adult rabbit cardiomyocytes.

PKG

Using phospho-specific antibodies, Yang L *et al.* (2007) found that the S496 amino acid residue on Cavβ2a is phosphorylated by the cyclic guanosine monophosphate (cGMP)-dependent protein kinase (PKG), an enzyme known to inhibit Cav1.2 activity (Jiang LH *et al.*, 2000). Alanine substitution at the PKG phosphorylation site in Cavβ2a significantly reduced the inhibition of Cav1.2 currents mediated by PKG in HEK-293 cells (Yang L *et al.*, 2007), but further experiments are needed to demonstrate that the site is actually phosphorylated in a physiological context.

PKC

Protein kinase C (PKC) phosphorylates Cavβ2a in *Spodoptera frugiperda* insect cells, but the functional relevance of this phosphorylation is still unknown (Puri TS *et al.*, 1997). More recently, Cav2.2 channels were expressed in Xenopus oocytes in various subunit combinations with or without Cavβ (Rajagopal S *et al.*, 2014a). In this model, Ca^{2+} currents were intensified by the PKC activator acetyl-β-methylcholine (MCh) when Cav2.2 was expressed alone, but not with Cavβ1b, Cavβ2a, Cavβ3 or Cavβ4. Moreover, MCh failed to potentiate Ca^{2+} currents in the T422A, S1757A and S2132A mutants of Cav2.2, which are putative PKC target sites. These findings suggest that Cavβ interferes with the interaction between PKC and the serine/threonine sites of Cav2.2. In addition, when Cavβ2 and Cavβ3 were downregulated via siRNA, PKC translocated to the membrane in pancreatic β cells, suggesting that these isoforms inhibit PKC activation by blocking its translocation to the membrane or by decreasing the interaction between the Cavα1 subunits and PKC (Rajagopal S *et al.*, 2014b).

Akt/PKB

A unique putative consensus phosphorylation site (RxRxxS) targeted by protein kinase B (PKB, also known as Akt) was identified in the C-terminal domain of Cavβ2, but is absent from the Cavβ1b, Cavβ3 and Cavβ4 subunits. Phosphorylation of Cavβ2a at S574 increased the trafficking of LTCC to the plasma membrane in neuronal cells (Viard P *et al.*, 2004) and was suggested as a mechanism whereby Cavα1 is protected from proteolytic degradation (Catalucci D *et al.*, 2009). Additionally, LTCC surface expression was reduced in cardiac-specific conditional knockout mice lacking active Akt/PKB (Catalucci D *et al.*, 2009). Cavα1 contains highly conserved PEST sequences (rich in proline, glutamic acid, serine, and threonine) that target proteins for rapid degradation, but these sequences are masked by Cavβ2 when it is phosphorylated by Akt/PKB, which in turn slows or prevents Cavα1 degradation.

1.2.2 GTPases

RGK GTPases

RGK (Rad, Rem, Rem2, Gem/Kir) proteins are a subfamily of the Ras superfamily of monomeric G-proteins and are inhibitors of Cav1 and Cav2 channels (Yang T and Colecraft HM, 2013). All RGK proteins bind to any of the Cavβ subunits (Buraei Z *et al.*, 2015). Béguin P *et al.* (2001) found that Gem interacts with Cavβ3 in a yeast two-hybrid assay. A structural model of the interaction showed that Gem binds to the GK domain of Cavβ3 and that amino acids D194, D270 and D272 in Cavβ3 and R196, V223 and H225 in Gem are critical for this interaction (Béguin P *et al.*, 2007). Additionally, alanine substitution at D258 in Cavβ4a decreased the RGK binding affinity and affected the ability of Rem2 to inhibit Cav2.1-mediated currents. Furthermore, mutations L173A and V303A in Cavβ4a blocked Rem2 binding and its ability to suppress Cav2.1 currents (Xu X *et al.*, 2015).

Several groups have addressed the question of how RGK inhibit Cav1 and Cav2 channels. A study using a mutated Cavβ unable to bind RGK showed that a direct interaction with Cavβ was not required for Gem to inhibit Cav2.1 channels in Xenopus oocytes (Fan M *et al.*, 2010). However, the binding of Cavβ to Cav2.1 was absolutely required for the Gem-mediated inhibition of Cav2.1 channels. In addition, Gem failed to inhibit Cavβ-less channels on the plasma membrane, although it could still bind to Cavα1. The above-mentioned findings suggest that an inhibitory site on the channel complex is probably exposed by Cavβ and then engaged by Gem to block Cav2.1 (Fan M *et al.*, 2010).

On the other hand, Cav1.2 channels containing a Cavβ2a mutant that is selectively unable to interact with RGK proteins were less potently inhibited (74% inhibition) by Rem than channels containing the wild-type Cavβ2a (96% inhibition). This suggests that the Rem-mediated inhibition of Cav1.2 channels occurs via a Cavβ-binding-dependent mechanism (Yang T *et al*., 2012). In the same study, the authors demonstrated that Rad (RGK family) can inhibit Cav1.2 via Cavβ-dependent and Cavβ-independent mechanisms. Mutations R208A and L235A in Rad or D244A, D320A and D322A in Cavβ2b reduce the binding of Rad to Cavβ subunits (Béguin P *et al.*, 2007; Yang T *et al*., 2012). Recently, Liu G *et al.* (2020) demonstrated that this interaction is essential for the cAMP/PKA-mediated upregulation of Ca^{2+} currents through Cav1.2. Using a flow-cytometry-based fluorescence resonance energy transfer two-hybrid assay, they detected a robust binding between Rad and Cavβ2b, which was reduced in the presence of PKA. The phosphorylation of Rad by PKA decreases Rad's affinity for Cavβ subunits and attenuates the constitutive inhibition

of Cav1.2, as detected by an increase in the open probability of the channel (Liu G *et al.*, 2020).

H-Ras and Ras/GRF1

Neuronal specific transcription factors like CREB and immediate-early genes can be regulated by signaling cascades triggered by LTCC-mediated depolarization. Accordingly, the recently demonstrated interaction between H-Ras and Cavβ2 seems to be crucial for depolarization-induced gene activation. Cavβ2 was shown to interact in human neuronal SH-SY5Y cells with H-Ras and the Ras-specific guanine nucleotide exchange factor (Ras/GRF1), an activator of Ras. Upon activation, H-Ras triggers the phosphorylation of Raf and the MEK/ERK/RSK/CREB signaling pathway. H-Ras is inactive in the absence of Cavβ2b, as confirmed by the loss of ERK/CREB phosphorylation when the single-point mutation W440A within the AID of Cav1.2 supresses its interaction with Cavβ2b. This strongly supports the hypothesis that depolarization-induced conformational changes at Cav1.2 mediate excitation-transcription coupling through Cavβ2b, but not Ca^{2+} entry during depolarization (Servili E *et al.*, 2018). However, the mechanism whereby the interaction between Cav1.2 and Cavβ2 activates Ras has yet to be determined.

Dynamin

Dynamin is a GTPase involved in the release of endocytic vesicles from the plasma membrane (Hinshaw JE, 2000; Praefcke GJ and McMahon HT, 2004). Its proline-rich region interacts with the SH3 domain of Cavβ2 and this interaction mediates the recruitment of dynamin to the plasma membrane (Gonzalez-Gutierrez G *et al.*, 2007). However, simulated docking predictions indicate that the conserved amino acids critical for binding to the PxxP motif are occluded in the crystal structure of the SH3 domain of Cavβ (Chen YH *et al.*, 2004; Opatowsky Y *et al.*, 2004; Van Petegem F *et al.*, 2004), which suggests that a structural rearrangement likely exposes this site to enable the binding of Cavβ to dynamin (Gonzalez-Gutierrez G *et al.*, 2007) .

Calcium channel surface expression is downregulated by the interaction between dynamin and the SH3 domain of Cavβ2 (Gonzalez-Gutierrez G *et al.*, 2007). Cavβ2-SH3 domains homodimerize through a single disulfide bond, a process that is crucial for channel endocytosis (Miranda-Laferte E *et al.*, 2011). Dimerization is reduced in the presence of the Cavα1 subunit, suggesting that the oligomerization of Cavβ2 is the functional switch between the channel-activating and channel-internalizing states of the subunit. The binding of dynamin to the SH3 domain of Cavβ2 could result in weaker intramolecular interactions that favor dimer formation and the dissociation of Cavβ2 from the channel (Miranda-Laferte E *et al.*, 2011).

1.2.3 Receptors and ion channels

Ryanodine receptor 1

RyR are large multiprotein complexes composed of four 560-kDa RyR subunits (Lanner JT *et al.*, 2010). The ryanodine receptor 1 (RyR1) is a Ca^{2+} channel isoform expressed in the sarcoplasmic reticulum (SR) of skeletal muscle cells. Its gating is stimulated by Ca^{2+} itself and inhibited by the alkaloid ryanodine (Bers DM, 2002). *In vitro* studies indicate that Cavβ1a binds to a RyR1 fragment containing amino acids K3494-K3502 (Cheng W *et al.*, 2005). However, deletion or substitution of these amino acids only partially reduced the interaction, indicating that other amino acids of RyR1 are also contributing to Cavβ1a binding.

According to studies using Cavβ1a/Cavβ2a chimeras and truncation mutants, some distinctive elements in the C-terminus of the Cavβ1a subunit are critical for both binding to and regulation of the RyR1 (Beurg M *et al.*, 1999; Sheridan DC *et al.*, 2003). A fivefold decrease in the Ca^{2+} transients peak amplitude was detected in the myotubes of Cavβ1a-null mice expressing a Cavβ1a mutant lacking the last 35 C-terminal amino acids (Beurg M *et al.*, 1999). This C-terminal tail of Cavβ1a (renamed Cavβ1a490-524) bound to the RyR1 and, like the full-length Cavβ1a subunit, increased the activity of the RyR1 (Rebbeck RT *et al.*, 2011).

Zinc transporter 1

The zinc transporter (ZnT) family consists of 10 proteins that are involved in either reducing cytoplasmic zinc or in zinc sequestration into secretory and synaptic vesicles (Nolte C *et al.*, 2004; Shusterman E *et al.*, 2014). ZnT-1 is a ubiquitously expressed protein that acts as an endogenous inhibitor of LTCC preventing excessive cation intake (Segal D *et al.*, 2004; Beharier O *et al.*, 2007). The inhibition of the LTCC by ZnT-1 depends on the presence of Cavβ2a leading to a reduction in the surface expression of Cavα1 (Levy S *et al.*, 2009). Coimmunoprecipitation experiments and fluorescence resonance energy transfer measurements have confirmed the interaction between ZnT-1 and Cavβ2a. Unlike other members of the ZnT family, ZnT-1 has a large C-terminus that seems to mediate its interaction with Cavβ. A peptide consisting of the ZnT-1 C-terminus inhibited the LTCC as efficiently as the wild-type ZnT-1 by an as yet unknown mechanism (Shusterman E *et al.*, 2017).

Bestrophin-1

Bestrophin-1 is a chloride anion channel expressed in the retinal pigment epithelium that can also regulate VGCC, including its activation kinetics, voltage-dependent activation

and current amplitude (Rosenthal R *et al.*, 2006; Yu K *et al.*, 2008). When heterologously expressed, bestrophin-1 coimmunoprecipitates with the Cavβ3 or Cavβ4 subunits. The binding of Cavβ and bestrophin-1 is thought to be mediated by the interaction between the SH3 domain of Cavβ and PxxP motifs located within amino acids 330-370 on the C-terminus of bestrophin-1 (Yu *et al.*, 2008; Reichhart *et al.*, 2010). A deletion mutant lacking the four PxxP motifs of another cluster, located between amino acids 468 and 486 of bestrophin-1, had a 20-30% lower coimmunoprecipitation efficiency with the Cavβ subunits and downregulated the cell membrane expression of Cav1.3. Therefore, the proline-rich motifs on the C-terminus of bestrophin-1 seem to help maintain the ability of Cavβ to regulate the surface expression of Cavα1 (Milenkovic VM *et al.*, 2011).

BKCa channels

Large-conductance Ca^{2+}-activated K^+ channels (BK_{Ca}) are dually activated by membrane depolarization and intracellular Ca^{2+} and modulate different physiological processes, including smooth muscle tone and neurotransmitter release (Salkoff L *et al.*, 2006; Fakler B and Adelman JP, 2008). The pore-forming subunit of the BK_{Ca} channel, Slo1, has a calcium bowl region that binds to the GK domain of Cavβ1 and also interacts with this protein through a non-canonical SH3-binding motif. This interaction is sufficient to modulate the gating of BK_{Ca} channels and significantly reduces their sensitivity to Ca^{2+} (Zou S *et al.*, 2008).

1.2.4 Ahnak

Ahnak is a large (700 kDa) ubiquitous signaling and scaffolding protein with a regulatory role in Ca^{2+} membrane permeability and intracellular Ca^{2+} homoeostasis (Shao Y *et al.*, 2009). It interacts with Cavβ (Haase H *et al.*, 1999; Alvarez J *et al.*, 2004) and has been reported to regulate VGCC in cardiomyocytes, T-lymphocytes, osteoblasts and neurons (Alvarez J *et al.*, 2004; Matza D *et al.*, 2008; Shao Y *et al.*, 2009; Jin J *et al.*, 2019).

The interaction of Cavβ2 with ahnak was originally detected by coimmunoprecipitation using cardiomyocytes isolated from rodent or human hearts (Haase H *et al.*, 1999). The high-affinity interaction (Kd ~50 nM) between Cavβ2 and ahnak is known to be mediated by the most carboxyl-terminal 382 amino acids of ahnak (Hohaus A *et al.*, 2002). The region on Cavβ2a responsible for the interaction with ahnak is unknown, but since ahnak coimmunoprecipitates with Cavβ1b, Cavβ2, Cavβ3 and Cavβ4b (Haase H *et al.*, 1999; Hohaus A *et al.*, 2002; Alvarez J *et al.*, 2004; Shao Y *et al.*, 2009; Jin J *et al.*, 2019), it is probably located in the conserved GK or SH3 domains.

It has been suggested that the ahnak-Cavβ2 interaction is important for the PKA-mediated upregulation of cardiac L-type Ca^{2+} currents (Haase H *et al.*, 2005; Pankonien I *et al.*, 2012). The phosphorylation of Cavβ2a and ahnak by PKA weakens the interaction between the two proteins and upregulates L-type Ca^{2+} currents (Haase H *et al.*, 2005, 2007). A novel PKA phosphorylation site (S296) was identified in the GK domain of Cavβ2 that reduces the Cavβ2-ahnak interaction by eliminating and/or masking a binding site (Pankonien I *et al.*, 2012).

1.2.5 Actin

The interaction of Cavβ2 with actin filaments seems to occur through the SH3 and GK domains of Cavβ2, suggesting that all the Cavβ isoforms can bind to actin (Stölting G *et al.*, 2015). On the other hand, overexpression of Cavβ2 in cardiomyocytes increases channel expression and stimulates L-type Ca^{2+} currents. This effect is dependent on the Cavβ-actin interaction and is abolished in the presence of cytochalasin D, a molecule that disrupts actin polymerization. It is known that ion channels trafficking to the cell surface are incorporated into vesicles that move along actin filaments and microtubules. Accordingly, Cavβ could promote channel recruitment via its direct interaction with actin, which would provide the tracks for transporting the channels to the cell surface.

1.2.6 Synaptic proteins: Rab-interacting molecules and synaptotagmin I

The four isoforms of the Rab3-interacting molecule (RIM1-4) protein family are presynaptic proteins that control VGCC-mediated neurotransmitter release by tethering the presyanptic Ca^{2+} channels to the active zone and by activating the priming of synaptic vesicles (Kaeser PS *et al.*, 2011). RIM1 was reported to associate with the Cavβ subunit via its C-terminus to significantly inhibit the voltage-dependent inactivation of different neuronal VGCC (Kiyonaka S *et al.*, 2007; Gandini MA and Felix R, 2012). Yeast two-hybrid assays using Cavβ4b mutants showed that amino acids 49-410, encompassing the major structural motifs SH3-HOOK-GK, were necessary for the interaction between Cavβ4b and RIM1 (Kiyonaka S *et al.*, 2007). Uriu Y *et al.* (2010) demonstrated the physical association of other family members RIM2α, RIM3γ, and RIM4γ with different Cavβ subunits, and this interaction decelerated VGCC inactivation to sustain depolarization-induced Ca^{2+} influx. Two mutations (E177A and M260V) in the C-terminus of RIM3 have been identified in patients with autism (Kumar RA *et al.*, 2010). Mutations at E176A and M259V in the mouse RIM3 protein affect its interaction with Cavβ and partially suppress the inhibitory effect of RIM3 on voltage-dependent inactivation of Ca^{2+} currents through Cav2.1 (Takada Y *et al.*, 2015).

The synaptic protein synaptotagmin I has also been shown to interact with the N-terminus of Cavβ4a (but not Cavβ4b) and this interaction is abolished by a high (10 mM) Ca^{2+} concentration (Vendel AC *et al.*, 2006). However, the physiological relevance of this interaction is yet unknown.

1.2.7 Voltage-gated calcium channel β-anchoring and -regulatory protein

VGCC-β-anchoring and -regulatory protein (BARP) is an integral membrane glycoprotein mainly expressed in neurons and neuroendocrine cells (Béguin P *et al.*, 2014). In COS-1 cells overexpressing the Cavβ subunits, BARP binds to all the different Cavβ isoforms, while in brain and cerebellum samples, it coimmunoprecipitates with Cavβ3 and Cavβ4, but not with Cavβ1. Two domains of BARP are involved in the interaction with Cavβ. The domain I binds to all Cavβ subunits, whereas the domain II interacts with Cavβ3, Cavβ2a, Cavβ2b and Cavβ4a, but not with Cavβ1a. Moreover, the domain I interacts with the AID-binding pocket in Cavβ and affects the binding of Cavβ to Cavα1. Interestingly, although BARP does not significantly hinder the Cavβ-mediated facilitation of Cavα1 expression on the plasma membrane, it blocks the calcium channel activity, leading to the inhibition of Ca^{2+}-elicited exocytosis. Thus, BARP acts as a negative regulator of VGCC activity by controlling the association of Cavβ with Cavα1 (Béguin P *et al.*, 2014).

A recent study investigating the role of BARP in higher brain functions found that, unexpectedly, BARP-knockout mice did not show behavioral phenotypes opposite to those of *Cacna1c* transgenic mice. Presumably, BARP´s failure to regulate VGCC activity is compensated by other Cavβ-interacting proteins (Nakao A *et al.*, 2015).

1.2.8 Gene transcription regulators

HP1 and B56δ/PP2A and TCF4

Cavβ4c is a truncated isoform of Cavβ4 lacking 90% of its GK domain and the complete C-terminus. This short splice variant interacts directly with heterochromatin protein 1 gamma (HP1γ), a nuclear protein that mediates gene silencing and transcription regulation (Hibino H *et al.*, 2003). The HP1 family has a chromo shadow domain (CSD) that acts as a scaffold assembling diverse nuclear proteins (Platero JS *et al*., 1995) and seems to mediate the interaction with Cavβ4c (Hibino H *et al.*, 2003). Cavβ4c and HP1γ colocalize in the nucleus of cochlear hair cells (Hibino H *et al.*, 2003).

Xu X *et al.* (2011) revealed that Cavβ4c interacts with the CSD of HP1 dimers through a C-terminal PxVxL consensus motif. They proposed that the conserved PVVLV sequence in the GK domains of all Cavβ contains the amino acids that are critical for binding to the

CSD. However, the PVVLV sequence is hidden in the GK domain of Cavβ, which explains the inability of the full-length protein to interact with the CSD. In contrast, in the shorter variant containing the truncated GK domain the PVVLV sequence can interact with HP1γ.

On the other hand, the interaction of Cavβ4b with B56δ (Ppp2r5d), a regulatory subunit of phosphatase 2A (PP2A), enables Cavβ4b to translocate to the nucleus and regulate gene activity (Tadmouri A *et al.*, 2012). This binding requires the interaction between the SH3 and GK domains of Cavβ4. Under electrical stimulation, Cavβ4b interacts with B56δ and translocates with PP2A to the nucleus, recruiting HP1γ in the process. The protein complex Cavβ4b/B56δ/PP2A was reported to bind to the promoter region of the tyrosine hydroxylase gene, thus repressing its expression in adult mouse brain (Tadmouri A *et al.*, 2012). Surprisingly, a transcriptome analysis of cerebellar neurons did not find tyrosine hydroxylase among the genes regulated by Cavβ4b (Etemad S *et al.*, 2014).

In mouse brain extracts, Cavβ4 interacts with the transcription factor TCF4, which prevents β-catenin from binding to TCF4 and thereby blocks the Wnt-responsive gene transcription (Rima M *et al.*, 2017), one of the main mechanisms controlling cell proliferation (Mulligan KA and Cheyette BN, 2012). This result is in line with a report showing that the proliferation of CHO cells, which do not endogenously express Cavβ4, was suppressed by the expression of this protein, an effect that required the presence of Cavβ4 in the nucleus (Rima M *et al.*, 2017).

Pax6(S)

The involvement of Cavβ in gene regulation was additionally suggested by a report showing that Cavβ3 binds to a splicing isoform of Pax6 (Zhang X *et al.*, 2010). Pax6 is a transcription factor that regulates the development of the eyes, nose, pancreas and nervous system. The splicing isoform Pax6(S) interacts with the Cavβ1b, Cavβ2a and Cavβ4 subunits, probably via a unique serine-rich tail in its C-terminus. This interaction does not modulate the properties of the channel, but enables Cavβ3 to translocate from the cytoplasm to the nucleus and block the transcriptional activity of Pax6(S).

1.3 Methods for the study protein-protein interactions

Identifying the interaction partners of a protein is essential to understand its biological functions. Protein-protein interactions are mediated primarily by non-covalent intermolecular forces, including electrostatic and hydrophobic interactions, hydrogen bonding and van der Waals forces (Leckband D, 2000; Crowley PB and Golovin A, 2005). Even though they are relatively weak individually, the effect of multiple interaction forces at the binding interface can be that of a strong association between proteins.

The yeast two-hybrid system has been used for the identification of protein-protein interaction networks. However, this technique has the drawback of artificially enclosing in the nucleus two foreign proteins that may have the appropriate cognate recognition sequences but unrelated cellular localizations and functions, leading to interactions that are not biologically relevant and represent false positives (Ratushny V and Golemis E, 2008). Therefore, an approach where proteins can interact in their native cellular environment, enabling unbiased detection, is highly desired.

Mass spectrometry (MS) has been combined with affinity purification (AP-MS) to interrogate protein-protein interactions (Dunham W *et al*., 2012; Meyer K and Selbach M, 2015). In this method the protein of interest is targeted with specific antibodies or antibodies against epitope tags (Gavin AC *et al.*, 2002; Ho Y *et al.*, 2002). However, antibodies targeting endogenous proteins are generally cross-reactive, requiring complex validation experiments such as quantitative immunoprecipitation combined with knockdown (Selbach M and Mann M, 2006).

The high affinity (Kd 10^{-14} M) of streptavidin for biotin has been exploited as an alternative to antibody-based affinity purification (Dundas CM *et al*., 2013). A method commonly referred to as BioID, based on the fusion of the protein of interest with a mutant form of the biotin ligase enzyme BirA, enables the biotinylation of all nearby proteins. This method has been used to identify interaction partners of the insoluble lamin A protein and the receptor tyrosine kinase EphA2 in their native cellular environment (Roux KJ *et al.*, 2012; Perez-White B *et al.*, 2017).

In parallel, a proximity-ligation method was developed based on engineered ascorbate peroxidase (APEX) labeling (Rhee HW *et al.*, 2013). APEX oxidizes biotin-phenol to biotin-phenoxyl radicals in the presence of H_2O_2. These radicals attack electron-rich amino acids such as tyrosine, tryptophan, histidine, cysteine and covalently attach biotin tags to targeted proteins (Amini F *et al.*, 2002; Bhaskar B *et al.*, 2003; Rogers M *et al.*, 2008; Minamihata K *et al.*, 2011) (Figure 4). Such phenoxyl free radicals are short-lived (≤ 1ms) (Mortensen A and Skibsted LH, 1997) and therefore have a small labeling radius (≤ 20 nm) (Mayer G and Bendayan M, 1997; Bendayan M, 2001). Thus, proteins in a radius under 20 nm can be covalently labeled with biotin-phenol, enriched using streptavidin-coated beads and identified by MS (Rhee HW *et al.*, 2013; Hung V *et al.*, 2014). The high affinity of the biotin-streptavidin complex allows biotinylated proteins to be efficiently separated after several stringent washes from proteins bound through unspecific interactions. This technique has the key advantage that the labeling is performed in living

cells with preserved membranes and protein-protein interactions, including transient interactions.

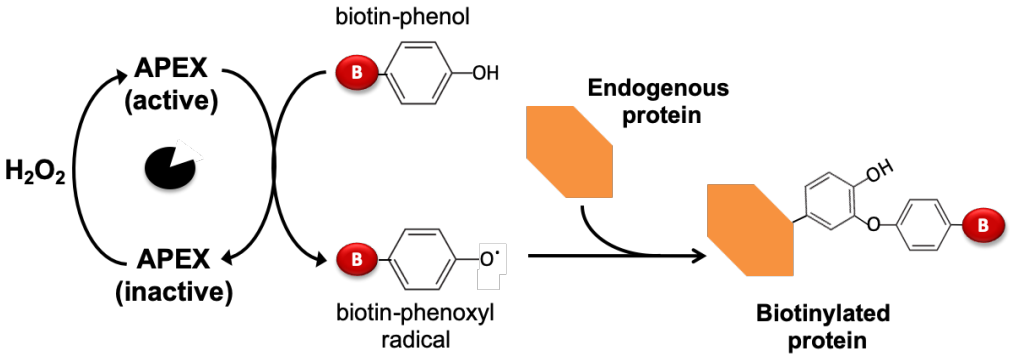

Figure 4. Schematic representation of the proximity labeling biotinylation of proteins. The ascorbate peroxidase (APEX) oxidizes biotin-phenol in the presence of H_2O_2 to biotin-phenoxyl radicals, which can covalently react with electron-rich amino acids such as tyrosine (reactive group shown in the figure), tryptophan, histidine and cysteine. Adapted from Chung C *et al.* (2017).

APEX is a triple mutant of soybean ascorbate peroxidase derived by structure-guided mutagenesis and screening (Martell JD *et al.*, 2012; Rhee H *et al.*, 2013). The introduction of an additional mutation (A134P) in APEX resulted in the improved version APEX2, with a higher activity that enables superior enrichment of proteins for proteomic studies. APEX2 is a monomeric protein with a molecular weight of 28 kDa, and is active under reducing conditions due to its lack of disulfide bonds (Lam S *et al.*, 2015). APEX2-based proximity labeling has the potential to provide higher spatial and temporal specificity based on its small labeling radius and short labeling time. This tool allows the development of proteomic maps of proteins located in challenging compartments such as the mitochondrial intermembrane space (Hung V *et al.*, 2014, 2016), ER-PM junctions (Jing J *et al.*, 2015), and primary cilia (Mick D *et al.*, 2015). In recent years, APEX2-based proximity labeling has been used to map the interactome of proteins like alpha-synuclein in living neurons (Chung C *et al.*, 2017), the vesicle-associated membrane protein-associated protein B (VAPB) (James C *et al.*, 2019) and emerin (Muller M *et al.*, 2020) at the inner nuclear membrane of HeLa P4 cells, and Cav1.2 in adult mouse cardiomyocytes (Liu G *et al.*, 2020).

The enzyme-based proximity labeling of proteins differs conceptually from traditional approaches like immunoprecipitation or cross-linking in that labeled proteins do not necessarily interact with the protein fused to the enzyme, but may localize at a limited distance in the nearby space. The direct *in vivo* labeling of neighboring proteins cannot differentiate between direct interactors and other nearby proteins. Importantly, however, labeling will be stronger for proteins remaining in close proximity to the one tagged with

the enzyme than for proteins passing by only randomly and fleetingly. Therefore, the identification of true neighbors should be based on the combination of enzyme-catalyzed proximity labeling experiments with proteomic quantitation.

1.3.1 Quantitative interaction proteomics

A single-step low-stringency affinity purification combined with quantitative proteomics is currently used to detect weak and transient interactions (Vermeulen M *et al.*, 2008; Smits AH and Vermeulen M, 2016). The unspecific binders that remain unchanged between a specific and a negative control (lacking the tagged bait protein) sample in a pull-down assay can be identified by comparing the differences in quantitative amounts of proteins (Figure 5).

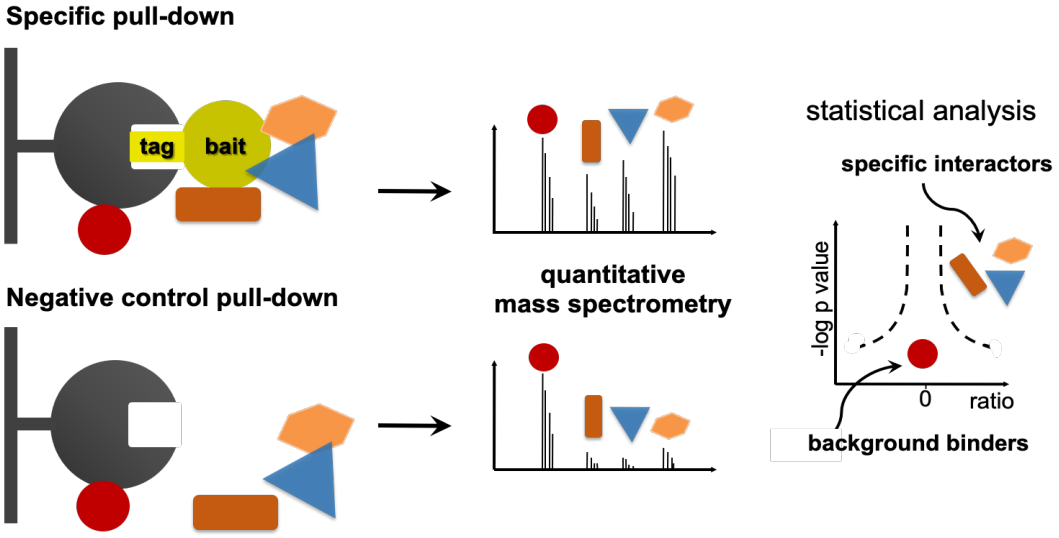

Figure 5. Quantitative interaction proteomics. A specific pull-down sample is compared with a negative control pull-down sample lacking the tagged bait protein. The differences in protein intensities between the samples are plotted in a volcano plot against the negative logarithmized p values. The unspecific binders appear close to the center, around zero, while the enriched interacting partners are located on the right side of the plot. Adapted from Hein MY *et al.* (2013).

Label-based or label-free approaches enable the quantification of pull-down experiments. In the former, the bait and the control samples are differentially labeled using heavy isotopes like 13C, 15N and 18O, or natural light isotopes such as 12C, 14N and 16O. The use of stable isotopes only changes the mass of the peptides resulting from the trypsin digestion of the proteins, while all their other physicochemical properties remain unaffected. Therefore, the heavy-labeled peptides behave like the light-labeled peptides but can be distinguished during the MS measurement. After the labeling step, the samples can then be mixed and analyzed in a single liquid chromatography-tandem mass spectrometry (LC-MS/MS) run.

Label-free quantification (LFQ) is an entirely computational method with no limitations concerning sample number. Intensity-based LFQ procedures are based on the linear correlation existing over a wide concentration range between peptide concentration and the peak intensities of individual peptide signals (Bondarenko PV *et al*., 2002). The peptide intensities are used to determine protein intensities by considering all available pairwise peptide ratios between the samples. The intensity-based LFQ analysis can be performed with the MaxQuant software (Cox J and Mann M, 2008; Cox J *et al.*, 2014) and provides an accurate approximation of the protein amounts in each sample.

1.4 Excitation-contraction coupling

Calcium ions are involved in multiple cellular processes like gene transcription, cellular proliferation and muscle contraction. For the heart to function as a pump, the intracellular Ca^{2+} concentration must increase during systole to activate contraction and then fall, during diastole, to levels that are sufficiently low to allow the myofilaments to relax and the heart to refill with blood. During cardiomyocyte contraction, the free cytosolic Ca^{2+} concentration increases from a resting level of ~100 nM to ~1 µM (Marks AR, 2013). Extracellular calcium is incorporated into cardiac muscle cells via LTCC. In ventricular myocytes, the systolic action potentials induce a depolarization that opens the LTCC located on the sarcolemma and T-tubules. The calcium ions that enter in the dyadic space (the region bounded by the T-tubule and the SR) cause the opening of the RyR and the release of a large amount of Ca^{2+} from the SR. This mechanism, known as Ca^{2+}-induced Ca^{2+} release (CICR), results in the activation of the actin-myosin contractile machinery and is important for the EC coupling (Bers D, 2002; Eisner D *et al.*, 2017) (Figure 6A).

In cardiac muscle, LTCC are irregularly and sparsely distributed in a couplon, the structural domain where EC coupling takes place (Stern MD *et al*, 1997). A couplon in cardiac myocytes can have around 100 RyR, with one Cav1.2 per 4 to 10 RyR tetramers (Bers DM, 2014). However, recent studies using electron microscopy and super-resolution imaging have indicated that RyR are often arranged in smaller clusters in dyads (Baddeley D *et al.*, 2009; Hayashi T *et al.*, 2009; Jayasinghe I *et al.*, 2018; Kolstad TR *et al.*, 2018). The isoforms of LTCC (Cav1.2) and RyR (RyR2) in cardiac myocytes project into the 12-20-nm space separating the plasma membrane and the SR at the junction (Shaw RM and Colecraft HM, 2013), but they are not known to mechanically interact (Franzini-Armstrong C and Protasi F, 1998). Since EC coupling requires Ca^{2+} influx via LTCC, the removal of extracellular Ca^{2+} or the inhibition of Ca^{2+} currents immediately (< 1 second) prevent cardiac Ca^{2+} transients from occurring (Bers DM, 2017).

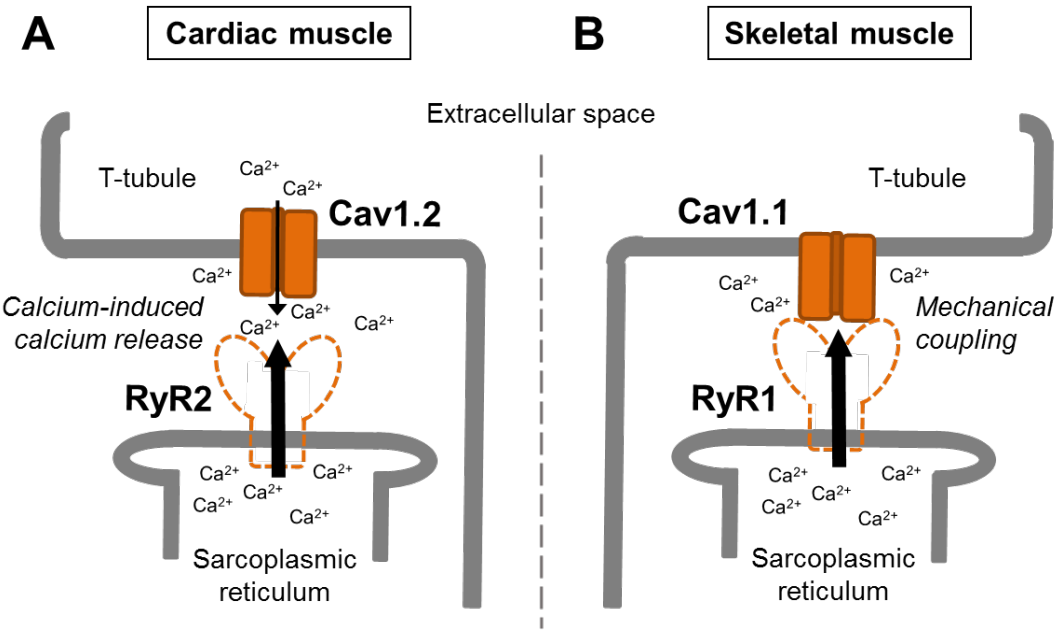

Figure 6. Excitation-contraction coupling in cardiac and skeletal muscles. In cardiomyocytes (A), the action potential propagates into the T-tubules, opening L-type voltage-gated Ca^{2+} channels (Cav1.2). The resulting Ca^{2+} influx triggers the opening of the ryanodine receptor 2 (RyR2) on the membrane of the sarcoplasmic reticulum and the release of Ca^{2+}, a mechanism known as Ca^{2+}-induced Ca^{2+} release. In the skeletal muscle (B), membrane depolarization induces conformational changes in Cav1.1, which activates the RyR1 by interacting with it. This mechanism is called mechanical coupling.

In skeletal muscle, couplons have a relatively rigid structure, with four LTCC directly above and communicating with four identical protomers of an underlying RyR in the junctional SR, the specialized region of the SR that is proximal to the T-tubules (Yin CC *et al*., 2005). The skeletal muscle isoforms of LTCC (Cav1.1) and RyR (RyR1) are physically in contact and a depolarization of the T-tubule membrane induces a conformational change of Cav1.1 that is sufficient to activate the RyR1 (Figure 6B). This occurs even in the absence of Ca^{2+} influx through the channel (Paolini C *et al.*, 2004; Allard B, 2018). The activation of RyR1 that are not connected to LTCC is the subject of controversy. Some authors suggest that this activation can be mediated by Ca^{2+} released from adjacent LTCC-connected RyR1 through a Ca^{2+}-induced Ca^{2+} release mechanism (Ríos E and Pizarro G, 1988), while others propose that unconnected RyR1 work as a structural and functional reserve to control muscle contraction (Ríos E *et al*, 2019).

Calcium removal from the cytoplasm is necessary for muscle relaxation and this function is parallelly performed by the sarcoplasmic/endoplasmic reticulum Ca^{2+}-ATPase (SERCA) and the Na^{+}/Ca^{2+} exchanger (Bers DM, 2017). Among different SERCA isoforms, the 110-kDa monomeric SERCA2a is predominantly expressed in the adult myocardium, accounting for approximately 40% of the total proteins of the SR (Marín-García J, 2014).

In rat and mouse ventricular myocytes, SERCA2a is the main contributor to calcium removal and transports two Ca^{2+} ions into the SR in exchange for one H^+ at the cost of one ATP molecule. Even though SERCA has a relatively low enzymatic activity, the high density of these pumps in the SR membrane ensures a rapid reduction of cytosolic calcium (Greig CA and Jones DA, 2016). In rat ventricles under normal conditions, SERCA2a takes up approximately 90% of the Ca^{2+} released by the SR, whereas nearly 10% is expelled from the cytoplasm via the Na^+/Ca^{2+} exchanger (Bers DM, 2002).

1.5 Aim of the project

LTCC are heteromultimeric proteins composed of a Cavα1 pore-forming subunit and the Cavβ, Cavα2δ and Cavγ accessory subunits. Cavβ binds with high affinity at an equimolar stoichiometry to the AID in the I-II loop of Cavα1 (Pragnell M *et al.*, 1994; De Waard M *et al.*, 1995). For many years, Cavβ was only considered as a regulator of LTCC trafficking and activity. Given its cytosolic character and high affinity for the LTCC, Cavβ could play an important role as a molecular scaffold by recruiting proteins from its nanoenvironments and organizing them in complexes around the LTCC in cardiomyocytes. Interestingly, several recent studies highlight new functions of Cavβ that are independent of its role in the regulation of LTCC and directly linked to diverse cellular processes like synaptic vesicle docking and fusion, endocytosis and gene expression (Rima M *et al.*, 2016). Of the four Cavβ isoforms, Cavβ2 is predominantly expressed in cardiomyocytes and is known to associate with diverse proteins besides LTCC, such as ahnak, dynamin and actin. However, the molecular composition of the nanoenvironments of Cavβ2 in cardiomyocytes, and specifically of Cavβ2b, its most abundant splice variant in these cells, is still unknown.

Therefore, this project had two main goals:

1) the identification of components of the nanoenvironments of Cavβ2b within its native environment in adult rat cardiomyocytes (ARC) by combining a proximity labeling biotinylation method based on APEX2 and quantitative proteomics.

2) the validation of the interaction between Cavβ2b and a potential binding partner identified with high accuracy by mass spectrometry. To reach this objective, we performed biochemical and functional experiments with cultured ARC and murine hearts by combining pull-down, coimmunoprecipitation, fluorescence microscopy and calcium current and transient measurements.

2. MATERIALS

2.1 Reagents

Acetonitrile	Merck, Darmstadt, GER
2,3-Butanedione monoxime	Sigma-Aldrich, Steinheim, GER
Ammonium bicarbonate	Sigma-Aldrich, Steinheim, GER
Avicel® PH-101	Sigma-Aldrich, Steinheim, GER
BCA (bicinchoninic acid) Assay Reagent A	Interchim, Montluçon Cedex, FRA
Biotin-phenol	Sigma-Aldrich, Steinheim, GER
Bradford reagent	Sigma-Aldrich, Steinheim, GER
Caffeine	Sigma-Aldrich, Steinheim, GER
Calcium chloride dihydrate ($CaCl_2$ x $2H_2O$)	Sigma-Aldrich, Steinheim, GER
Calpeptin	Sigma-Aldrich, Steinheim, GER
Coomassie Brilliant Blue G250	Sigma-Aldrich, Steinheim, GER
Crystal violet	Sigma-Aldrich, Steinheim, GER
D-(+)-Glucose	Sigma-Aldrich, Steinheim, GER
Dithiothreitol	AppliChem, Darmstadt, GER
Dulbecco's Modified Eagle Medium (DMEM)	Biochrom, Berlin, GER
Ethylenediaminetetraacetic acid (EDTA)	Sigma-Aldrich, Steinheim, GER
Fetal bovine serum (heat inactivated)	Gibco, Grand Island, USA
Fluo-4AM (Cat No. F14201)	Thermo Fisher Scientific, Rockford, USA
Gluthathione	Sigma-Aldrich, Steinheim, GER
Glycerol	Merck, Darmstadt, GER
Halt™ Protease Inhibitor Cocktail	Thermo Fisher Scientific, Rockford, USA
HEPES sodium salt	Sigma-Aldrich, Steinheim, GER
Imidazole	Sigma-Aldrich, Steinheim, GER
ImmunoSelect®Antifading Mounting Medium DAPI	Dianova, Hamburg, GER
Insulin	Sigma-Aldrich, Steinheim, GER
Iodoacetamide	Merck, Darmstadt, GER
Isoflurane	CP-Pharma, Burgdorf, GER
Isoprenaline hydrochloride	Sigma-Aldrich, Steinheim, GER
isopropyl-β-D-thiogalactopyranosid (IPTG)	Sigma-Aldrich, Steinheim,GER
L-Glutamine Solution 200 mM	Sigma-Aldrich, Munich, GER
Laminin	Roche, Mannheim, GER
Luria-Bertani (LB)-Medium-Powder	AppliChem, Darmstadt, GER
M199 medium	Gibco, Grand Island, USA
Magnesium sulfate heptahydrate ($MgSO_4$ x 7 H_2O)	Sigma-Aldrich, Steinheim, GER
Na^+-selenite	Sigma-Aldrich, Steinheim, GER

Normal goat serum	Sigma-Aldrich, Steinheim, GER
NP-40	Merck, Darmstadt, GER
Paraformaldehyde solution 4% in PBS (phosphate-buffered saline)	Santa Cruz Biotechnology, Dallas, USA
Penicillin-Streptomycin	Sigma-Aldrich, Steinheim, GER
Pierce® ECL Western Blotting Substrate	Thermo Fisher Scientific, Rockford, USA
Potassium bicarbonate ($KHCO_3$)	Merck, Darmstadt, GER
Potassium chloride (KCl)	Sigma-Aldrich, Steinheim, GER
Potassium dihydrogen phosphate (KH_2PO_4)	Merck, Darmstadt, GER
Protease Inhibitor Cocktail tablets (cOmplete Mini)	Roche, Mannheim, GER
Sodium ascorbate	Sigma-Aldrich, Steinheim, GER
Sodium azide	Sigma-Aldrich, Steinheim, GER
Sodium bicarbonate ($NaHCO_3$)	Merck, Darmstadt, Germany
Sodium chloride (NaCl)	Merck, Darmstadt, Germany
Sodium dodecyl sulfate (SDS)	Sigma-Aldrich, Steinheim, GER
Sodium phosphate dibasic (Na_2HPO_4)	Sigma-Aldrich, Steinheim, GER
Taurine	AppliChem, Darmstadt, GER
Transferrin	Sigma-Aldrich, Steinheim,GER
Trifluoroacetic acid	Merck, Darmstadt, GER
Triton X-100	Sigma-Aldrich, Steinheim, GER
Trizma® base	Sigma-Aldrich, Steinheim, GER
Trolox	Sigma-Aldrich, Steinheim, GER
Tween® 20	Sigma-Aldrich, Steinheim,GER
β-mercaptoethylamine	Sigma-Aldrich, Steinheim, GER

2.2 Equipment

Confocal Microscope TCS SP5	Leica Microsystems, Wetzlar, GER
Eclipse Ti microscope	NIKON, New York, USA
EPC-10 amplifier	HEKA Elektronik, Pfalz, GER
FluorChem SP Gel Imaging System	Alpha Innotech, San Leandro, USA
Linear Trap Quadruple Orbitrap Elite mass spectrometer	Thermo Fisher Scientific, Rockford, USA
Mikro Dismembrator U	Sartorius, Göttingen, GER
Mini-Trans-Blot-Cell	Bio-Rad, Hercules, USA
Myocyte Calcium and Contractility System	IonOptix, Westwood, USA
Photomultiplier (PMT400)	IonOptix, Westwood, USA
SimpliNano spectrophotometer	GE Healthcare, Freiburg, GER
Sonopuls Ultrasonic Homogenizer HD 2070	Bandelin, Berlin, GER

UltiMate™ 3000 RSLCnano system	Thermo Fisher Scientific, Rockford, USA
UXL-75XE xenon short ARC lamp	Ushio America, Cypress, USA
Vacuum concentrator (RVC2-25CD plus)	Martin Christ Gefriertrocknungs-anlagen, Osterode am Harz, GER

2.3 Kits

Quick Blunting™ Kit	NewEngland Biolabs, Frankfurt, GER
pAd/BLOCK-iT™-DEST Gateway Vector	Thermo Fisher Scientific, Rockford, USA
pAd/CMV/V5-DEST™ Gateway® Vector	Thermo Fisher Scientific, Rockford, USA
pAd/PL-DEST™Gateway® Vector	Thermo Fisher Scientific, Rockford, USA
Subcellular Protein Fractionation Kit for Cultured Cells	Thermo Fisher Scientific, Rockford, USA
X-tremeGENE™ HP DNA Transfection Reagent	Roche, Mannheim, GER

2.4 Enzymes

All enzymes for cloning or restriction control experiments were purchased from NewEngland Biolabs, Frankfurt, Germany. The enzymes bought from other companies are listed below:

Liberase, Cat No. 05401151001	Roche, Mannheim, GER
Trypsin, Cat No. 37286	Serva, Heidelberg, GER
Trypsin, Cat No. T4799-10g	Sigma-Aldrich, Steinheim, GER

2.5 Vectors

pTRC-APEX2	Addgene, Watertown, USA
pAd/BLOCK-iT™-DEST	Thermo Fisher Scientific, Rockford, USA
pENTR 3C	Thermo Fisher Scientific, Rockford, USA
pENTR/U6	Thermo Fisher Scientific, Rockford, USA
pGEX-6P-1	Sigma-Aldrich, Steinheim, GER
pRSET B	Thermo Fisher Scientific, Rockford, USA

2.6 Antibodies and conjugates

	Host species	Dilution WB	Dilution ICC	Manufacturer	Cat. No
Primary antibodies					
Anti-Cavβ2	rabbit	1:1000	1:400	Novus Biologicals	NBP1-86680
Anti-Cavβ2b	rabbit	1:250	1:250	Homemade	
Anti-Ryanodine receptor 2 (C3-33)	mouse	1:1000	1:400	Thermo Fisher Scientific	MA3-916
Anti-Junctophilin 2	mouse	1:1000	-	Santa Cruz Biotechnology	sc-377086
Anti-α-actinin 2	mouse	1:1000	1:400	Santa Cruz Biotechnology	sc-17829
Anti-VDAC1	mouse	1:1000	-	Santa Cruz Biotechnology	sc-390996
Anti-SERCA2a	mouse	1:1000	-	Thermo Fisher Scientific	MA3-919
Anti-Cav1.2	rabbit	1:500	-	Alomone Labs	ACC-003
Anti-V5 epitope tag	rabbit	1:1000	-	Cell Signaling	R960-25
Anti-Na^+/K^+ ATPase	rabbit	1:5000	-	Abcam	ab76020
Anti-GAPDH	rabbit	1:5000	-	Cell Signaling	2118
Anti-Histone H3	rabbit	1:2000	-	Abcam	ab1791
Secondary antibodies					
Anti-mouse IgG	goat	1:10000	-	Jackson ImmunoResearch laboratories	115-035-003
Anti-rabbit IgG	goat	1:10000	-	Jackson ImmunoResearch laboratories	111-035-144
Anti-rabbit IgG conjugated-Alexa Fluor 488	goat	-	1:300	Thermo Fisher Scientific	A-11008
Anti-mouse IgG conjugated-Alexa Fluor 633	goat	-	1:300	Thermo Fisher Scientific	A-21052
Biotinylation detection conjugate					
Streptavidin-HRP	-	1:2000	-	Thermo Fisher Scientific	N100

WB: western blot; ICC: immunocytochemistry; GAPDH: glyceraldehyde-3-phosphate dehydrogenase; HRP: horseradish peroxidase; SERCA2a: sarcoplasmic/endoplasmic reticulum Ca^{2+}-ATPase 2a; VDAC1: voltage-dependent anion-selective channel protein 1.

2.7 Other materials

HiLoad 16/60 Superdex 200 pg gel filtration column	GE Healthcare, Freiburg, GER
Amersham Protran 0.2 µm NC nitrocellulose	GE Healthcare, Freiburg, GER
Amicon® Ultra centrifugal filter	Merck KGaA, Darmstadt, GER
BL21 (DE3) Competent *E. coli*	New England Biolabs, Frankfurt, GER
Cell Culture Multiwell Plate, 6 well	Greiner Bio-One, Frickenhausen, GER
Cover Glass (25 x 25 mm)	Corning, Kaiserslautern, GER
Dynabeads Protein G	Thermo Fisher Scientific, Rockford, USA
GST HiTrap™ column	GE Healthcare, Freiburg, GER
HisTrap histidine-tagged protein purification column	GE Healthcare, Freiburg, GER
MagStrep type3 XT beads	IBA Lifesciences, Göttingen, GER
MBPtrap™ column	GE Healthcare, Freiburg, GER
NEB 5-alpha Competent *E. coli*	New England Biolabs, Frankfurt, GER
Streptavidin Magnetic Beads	Thermo Fisher Scientific, Rockford, USA
Zeba™ Spin Desalting Columns 7K MWCO	Thermo Fisher Scientific, Rockford, USA

3. METHODS

3.1 RT-PCR

The expression of the RNA encoding the different Cavβ2 splice variants in ARC was detected by RT-PCR. After isolation of total RNA from the cells using a TRIzol™-based method, RT-PCR was performed with the following forward primers:

5′-ATGCAGTGCTGCGGGCTGG-3′ for Cavβ2a

5′-ATGCTTGACAGGCAGTTGGTGTCTTC-3′ for Cavβ2b

5′-ATGGACCAGGCGAGTGGACTGG-3′ for Cavβ2c

5′-TGATGACATCTGTATCTGGCAAACCAG-3′ for Cavβ2d

5′-ATGAAGGCCACCTGGATCAGGC-3′ for Cavβ2e

The common antisense primer was 5′-CCACCAACACCACTGGTCTCATGG-3′.

3.2 Antibody preparation and validation

To prepare an antibody specifically recognizing Cavβ2b, the cDNA encoding the variable N-terminus (NT) from rat Cavβ2b (amino acids 1-17; accession number Q8VGC3-5) was amplified by PCR from the pcDNA3.1-Cavβ2b vector and cloned into the PGEX-6P-1 vector to fuse a glutathione S-transferase (GST) moiety at the N-terminus of Cavβ2b-NT. Competent *E. coli* BL21 (DE3) cells were transformed with the PGEX-6P-1-GST-Cavβ2b-NT plasmid and the GST-Cavβ2b-NT recombinant protein was expressed by a 3-h induction with 0.5 mM IPTG. After that, cells were harvested by centrifugation, resuspended in phosphate-buffered saline (PBS) pH 7.4 and lysed by sonication. The GST-Cavβ2b-NT recombinant protein was purified from the lysate by affinity chromatography using a GST HiTrap™ column followed by size exclusion chromatography. The purified protein was concentrated by ultrafiltration using an Amicon® Ultra centrifugal filter and its concentration was measured spectrophotometrically at 280 nm. The recombinant protein GST-Cavβ2b-NT was used as antigen for the production of the anti-Cavβ2b antibody by the company ImmunoGlobe GmbH (Himmelstadt, GER) using their own protocols. The serum collected from rabbits 8 weeks after immunization was purified by affinity chromatography using maltose-coated beads previously incubated with the maltose binding protein (MBP)-Cavβ2b-NT fusion protein. This protein was prepared after cloning the Cavβ2b-NT fragment into the pMAL5 vector and following the same protein purification steps described for the GST-Cavβ2b-NT recombinant protein, but using an MBPtrap™ column to perform the affinity chromatography step.

To validate the specificity of the anti-Cavβ2b antibody, HEK-293 cells were grown in DMEM supplemented with 10% [v/v] fetal bovine serum and L-glutamine (2 mM) and incubated in a 5% [v/v] CO_2 humidified atmosphere. Cells were transfected with the corresponding plasmids encoding either of the five different Cavβ2 splice variants. The X-tremeGENE™ HP DNA Transfection Reagent was used for transfection following the manufacturer's instructions. Twenty-four hours after transfection the cells were lysed on ice using cell lysis buffer containing 20 mM Tris pH 7.5, 150 mM NaCl, 1% [v/v] NP-40, 1x Halt protease inhibitor cocktail and 1 mM EDTA. The cell lysate was then centrifuged at 16000 g for 15 min at 4 ºC. The supernatants were collected and stored at -80 ºC until used in western blot analyses.

3.3 Production of recombinant adenovirus

For protein overexpression using an adenovirus expression system, the cDNA fragment containing the APEX A134P (APEX2) open reading frame was obtained by PCR amplification from the vector pTRC-APEX2 and cloned into the pENTR 3C vector to produce the pENTR 3C-APEX2 plasmid. To generate the pENTR 3C-Cavβ2b-V5-APEX2 construct, the cDNA encoding the full rat Cavβ2b (accession number Q8VGC3-5) was amplified by PCR from the pcDNA3.1-Cavβ2b vector and inserted in frame upstream of the APEX2 sequence into the pENTR 3C-APEX2 plasmid using standard overlapping PCR methods (Figure S1, supplementary information). For the pENTR 3C-SH3-V5 construct, the cDNA encoding the SH3 domain of the rat Cavβ2b (residues 25-137) was also amplified by PCR from the pcDNA3.1-Cavβ2b vector and cloned into the pENTR 3C vector using conventional molecular biology methods (Figure S2, supplementary information). The pENTR 3C-SH3-V5 construct contains the sequence for the V5 tag at its 3' end, while in the pENTR 3C-Cavβ2b-V5-APEX2 construct the sequence for the V5 tag was inserted between Cavβ2b and APEX2. The proteins encoded by the pENTR 3C-Cavβ2b-V5-APEX2 and pENTR 3C-SH3-V5 constructs are referred to in this work as Cavβ2b-V5-APEX2 and Cavβ2b-SH3 domain, respectively.

The adenoviral vectors for the overexpression of proteins Cavβ2b-V5-APEX2 and Cavβ2b-SH3 domain were generated by homologous DNA recombination between each pENTR3C plasmid and the pAD/CMV/V5-DEST vector using the pAd/CMV/V5-DEST™ Gateway® Vectors kit according to the manufacturer´s instructions. To generate a control viral vector that does not encode the Cavβ2b-SH3 domain, the incompatible overhangs of the empty linear pENTR/U6 vector were converted to blunt-ended DNA using the Quick Blunting™ Kit. The vector was then circularized by blunt-end ligation with standard

molecular biology methods and used to produce the control virus by homologous DNA recombination with the pAd/BLOCK-iT™-DEST plasmid. This virus was used for the transduction of cells used as negative control in the electrophysiological experiments and Ca^{2+} transient measurements. The recombinant adenoviral plasmids were linearized with the PacI restriction enzyme and purified by phenol/chloroform extraction followed by ethanol precipitation, as described by Steward GF and Culley AI (2010). HEK-293A cells cultured on 6-well plates were transfected with 1 µg of plasmids linearized with PacI using the X-tremeGENE™ HP DNA Transfection Reagent, following the manufacturer's instructions. The cells were harvested 14 days after transfection, when 70-80% cytopathic effect was observed, and subjected to three freeze-thaw cycles by freezing at -80 °C and thawing at 37 °C in a water bath to release the virus from the cells. The supernatants were collected by centrifugation at 1700 g for 10 min and the aliquots were stored at -80 °C. Virus titers were determined by plaque assay, as described in section 3.4.

3.4 Titration of viruses

HEK-293A cells were seeded at a density of 5 x 10^5 cells/well onto 6-well plates and grown for 24 h prior to infection until reaching 90-100% confluence. Ten-fold serial dilutions of the adenoviral stocks were prepared in serum-free DMEM over a range of 10^{-4} to 10^{-9}. The culture medium was removed and 100 µL of each virus dilution were added to the cells. Plates were then incubated for 2 h at 37 °C/5% [v/v] CO_2, and shaken every 20 min to ensure totally covering the cell monolayers. Thereafter, the virus inocula were removed and 3 mL of immobilizing medium were gently added to each well. The immobilizing medium consisted of a 1:1 [v/v] mixture of 2x plaque medium (DMEM supplemented with 5% [v/v] fetal bovine serum, 2 mM glutamine, 100 U/mL penicillin, 100 µg/mL streptomycin) and 2.4% [w/v] Avicel overlay medium. Plates were incubated for 7 days at 37 °C/5% [v/v] CO_2 until distinct plaques (areas of cell lysis) developed. The overlay was then removed and the cells were fixed for 30 min at room temperature (RT: 20-25 °C) with 4% [v/v] formaldehyde in PBS. After withdrawing the fixative, the cells were washed with water and plaques were visualized by staining with 1% [w/v] crystal violet (1 g of crystal violet powder in 20 mL of ethanol and 80 mL of distilled H_2O) for 15 min, followed by rinsing with water. Plaques were counted and viral titers determined as plaque-forming-units per mL of virus (pfu/mL) using the formula: pfu/mL = average number of plaques/(dilution x volume of diluted virus added to the plate).

3.5 Isolation and adenoviral transduction of adult rat cardiomyocytes

The following solutions were used for the isolation and culture of ARC:

- **Buffer A**: 113 mM NaCl, 12 mM $NaHCO_3$, 10 mM HEPES, 0.6 mM KH_2PO_4, 1.22 mM Mg_2SO_4 x $7H_2O$, 10 mM $KHCO_3$, 0.6 mM Na_2HPO_4, 4.69 mM KCl, 0.03 mM phenol red, 5.5 mM glucose, 30 mM taurine, 10 mM 2,3-butanedione monoxime, pH 7.46 adjusted with NaOH.
- **Enzyme buffer:** 20 mL of buffer A supplemented with 1.44 mg liberase, 5.6 µg trypsin (0.14 µg/µL, Sigma-Aldrich), 12.5 µM $CaCl_2$.
- **Stop buffer 1:** 9 mL of buffer A, 1 mL of fetal bovine serum, 12.5 µM $CaCl_2$.
- **Stop buffer 2:** 28.5 mL of buffer A, 1.5 mL of fetal bovine serum, 12.5 µM $CaCl_2$.
- **Modified M199 medium:** medium 199 supplemented with 870 nM insulin, 65 nM transferrin, 29 nM Na^+-Selenite, antibiotics (100 U/mL penicillin, 100 µg/mL streptomycin).

The animal experiments were approved by the authority of Unterfranken and the standing authority of the University of Würzburg (under reference number 55.2-2532-468). Wistar rats (250-300 g, Charles River Laboratories, Sulzfeld, GER) were anaesthetized by inhalation of 2% isoflurane - 98% oxygen in a chamber and then killed by cervical dislocation. Hearts were surgically excised, immediately washed with buffer A and suspended in a Langendorff perfusion apparatus via cannulation of the aorta. Then, the hearts were flushed blood-free with buffer A for 4 min and subsequently perfused with recirculating enzyme buffer during 7 min at a rate of 1 drop per second. After perfusion, the aorta and atria from each heart were removed and the ventricles cut into 4 pieces. The ventricular tissue was transferred to a dish with 5 mL of buffer A and 5 mL of stop buffer 1. Cells were further dissociated by gently shaking the tissue several times in the solution until reaching a single-cell suspension. The suspension was allowed to settle for 10 min at RT and the resulting pellet was resuspended in stop buffer 2 and subjected to several Ca^{2+} toleration steps of 4 min each, increasing the Ca^{2+} concentration in buffer A stepwise (0.05 mM, 0.1 mM, 0.2 mM, 0.5 mM, 1 mM). After the last step, the cells were again allowed to settle for 10 min at RT and resuspended in modified M199 medium with additional 5% [v/v] fetal bovine serum, resulting in a suspension with 75-90% rod-shaped living cells. Cells were plated in 6-well plates or onto glass coverslips, previously coated with 15 µg/mL of laminin for 1 h. After 3 h of incubation, the medium was replaced with serum-free modified M199 medium to perform viral transduction. These procedures were

conducted with the support of Michelle Gulentz and Dr. Michael Kohlhaas, from the Comprehensive Heart Failure Center, University Hospital Würzburg.

For viral transduction, ARC were seeded in 6-well plates and infected with adenovirus at a multiplicity of infection of 75 during 4 h at 37 °C. Following infection, the adenovirus-containing medium was replaced with modified M199 medium and the cells incubated at 37 °C for 24 h.

3.6 Mouse heart lysates preparation

Frozen hearts were powdered using a Mikro-Dismembrator U at 2000 rpm for 1 min. Proteins were extracted with lysis buffer (20 mM Tris pH 7.5, 150 mM NaCl, 1% [v/v] NP-40, 1x Halt protease inhibitor cocktail, 1 mM EDTA, 25 mM calpeptin) by vortexing every 5 min during 15 min on ice. Insoluble components were removed by centrifugation at 16000 g for 15 min at 4 °C. The supernatant was used for strep-tag pull-down and coimmunoprecipitation experiments.

3.7 Protein expression and purification

For protein purification, we amplified by PCR the cDNA of the rat Cavβ2b (accession number Q8VGC3-5) and its NT (amino acids 1-24), SH3 (amino acids 25-137), HOOK (amino acids 138-225) and CT (amino acids 424-605) domains using the pcDNA3.1-Cavβ2b vector. Each specific forward primer contained as overhang the cDNA sequence encoding the Twin-Strep-tag peptide (WSHPQFEKGGGSGGGSGGSAWSHPQFEK). Then, the PCR fragments were cloned in frame into the pGEX-6P-1 vector to fuse a GST moiety at the N-terminus of the resulting proteins (Figure S3, supplementary information). In parallel, the construct pRSET B-His-Twin-strep-Cavβ2b was generated by cloning in frame into the pRSET B vector the PCR fragment corresponding to the full-length Cavβ2b. This construct carries at its 5' end the sequence coding for a polyhistidine tag, followed by the Twin-strep-tag (Figure S4, supplementary information).

The sequences encoding Cavβ2b and its different domains (NT, SH3, HOOK, CT) fused to Twin-strep-tag were cloned into the pGEX-6P-1 vector and the fusion proteins expressed in competent *E. coli* BL21 (DE3) cells to allow for the inducible expression of the transformed vector after IPTG addition. For large scale expression, transformed cells were grown at 37 °C in 10 mL of Luria-Bertani (LB) medium with ampicillin (100 µg/mL) at a shaking speed of 250 rpm, and used to inoculate up to 200 mL of LB medium with ampicillin (100 µg/mL). When the bacterial culture had grown to an optical density of 0.6-0.7 at 600 nm, protein expression was induced during 3 h with 1 mM of IPTG. Following

IPTG treatment, the cells were harvested and resuspended in 10 mL of lysis buffer (20 mM Tris, 300 mM NaCl, pH 8 supplemented with one Complete Mini Protease Inhibitor cocktail tablet). Cells were lysed during 2 min by sonication at 40% amplitude using a Sonopuls Ultrasonic Homogenizer HD 2070, with 30-second pulses given every 30 seconds. The supernatant was recovered after centrifugation of the cell lysate at 20000 g for 20 min at 4 °C and passed through a 0.2-µm filter. The filtrate was then transferred onto a 1-mL GST-tagged protein purification column (GST HiTrap) previously loaded with equilibration buffer (20 mM Tris, 300 mM NaCl, pH 8). The column was washed with five column volumes (5 mL) of equilibration buffer and the protein was eluted in two column volumes (2 mL) of equilibration buffer containing 15 mM gluthathione, 10 mM dithiothreitol. The eluate was loaded onto a HiLoad 16/60 Superdex 200 pg gel filtration column and run at 1 mL/min in a solution containing 20 mM Tris, 300 mM NaCl, 1 mM EDTA, pH 8 for one column volume (120 mL). Peak elution fractions were pooled and concentrated to 300 µL by ultrafiltration with a 10-kDa cutoff membrane using an Amicon® Ultra centrifugal filter. Protein concentration was measured with a SimpliNano spectrophotometer at an absorbance of 280 nm. The proteins were separated by sodium dodecyl sulfate-polyacrylamide gel electrophoresis (SDS-PAGE) using the standard Laemmli method as described by Gallagher S (2006) and visualized by Coomassie Blue staining.

The purification of the His-Twin-strep-Cavβ2b protein was performed as described above for the GST-recombinant proteins, but with some modifications in the affinity purification. Specifically, transformed *E. coli* BL21 (DE3) cells expressing the His-Twin-strep-Cavβ2b protein were resuspended using 20 mM imidazole in PBS, pH 7.4 adjusted with HCl. Then, they were sonicated, centrifuged, and the lysate was loaded onto a 1-mL HisTrap histidine-tagged protein purification column. The elution buffer contained 500 mM imidazole, PBS pH 7.4 adjusted with HCl.

3.8 Proximity labeling biotinylation

Proximity labeling biotinylation was performed as described by Hung V *et al.* (2016). ARC were infected with the Cavβ2b-V5-APEX2 adenovirus. After 24 h, the cells were incubated with 0.5 mM biotin-phenol in modified M199 medium for 30 min at 37 °C under 5% [v/v] CO_2. Then, H_2O_2 was added to each well for a final concentration of 1 mM and the plate was gently agitated during 1 min. To stop the reaction, the labeling solution was suctioned and the cells were washed three times with a quenching solution (5 mM Trolox, 10 mM sodium azide and 10 mM sodium ascorbate in PBS). The cells were lysed on ice using

lysis buffer (20 mM Tris pH 7.5, 150 mM NaCl, 1% [v/v] NP-40, 1x Halt protease inhibitor cocktail, 1 mM EDTA, 25 µM calpeptin) with quenchers (10 mM sodium azide, 10 mM sodium ascorbate and 5 mM Trolox) and vortexing every 5 min. A volume of 100 µL of lysis buffer was used for each pellet derived from one well of a 6-well plate. The samples were centrifuged at 15000 g during 15 min at 4 °C to remove insoluble debris.

Protein samples were subjected to enrichment of biotinylated proteins. To this end, the samples were first applied to Zeba™ Spin Desalting Columns 7K MWCO and eluted in 100 µL of lysis buffer. Protein concentration was determined using the Bradford assay. Then, 200 µg of protein from each reaction were incubated with 50 µL of streptavidin-coated magnetic bead slurry for 3 h at 4 °C. After washing the streptavidin-coated beads four times with 20 mM Tris pH 7.5, 150 mM NaCl, 1% [v/v] NP-40, the biotinylated proteins were eluted with 35 µL of 2x SDS sample-loading buffer (4% [w/v] SDS, 0.2% [w/v] bromophenol blue, 20% [v/v] glycerol, 100 mM Tris pH 6.8, 200 mM dithiothreitol) and boiled for 5 min.

3.9 Strep-tag pull-down

Forty microliters of Strep-Tactin matrix slurry (MagStrep type3 XT beads) were incubated with equal amounts of moles of the Twin-strep-tagged proteins (0.21 nmol) for 1 h at 4 °C in a final volume of 250 µL of washing buffer (20 mM Tris pH 7.5, 150 mM NaCl, 1% [v/v] NP-40). Then, the matrix was washed three times with 500 µL per wash of chilled washing buffer. Mouse heart lysates were prepared as described in section 3.6 and incubated for 3 h at 4 °C in a rotating mixer with the Twin-strep-tagged proteins previously bound to the Strep-Tactin matrix. Following incubation, samples were washed three times using washing buffer. Next, 35 µL of 2x SDS sample-loading buffer were added to the samples, which were then boiled at 95 °C for 5 min or incubated at RT for 45 min and subsequently loaded onto polyacrylamide gels and analyzed by western blot.

3.10 Coimmunoprecipitation

Mouse heart lysates were prepared as described in section 3.6 and incubated overnight at 4 °C in a mechanical tube roller with 30 µL of Protein G matrix slurry (Dynabeads Protein G) and 8 µg of either anti-Cavβ2b antibody (homemade; preparation described in section 3.2) or normal mouse IgG as a negative control. Then the matrix was washed three times with 500 µL per wash of pre-chilled washing buffer (20 mM Tris pH 7.5, 150 mM NaCl, 1% [v/v] NP-40). Elution was performed by adding 40 µL of loading buffer 2x to the beads, which were then incubated for 45 min at RT.

3.11 Cell fractionation and western blot

Cellular fractionations of ARC were performed following the manufacturer's instructions provided with the Subcellular Protein Fractionation Kit for Cultured Cells. Protein lysates were obtained from cells plated on 6-well plates and prepared by adding 100 µL of ice-cold buffer (25 mM Tris/HCl pH 7.5, 150 mM NaCl, 1% [v/v] NP-40, 1 mM EDTA, 25 µM calpeptin) supplemented with 1x Halt protease inhibitor cocktail and incubated for 15 min. Supernatants were collected after centrifugation at 16000 g for 15 min at 4 °C. Protein concentration was measured using the bicinchoninic acid assay.

For western blot analyses, 40 µg of cellular fractions or total protein lysates were resolved by SDS-PAGE for 1 h at 180 V. Thereafter, the proteins were transferred onto nitrocellulose membranes during 1 h at 100 V using a Mini Trans-Blot Cell and ice-cold transfer buffer (25 mM Tris, 192 mM glycine, 20% [v/v] methanol). Following transfer, membranes were blocked for 1 h at RT in Tris-buffered saline (TBS) containing 5% [w/v] BSA and 0.1% [v/v] Tween-20. The membranes were subsequently incubated overnight at 4 °C in blocking buffer with the corresponding primary antibody (section 2.6). Afterwards, the membranes were washed three times for 10 min with TBS plus 0.1% [v/v] Tween-20 and incubated with horseradish peroxidase (HRP)-conjugated secondary antibody for 1 h at RT. After three further washing steps, the membranes were incubated with enhanced chemiluminescence reagent, visualizing the blots with a FluorChem SP Gel Imaging System and digitizing the results with the AlphaView software (version 1.3.0.7, ProteinSimple; San Jose, USA). The ImageJ software (version 1.51n, National Institutes of Health, Bethesda, USA) was used for the densitometry analysis of protein band images from various acquisition times (3-15 min). Thereafter, the membranes were stripped with 2% [w/v] SDS, 62.5 mM Tris pH 6.8, 0.8% [v/v] β-mercaptoethanol for 45 min at 50 °C and probed again with additional antibodies.

3.12 Immunocytochemistry

ARC were plated on 25 x 25 mm glass coverslips previously coated with 10 µg/mL of laminin for 1 h. After 3 h of incubation, the cells were washed and fixed in 4% [v/v] paraformaldehyde in PBS for 10 min at RT. Fixed cells were permeabilized with 0.2% [v/v] Triton X-100 in PBS, then washed again and incubated for 1 h at RT in blocking solution containing 5% [v/v] normal goat serum. Cells were then rinsed and incubated overnight at 4 °C with the corresponding primary antibodies (section 2.6) diluted in 1.5% [v/v] normal goat serum in PBS. Coverslips were washed to remove excess primary antibody and then incubated with the appropriate secondary antibody for 2 h at RT. Finally, cells were

washed and mounted on glass slides using DAPI mounting medium. All the washing steps consisted of three washes with PBS. Images were acquired on a Leica inverted confocal microscope using a 60x oil-immersion objective. DAPI was excited with a 401-nm laser and detected in the 425-475-nm range. Alexa Fluor 488 dye was excited with a 488-nm argon-ion laser and the fluorescence signal acquired between 490-515 nm. Finally, Alexa Fluor 633 dye was excited at 630 nm and signal detected at 640-700 nm. Images were analyzed using the ImageJ software (version 1.51n, National Institutes of Health, Bethesda, USA).

3.13 Sample preparation and tryptic digestion for mass spectrometry

These experiments were performed in collaboration with Dr. Katalin Barkovits and Prof. Katrin Marcus, from the Medical Proteome Center, Ruhr University Bochum.

The samples prepared as described in section 3.8 were loaded on a 12% Tris-glycine polyacrylamide gel and allowed to run for 8 min at 25 mA. The protein bands were stained with Coomassie Blue and cut out of the gel and into smaller pieces. The bands were destained by incubating the gel pieces three times with 100 mM ammonium bicarbonate for 10 min, alternated with three 10-min incubations with a 1:1 [v/v] mixture of 100 mM ammonium bicarbonate and 100% acetonitrile. Finally, the gel pieces were dried in a vacuum concentrator for 10 min and resuspended each in 30 µL of 100 mM ammonium bicarbonate. Protein digestion was performed overnight with 0.006 µg/µL of trypsin (> 6000 U/g, Serva) at 37 °C and a shaking speed of 300 rpm. The peptides were eluted from the gel pieces by incubating two times during 10 min with 40 µL of a 1:1 [v/v] solution containing 100% acetonitrile and 0.1% [v/v] trifluoroacetic acid in an ice-cooled ultrasonic bath. Samples were dried in a vacuum concentrator and resuspended in 15 µL of 0.1% [v/v] trifluoroacetic acid. Afterwards, the peptide concentration was determined by amino acid analysis as previously described (Plum S *et al.*, 2013). Based on this analysis, 200 ng of peptides from each sample were used for MS analysis.

3.14 Identification and quantification of proteins by mass spectrometry

These experiments were performed in collaboration with Dr. Katalin Barkovits and Prof. Katrin Marcus, from the Medical Proteome Center, Ruhr University Bochum.

Nano-HPLC-MS/MS was performed as previously described (Maerkens A *et al.*, 2016) by means of LC-MS/MS on an UltiMate 3000 RSLCnano system coupled online to an Linear Trap Quadruple Orbitrap Elite mass spectrometer. For protein identification via database searches, the raw files were analyzed with the Proteom Discoverer software (version

1.4.1.14, Thermo Fisher Scientific, Rockford, USA) using the Mascot search algorithm (version 2.5, Matrix Science Ltd., Boston, USA) and searching against the UniProtKB/Swiss-Prot database using rat taxonomy (released 2018/11, 36075 entries). The database search was performed with the following parameters: mass tolerance 5 ppm for precursor and 0.4 Da for fragment ions; 1 missed cleavage; methionine oxidation and biotinylation as variable modifications; false discovery rate threshold of 1%. We accepted all proteins identified in MS analyses by more than two different peptides. Label-free quantification of proteins was performed using the MaxLFQ algorithm (Cox J *et al.*, 2014) integrated into the MaxQuant software (version 1.5.3.8, Max Planck Institute of Biochemistry, Martinsried, GER) (Cox J and Mann M, 2008). Only unique peptides were used for the quantification. We eliminated proteins that were only identified with modified peptides or matched to the reverse database or to the list of common contaminants provided by MaxQuant.

3.15 Analysis of the mass spectrometry data

The analysis of the LFQ data was performed using the Perseus software (version 1.6.5.0, Max Planck Institute of Biochemistry, Martinsried, GER), as previously described (Keilhauer EC *et al*., 2015). The "proteingroups.txt" file generated by MaxQuant was loaded into Perseus and LFQ intensities were transformed to a logarithmic scale. Only the proteins containing LFQ intensity values in all the three replicates of the pull-down of Cavβ2b-V5-APEX2-biotinylated proteins were used for the analysis. The resulting differences between the means of the logarithmized LFQ intensities for each protein in the samples from H_2O_2-treated and untreated Cavβ2b-V5-APEX2-expressing cells [$\log_2(+H_2O_2/-H_2O_2)$] were plotted in a volcano plot against the negative logarithmized p values. The classification of proteins as interactors was based on a cutoff value separating enriched proteins from background binders. To determine the cutoff value, the standard deviation was calculated from the difference between the mean logarithmized LFQ intensity values of the samples from Cavβ2b-V5-APEX2-expressing cells treated with H_2O_2 and those from untreated cells (negative control). Only proteins enriched by more than one standard deviation of the distribution compared with the negative control were accepted at $p < 0.01$.

3.16 Electrophysiology

These experiments were performed by Dr. Michael Kohlhaas from the Comprehensive Heart Failure Center, University Hospital Würzburg.

Calcium currents were recorded in whole-cell voltage-clamp mode using an EPC-10 amplifier and the Patchmaster software (HEKA Elektronik, Pfalz, GER). Glass pipettes were pulled to a resistance of 2-4 MΩ and filled with internal solution containing 125 mM CsCl, 20 mM HEPES, 5 mM Mg-ATP, pH 7.2 adjusted with CsOH. ARC were perfused with K^+-free external solution containing 140 mM NaCl, 4 mM CsCl, 1 mM $MgCl_2$, 5 mM HEPES, 10 mM glucose, 1.8 mM $CaCl_2$, pH 7.4 adjusted with NaOH. Current-voltage relationships were established using a voltage step protocol from -40 mV to +50 mV in 10-mV increments at 0.4 Hz over 200 ms, with a holding potential set to -70 mV. Isoprenaline at a concentration of 30 nM was applied after calcium currents stabilized. Data were acquired with Patchmaster and analyzed using the Fitmaster software (HEKA Elektronik, Pfalz, GER) and Microsoft Excel.

3.17 Calcium measurements

These experiments were performed in collaboration with Dr. Michael Kohlhaas from the Comprehensive Heart Failure Center, University Hospital Würzburg.

ARC were cultured on cover slides coated with laminin and loaded for 20 min at RT with 1 µM Fluo-4AM in a Ca^{2+}-free normal Tyrode's solution containing 130 mM NaCl, 5 mM KCl, 1 mM $MgCl_2$, 10 mM HEPES, 0.3 mM ascorbic acid, 2 mM pyruvate, 10 mM glucose, pH 7.4. Calcium measurements were performed using a customer-modified Myocyte Calcium Photometry and Contractility System. Prior to fluorescence recording with an Eclipse Ti microscope, a rectangular frame of the microscope´s field of view was adjusted to fit around individual cells. Using the same frame size, fluorescence was then recorded in a cell-free area to allow for background fluorescence subtraction. ARC were paced at 3.0- and 4.0-Hz stimulation frequencies, while perfused with normal Tyrode's solution containing 1.8 mM Ca^{2+}. The whole experiment was conducted at 37 °C. The dye was excited at 480 nm using a xenon lamp and the emitted fluorescence was measured at 535 nm using a photomultiplier. Fluorescence was recorded for 1 min and the means of ten Ca^{2+} transients for each stimulation frequency were used for the analysis (Ionwizard software, version 6.3, IonOptix, Westwood, USA). The assessed parameters included amplitude, departure velocity and time to 50% and 90% transient decay.

The SR Ca^{2+} content was estimated by rapid application of a caffeine pulse. In this case, ARC were paced at 1.0 Hz for 1 min to establish steady-state contractions. Then, the pacing was paused and SR Ca^{2+} release was induced by fast perfusion of normal Tyrode's solution supplemented with 1.8 mM Ca^{2+} and 10 mM caffeine. The SR Ca^{2+} content was calculated by subtracting the baseline from the peak Ca^{2+} release (when the solution containing caffeine was added).

3.18 Statistical analysis

All data are presented as the mean ± SEM (standard error of the mean). Differences were considered statistically significant when $p < 0.05$. Statistical analyses were performed using the unpaired *t*-test, 1- or 2-way ANOVA as appropriate. To detect significant differences between more than two groups, post-hoc multiple comparisons were performed using the Bonferroni correction. The analyses were performed with GraphPad Prism (version 8, GraphPad Software Inc., San Diego, USA) and Microsoft Excel.

4. RESULTS

4.1 Evaluation of Cavβ2 splice variants expression in cardiomyocytes and validation of the Cavβ2b antibody

We assessed the expression pattern of the five Cavβ2 splice variants (Cavβ2a-e) in cultured ARC. RT-PCR analyses demonstrated that the mRNA encoding Cavβ2b is predominantly expressed, while the ones encoding for the other splice variants are detected at very low levels (Figure 7A). In order to confirm the expression of protein Cavβ2b in cardiomyocytes, we produced an antibody that specifically targets this Cavβ2 splice variant by recognizing the N-terminus of the protein. Western blot analyses using lysates from HEK-293 cells overexpressing each Cavβ2 splice variant confirmed the high specificity of this antibody for Cavβ2b (Figure 7B).

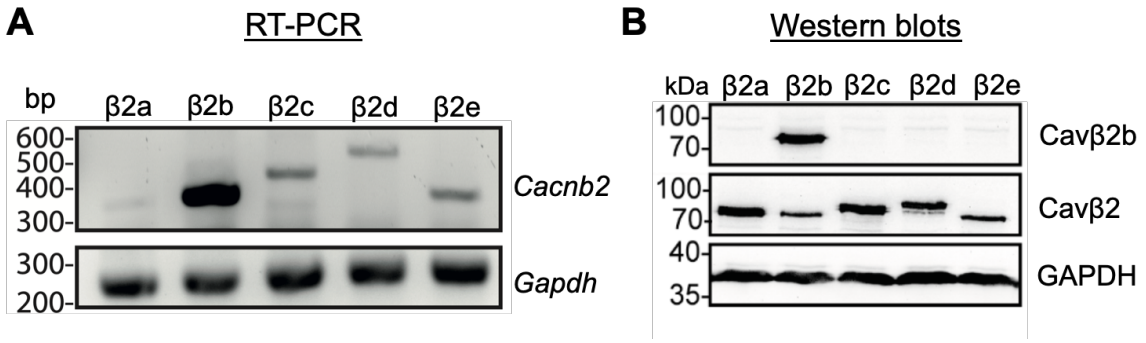

Figure 7. Expression levels of the mRNAs encoding the Cavβ2 splice variants in adult rat cardiomyocytes and validation of the Cavβ2b antibody. (A) Analysis of the expression pattern of the mRNAs encoding each of Cavβ2 splice variants (Cavβ2a, Cavβ2b, Cavβ2c, Cavβ2d and Cavβ2e) in ARC. The sequence of the *Cacnb2* genes encoding the N-terminus of each Cavβ2 splice variant was amplified by RT-PCR. Housekeeping gene *Gapdh* was used as a control. (B) Western blot analyses to validate the specificity of the anti-Cavβ2b antibody using lysates from HEK-293 cells overexpressing the different Cavβ2 splice variants. A commercial anti-Cavβ2 antibody and an anti-GAPDH antibody were used as expression and loading controls, respectively. ARC: adult rat cardiomyocytes; GAPDH: glyceraldehyde-3-phosphate dehydrogenase.

4.2 Proximity labeling biotinylation for the identification of Cavβ2b protein interactors

APEX2-mediated proximity labeling biotinylation in living cells combined with quantitative proteomics has emerged as a powerful method to map protein networks (Rhee RW *et al.*, 2013; Hung V *et al.*, 2014; James C *et al.*, 2019; Liu G *et al.*, 2020). The treatment with biotin-phenol and H_2O_2 of cells expressing an engineered ascorbate peroxidase APEX2 results in the covalent labeling of proteins located within a 20-nm radius of each APEX2 molecule (Rhee RW *et al.*, 2013; Lam S *et al.*, 2015). As shown by Link S *et al.* (2009) and confirmed in our work (section 4.1), Cavβ2b is the predominant Cavβ isoform

expressed in cardiomyocytes. Therefore, the fusion of APEX2 to Cavβ2b could offer a means to detect proteins in the nanoenvironments of Cavβ2b in cardiomyocytes.

In this experiment, APEX2 was genetically linked to the C-terminus of a V5 epitope-tagged Cavβ2b and the resulting Cavβ2b-V5-APEX2 construct was cloned into an adenoviral vector and transduced in ARC. The biotinylation of proteins proximal to Cavβ2b-V5-APEX2 was triggered by incubating the cells with the substrates biotin-phenol and H_2O_2. After cell lysis, biotinylated proteins were subsequently enriched using streptavidin-coated beads and analyzed by western blot and MS. For a better understanding of the results presented in this work, an overview of the strategy followed for the biotin labeling of the proteins in the Cavβ2b nanoenvironments is provided in figure 8.

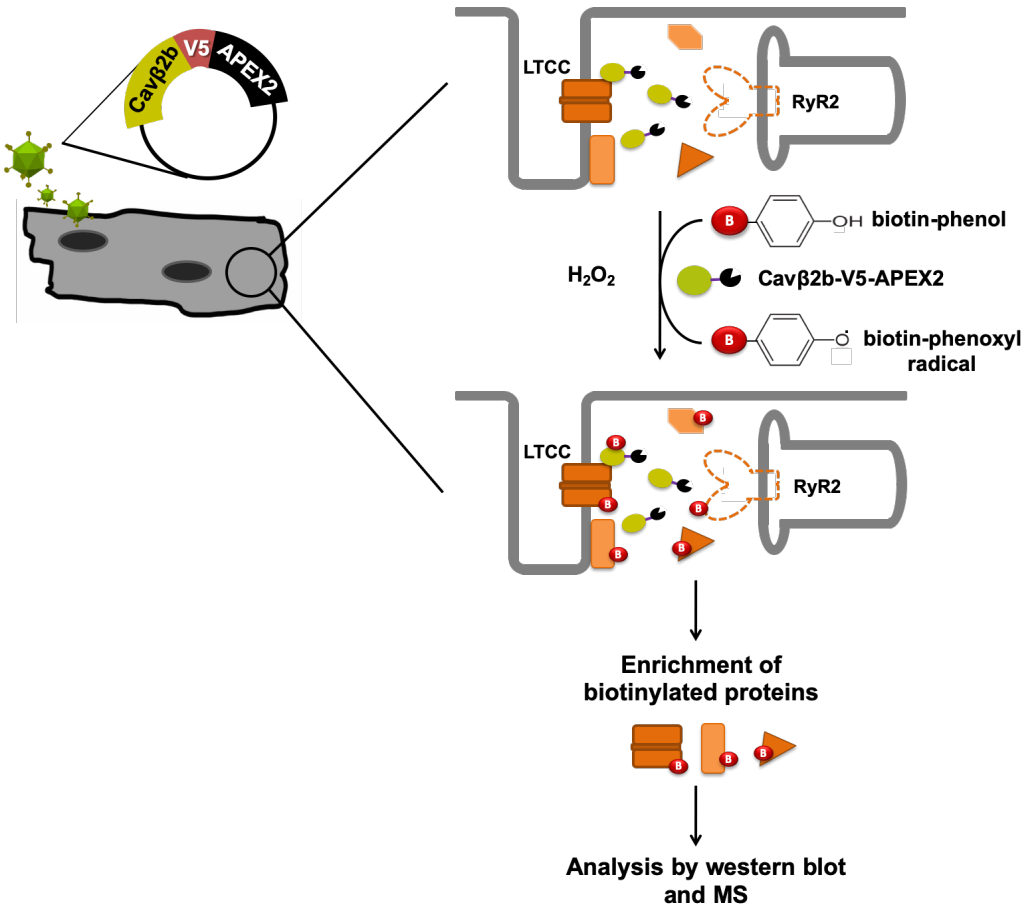

Figure 8. Schematic representation of the proximity labeling biotinylation workflow. ARC are transduced with Cavβ2b-V5-APEX2 using an adenovirus expression system. APEX2 fused to Cavβ2b enables biotin labeling of proteins located < 20 nm from Cavβ2b when the substrates biotin-phenol and H_2O_2 are present. Biotinylated proteins are further enriched by streptavidin-coated beads through affinity purification and bound proteins are analyzed by MS. This scheme shows only the dyadic junction, the main location of Cavβ2b in cardiomyocytes and where the LTCC and the RyR2 are 12-20 nm apart (Shaw RM and Colecraft HM, 2013). APEX2: ascorbate

peroxidase 2; ARC: adult rat cardiomyocytes; LTCC: L-type voltage-gated calcium channel; MS: mass spectrometry; RyR2: ryanodine receptor 2.

The western blot analysis performed after 24 hours of incubation with the adenovirus and using the anti-Cavβ2b antibody showed a ~100-kDa band corresponding to the expression of the Cavβ2b-V5-APEX2 construct. Additionally, a ~70-kDa band corresponding to the endogenous Cavβ2b was detected in non-transduced and Cavβ2b-V5-APEX2-expressing cardiomyocytes (Figure 9A). Immunocytochemistry analyses of non-transduced and Cavβ2b-V5-APEX2-expressing cells, using the anti-Cavβ2b antibody and an anti-V5 antibody, respectively, showed a similar fluorescence pattern for the endogenous Cavβ2b and the overexpressed Cavβ2b-V5-APEX2 fusion protein (Figure 9B), demonstrating that the exogenous Cavβ2b-V5-APEX2 is not mislocalized in ARC.

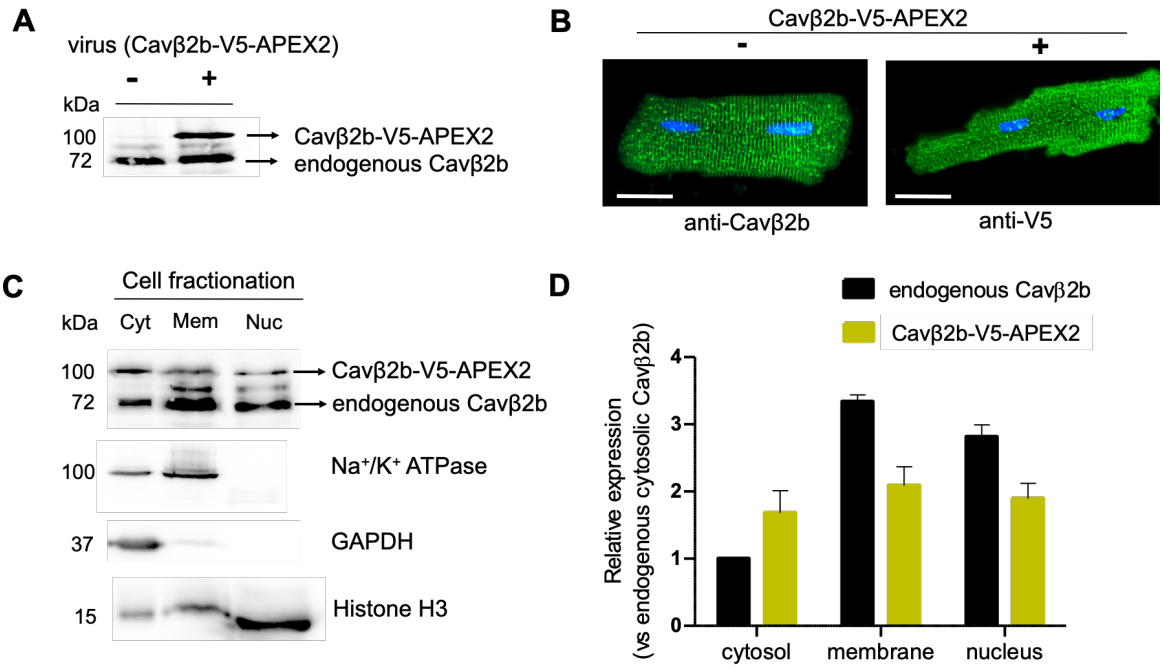

Figure 9. Expression levels and subcellular localization of Cavβ2b-V5-APEX2. ARC were infected with adenovirus at a MOI of 75 for the expression of the recombinant protein Cavβ2b-V5-APEX2. (A) Western blot to confirm the expression of the recombinant protein Cavβ2b-V5-APEX2. (B) Confocal fluorescence images of ARC infected or not with a Cavβ2b-V5-APEX2-coding adenovirus and visualized using an anti-Cavβ2b antibody to recognize the endogenous Cavβ2b and an anti-V5 antibody to recognize the recombinant Cavβ2b-V5-APEX2. Scale bar represents 15 µm. (C) Left panel: western blot with an anti-Cavβ2b antibody to detect the recombinant Cavβ2b-V5-APEX2 and the endogenous Cavβ2b in subcellular fractions. Marker-specific antibodies: anti-GAPDH (cytosol); anti-Na^+/K^+ ATPase (membrane); anti-histone H3 (nucleus). Right panel: bar plots (mean ± SEM) of densitometric measurements from the western blots. ARC: adult rat cardiomyocytes; GAPDH: glyceraldehyde-3-phosphate dehydrogenase; MOI: multiplicity of infection.

Cell fractionation samples of Cavβ2b-V5-APEX2-expressing ARC were analyzed by western blot using the anti-Cavβ2b antibody. As shown in figure 9C, the recombinant and the endogenous Cavβ2b were located in the same subcellular fractions: cytosol, membrane and nucleus. However, the endogenous Cavβ2 was mainly membrane-associated, as previously reported (Gao T *et al.*, 1997; Foell JD *et al.*, 2004), whereas the recombinant Cavβ2b-V5-APEX2 had a more homogenous distribution among the three subcellular fractions.

The purity of the cellular fractions was assessed by western blot against specific markers (Figure 9C). GAPDH was used as a cytosolic marker (Tristan C *et al.*, 2011) and was found in the cytosolic, but not in the nuclear or membrane fractions of ARC. Na^+/K^+ ATPase and histone H3 were used as membrane and nuclear markers, respectively (Clément C *et al.*, 2018; Kong Y *et al.*, 2018). The bulk of histone H3 was found in the nuclear fraction isolated from ARC, appearing substantially less in the membrane and cytosolic fractions. Na^+/K^+ ATPase was mainly present in the membrane fraction, although 25% of the total protein was detected in the cytosolic fraction. This indicates that the cytosolic fraction was contaminated with membrane-associated proteins, a fact that could have influenced the amount of endogenous Cavβ2b and recombinant Cavβ2b-V5-APEX2 observed in this fraction.

Twenty-four hours after transduction, live cells were pre-incubated with biotin-phenol for 30 min and then treated with H_2O_2 for 1 min. The activity of Cavβ2b-V5-APEX2 was assessed by incubating the whole-cell lysate with streptavidin-coated beads in order to capture the biotinylated proteins interacting with the matrix. After the pull-down assay, the samples were eluted and analyzed by streptavidin blot. Multiple bands spanning a large-molecular-weight range were detected in the sample treated with both substrates. In the negative control without H_2O_2, only the bands corresponding to endogenously biotinylated proteins were visible (Figure 10A and Figure S5, supplementary information). Four endogenously biotinylated proteins have been described in mammals: propionil-CoA carboxylase (750 kDa), acetyl CoA carboxylase (280 kDa), pyruvate carboxylase (130 kDa) and methylcrotonyl-Coa carboxylase (80.4 kDa) (Chapman-Smith A and Cronan JE, 1999).

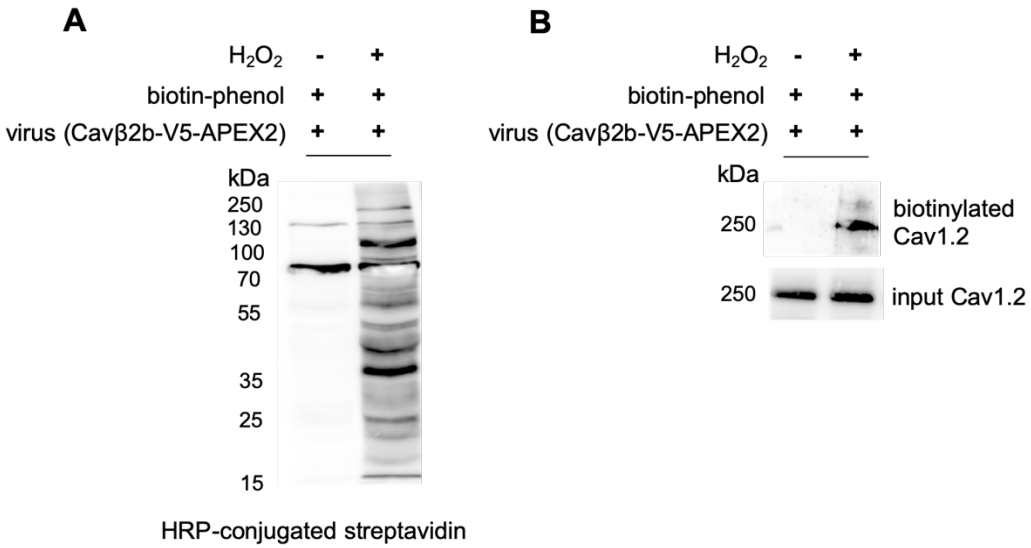

Figure 10. Functionality of Cavβ2b-V5-APEX2 in adult rat cardiomyocytes. (A) Streptavidin blot analysis of endogenous proteins biotinylated by Cavβ2b-V5-APEX2. ARC were infected with adenovirus at a MOI of 75 for the expression of the recombinant protein Cavβ2b-V5-APEX2. Transduced cells were incubated with biotin-phenol for 30 min and then treated with H_2O_2 for 1 min to initiate biotinylation. The cells were lysed and the biotinylated proteins were enriched using streptavidin-coated beads and analyzed by western blot with streptavidin-HRP conjugate. (B) Western blot using an antibody against Cav1.2 after streptavidin-mediated enrichment of biotinylated proteins. H_2O_2 was omitted in the negative control. The data shown are representative of three independent experiments (Figure S5, supplementary information). ARC: adult rat cardiomyocytes; HRP: horseradish peroxidase; MOI: multiplicity of infection.

As the main binding partner of Cavβ2b in cardiomyocytes, Cav1.2 was expected to interact with and be biotinylated by the recombinant protein Cavβ2b-V5-APEX2. In accordance, western blot analysis after the streptavidin enrichment of biotinylated proteins revealed a robust biotinylation of Cav1.2 only in the sample treated with both biotin-phenol and H_2O_2, but not in the negative control, where H_2O_2 was omitted (Figure 10B and Figure S5, supplementary information). This shows that Cavβ2b-V5-APEX2 mediates the biotin labeling of neighboring proteins in living cells.

4.3 Proteins in the Cavβ2b nanoenvironments identified by mass spectrometry

Proteins in the nanoenvironments of Cavβ2b were identified using the biotin labeling strategy followed by single-shot LC-MS/MS using an Orbitrap instrument, which provides better reproducibility and higher sensitivity. Three biological replicates of the samples of ARC infected with adenovirus carrying the Cavβ2b-V5-APEX2 sequence were analyzed for each of the conditions used: treatment with biotin-phenol in the presence or absence of H_2O_2.

Three staged filters were used to extract high-confidence protein constituents of the Cavβ2b nanoenvironments (Figure 11). First, only proteins identified by MS with more than two different peptides, at a false discovery rate of 1% and quantified with unique peptides were included (603 proteins). This step reduces the inaccuracy resulting from the operation of the mass spectrometer or the peptide searching/matching processes. Then, a consistency filter was applied by including only the proteins containing LFQ intensity values (quantification values) in all the replicates (440 proteins). Finally, the exclusion filter accepted only the proteins enriched by more than one standard deviation of the distribution at a $p < 0.01$. This cutoff value would separate enriched proteins from background binders. The top right corner of the plot is the area of highest confidence for a true interaction and is occupied by the interactors with the highest difference between the group means. Accordingly, these filters eliminated candidates with either lower abundance in cardiomyocytes or less stable interaction with Cavβ2b-associated networks and enriched for candidates that robustly integrate into the Cavβ2b nanoenvironments.

Sixty-one proteins met the criteria set in the three-stage filtering outlined above (Figure 11). These proteins were annotated as final constituents of the Cavβ2b nanoenvironments in ARC and are listed in table S1(supplementary information) together with their corresponding genes and the number of peptides used for their identification.

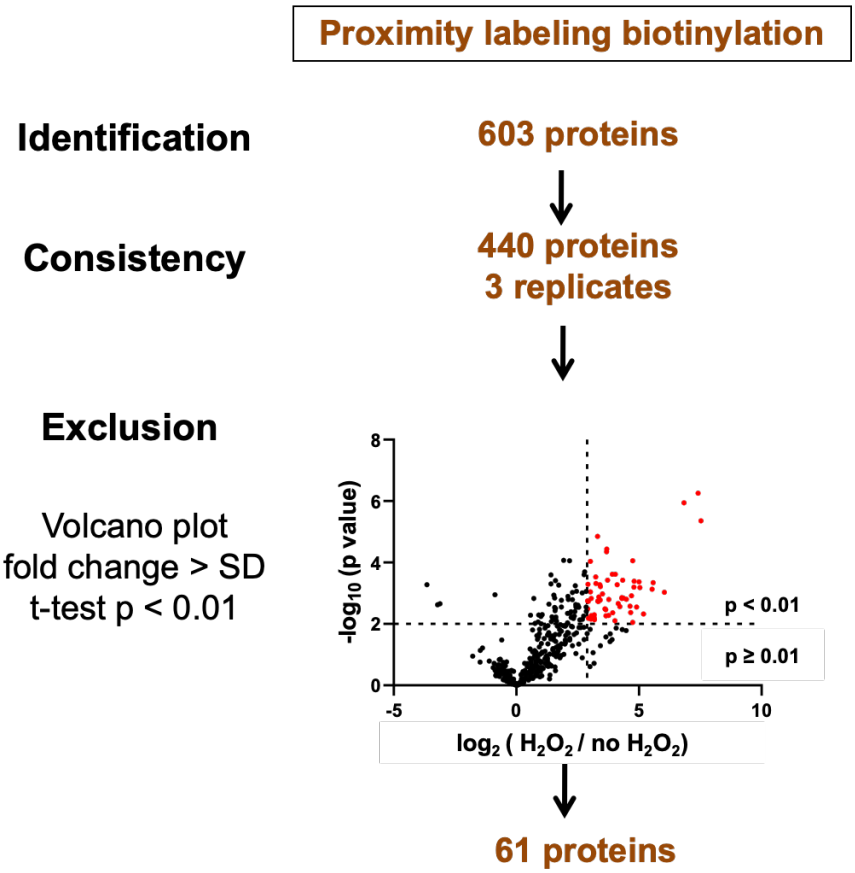

Figure 11. Summary of the mass spectrometry analyses used for the identification of proteins in the Cavβ2b nanoenvironments by proximity labeling biotinylation. Three staged filters (identification, consistency and exclusion) were used to extract high-confidence protein constituents of the Cavβ2b nanoenvironments. Identification filter: included the proteins identified with more than two different peptides, at a false discovery rate of 1% and quantified with unique peptides. Consistency filter: included the proteins containing quantification values in all the replicates. Exclusion filter: included only the proteins enriched by more than one SD at a $p < 0.01$. Differences between the means of the logarithmized LFQ intensities for each protein in the samples from H_2O_2-treated and untreated Cavβ2b-V5-APEX2-expressing cells are plotted against the $-\log_{10}$ (p value) in a volcano plot. Statistical significance was set at $p < 0.01$, corresponding to $-\log_{10}$ (p value) = 2 on the y-axis, and is represented by the dashed line plotted parallel to the x-axis. The dashed line perpendicular to the x-axis represent a cutoff that was chosen accordingly at one SD of the mean, corresponding to $\log_2$ (H_2O_2/no H_2O_2) = 2.90 on the x-axis. Experiments were performed in triplicate. LFQ: label-free quantification; SD: standard deviation.

The results of our database search using information from the Uniprot/Swissprot, Pubmed databases and the DAVID Functional Annotation Tool (http://david.abcc.ncifcrf.gov) (Huang DW *et al.*, 2009) revealed that most of the proteins identified as constituents of the Cavβ2b nanoenvironments reside in the cytosol (35%), although plasma membrane (20%), nuclear (19%) and cytoskeleton-associated (19%) proteins were also detected (Figure 12A and Table S2, supplementary information). The remaining constituents of the Cavβ2b nanoenvironments were annotated as proteins from the sarcoplasmic reticulum

(6%) or having an unknown localization. It is worth mentioning that the proteins classified as having a nuclear localization are also located in the cytosol.

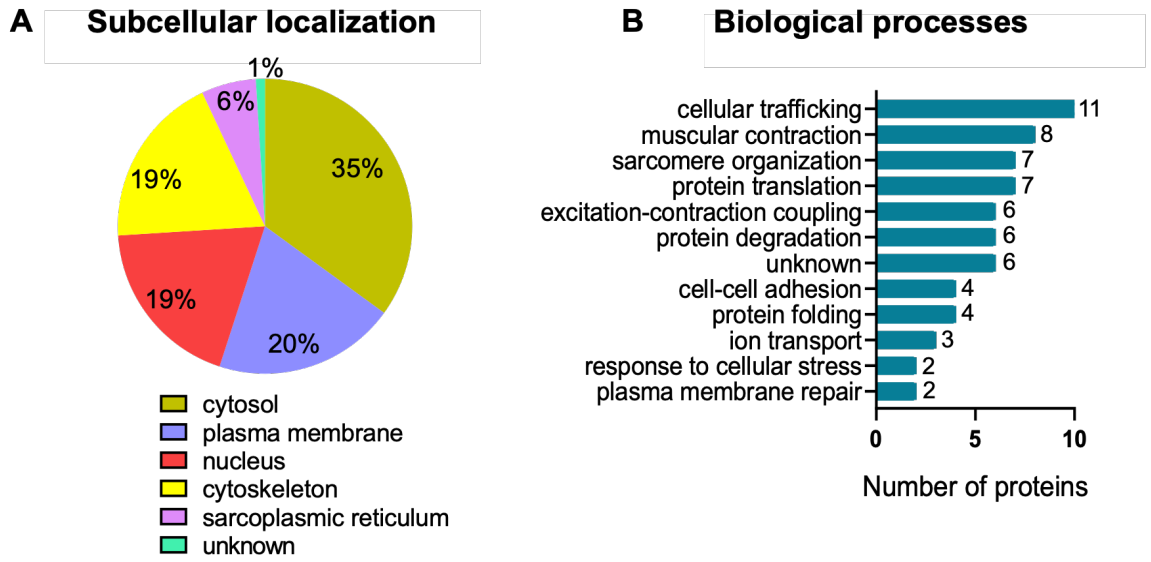

Figure 12. Annotation of proteins in the nanoenvironments of Cavβ2b. (A) Subcellular localization of the proteins and (B) biological processes in which these proteins are involved. The number of proteins associated with these processes is shown in the graph.

The 61 proteins identified were further classified according to 11 different biological processes. The most relevant functions included cellular trafficking (11 of 61 proteins; 18%), muscular contraction (8; 13%), sarcomere organization (7; 11%), protein translation (7; 11%), EC coupling (6; 10%) and protein degradation (6; 10%) (Figure 12B and Table S2, supplementary information). Figure 13 groups some representative proteins participating in these processes.

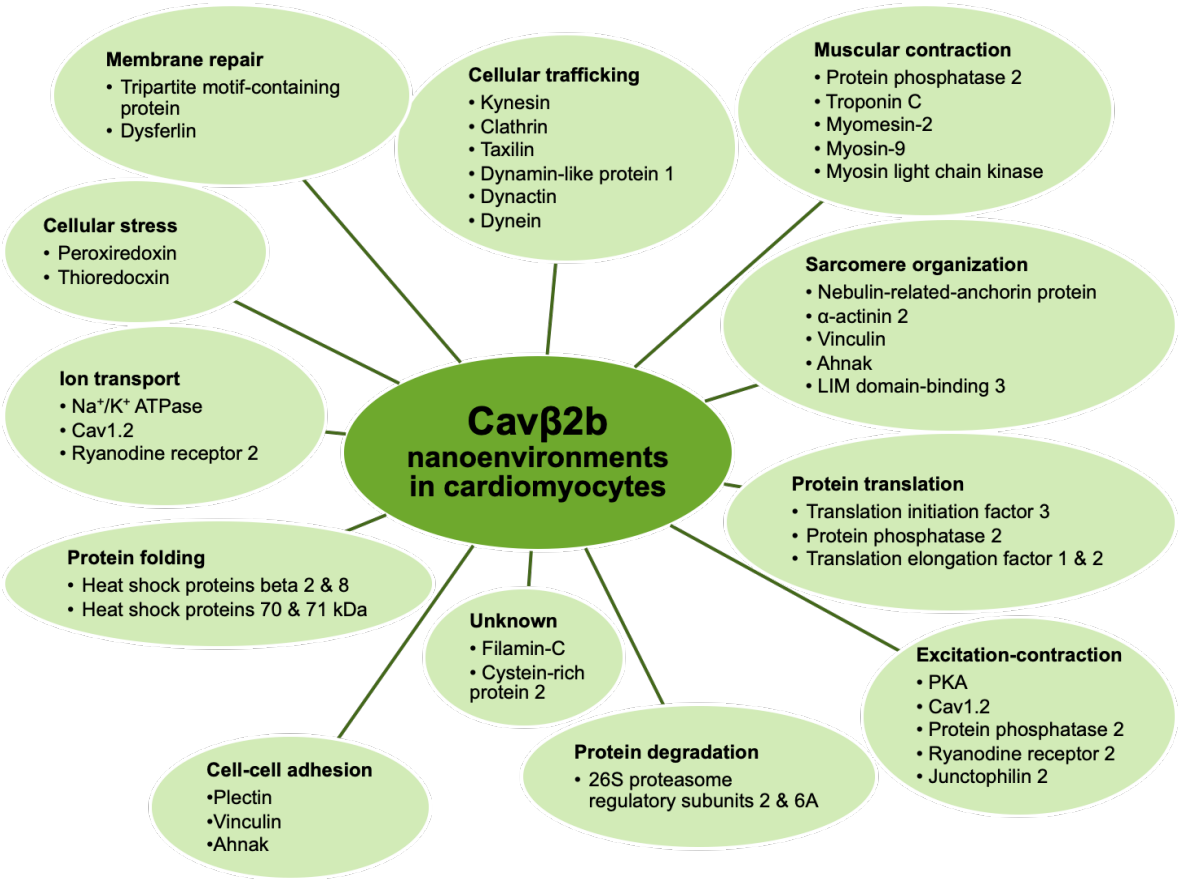

Figure 13. Subset of the proteins identified in the Cavβ2b nanoenvironments in cardiomyocytes. Proteins were grouped according to the biological processes in which they are involved. A complete list of proteins is provided in table S2, supplementary information.

4.4 Interaction of Cavβ2b with proteins of its nanoenvironments

Of the 61 proteins identified as final constituents of the Cavβ2b nanoenvironments in cardiomyocytes, we selected the RyR2 and junctophilin 2 (JPH2) to evaluate the interaction with Cavβ2b using pull-down assays. The RyR2 and JPH2 are known to be localized near Cav1.2 at the dyadic junctions and were thus expected to be in close proximity to Cavβ2b. Western blot analysis after streptavidin enrichment of biotinylated proteins clearly detected the RyR2 and JPH2 only in the sample of ARC expressing Cavβ2b-V5-APEX2 and treated with biotin-phenol and H_2O_2 (Figure 14 and Figure S5, supplementary information), confirming the LC-MS/MS results and the close proximity between Cavβ2b and these two proteins.

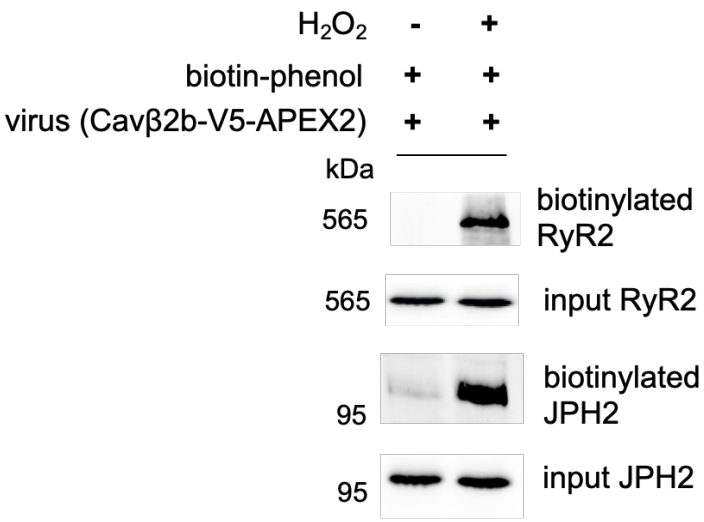

Figure 14. Biotinylation of the RyR2 and JPH2 by Cavβ2b-V5-APEX2. ARC were infected with adenovirus at a MOI of 75 for the expression of the recombinant protein Cavβ2b-V5-APEX2. After 24h, transduced cells were incubated with biotin-phenol for 30 min and then treated with H_2O_2 for 1 min to initiate biotinylation. The cells were lysed and the biotinylated proteins were enriched using streptavidin-coated beads and analyzed by western blot using antibodies against the RyR2 or JPH2. H_2O_2 was omitted in the negative control. Replicates of the assay for the biotinylation of the RyR2 by Cavβ2b-V5-APEX2 are shown in figure S5, supplementary information. ARC: adult rat cardiomyocytes; JPH2: junctophilin 2; MOI: multiplicity of infection; RyR2: ryanodine receptor 2.

Since APEX2-mediated proximity labeling biotinylation targets proteins located within 20 nm of the APEX2 molecule, the biotin labeling of one such protein does not necessarily imply a physical interaction with the protein fused to APEX2. In order to assess whether Cavβ2b interacts with the RyR2 and JPH2, we performed pull-down assays using a recombinant strep-tagged Cavβ2b as bait. Whole mouse heart extracts were incubated with the bait and the eluates then were analyzed by western blot (Figure 15A). In our experiment, we genetically fused the Twin-strep-tag peptide (28 amino acids, WSHPQFEKGGGSGGGSGGSAWSHPQFEK) to the N-terminus of a His-tagged Cavβ2b and the recombinant protein (His-strep-Cavβ2b) was expressed in *E. coli* and purified by Ni^{2+}-affinity chromatography. The strep-tag system is based on the streptavidin-biotin interaction, with the Twin-strep-tag peptide binding with high selectivity to Strep-Tactin, an engineered streptavidin (Schmidt TG *et al.*, 2013). As shown in figure 15B, the RyR2 and JPH2 bind to His-strep-Cavβ2b, but they do not appear in the negative control, where the recombinant protein is omitted. These data corroborate the results obtained by MS.

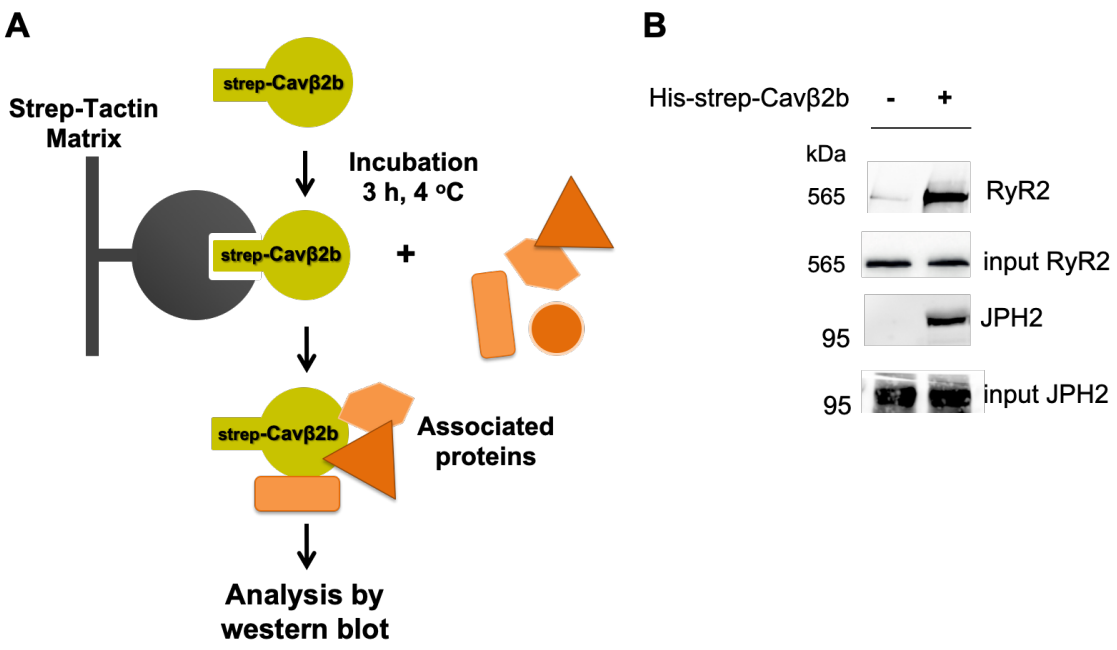

Figure 15. Evaluation of the interaction of Cavβ2b with the RyR2 and JPH2 by strep-tag pull-down assay. (A) Schematic representation of the strep-tag pull-down. Mouse heart lysates and the rat Cavβ2b recombinantly tagged with Twin-strep were incubated together with a Strep-Tactin matrix during 3 h at 4 °C and the eluates analyzed by western blot using antibodies against the RyR2 and JPH2, as shown in (B). Replicates of the pull-down assay for the RyR2 using the recombinant strep-Cavβ2b protein are shown in figure S6, supplementary information. JPH2: junctophilin 2; RyR2: ryanodine receptor 2; strep: Twin-strep-tag.

The sarcomeric α-actinin isoform (α-actinin 2), which is known to connect the cardiac T-tubule membrane with the sarcomere's Z-lines (Beggs AH *et al.*, 1992; Grison M *et al.*, 2017), was also identified in the nanoenvironments of Cavβ2b (Figure 13 and Tables S1-S2, supplementary information). By contrast, the voltage-dependent anion-selective channel protein 1 (VDAC1) was detected by LC-MS/MS, but excluded as a final constituent of the Cavβ2b nanoenvironments after the proteomic analysis. Pull-down assays were performed using the recombinant protein GST-strep-Cavβ2b and, as a negative control, GST-strep. The Twin-strep-tag peptide was genetically fused to the N-terminus of Cavβ2b and then fused to the GST for its purification by glutathione-affinity chromatography. As shown in figure 16, pull-down assays followed by western blot using α-actinin 2 and VDAC1 antibodies confirmed that the recombinant protein GST-strep-Cavβ2b interacts with α-actinin 2, but not with VDAC1. The fact that the recombinant GST-strep-Cavβ2b protein does not interact with VDAC1 corroborates the results of our proteomics study, implying that this channel is not part of the Cavβ2b nanoenvironments.

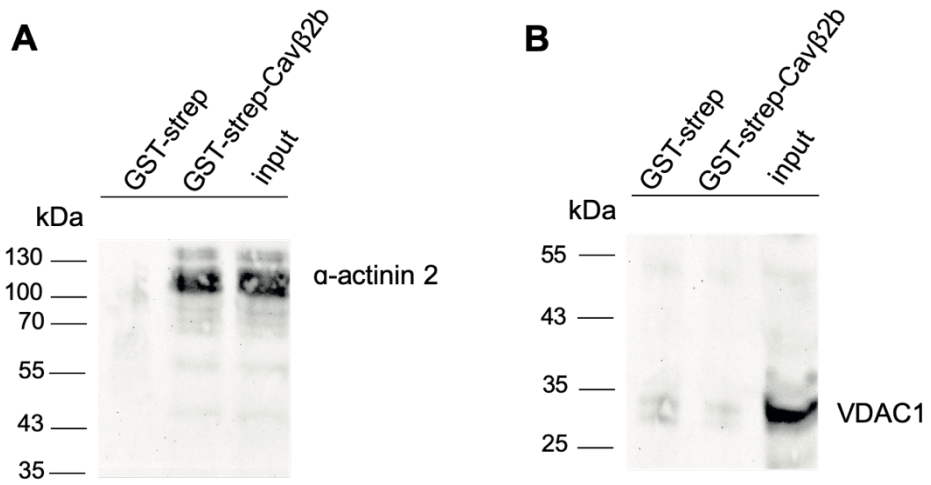

Figure 16. Evaluation of the interaction of Cavβ2b with α-actinin 2 and VDAC1 by strep-tag pull-down assay. Mouse heart lysates were incubated with GST-strep (negative control) or with GST-strep-Cavβ2b and the eluates were analyzed by western blot using antibodies against (A) α-actinin 2 or (B) VDAC1. GST: glutathione S-transferase; strep: Twin-strep-tag; VDAC1: voltage-dependent anion-selective channel protein 1.

4.4.1 Distribution pattern of Cavβ2, the RyR2 and α-actinin 2 in adult rat cardiomyocytes

Figure 17 shows confocal fluorescence images of ARC labeled with an anti-Cavβ2 antibody and specific antibodies for either the RyR2 or α-actinin 2. The distribution pattern of Cavβ2 resembles the arrangement of T-tubules previously revealed with other markers (Hong T and Shaw RM, 2017; Wong J *et al.*, 2013). The superposition of the fluorescence microscopy images obtained with equal intensities for the two probes indicated that Cavβ2 and the RyR2 colocalized in the T-tubules in ARC. A similar result was obtained with the immunostaining using anti-Cavβ2 and anti-α-actinin 2 antibodies. The predominant yellow color in the merged image confirmed that in cardiomyocytes the Cavβ2 subunit is, as previously described (Gao T *et al.*, 1997), distributed along the T-tubules at the level of the Z-lines, where α-actinin 2 is found.

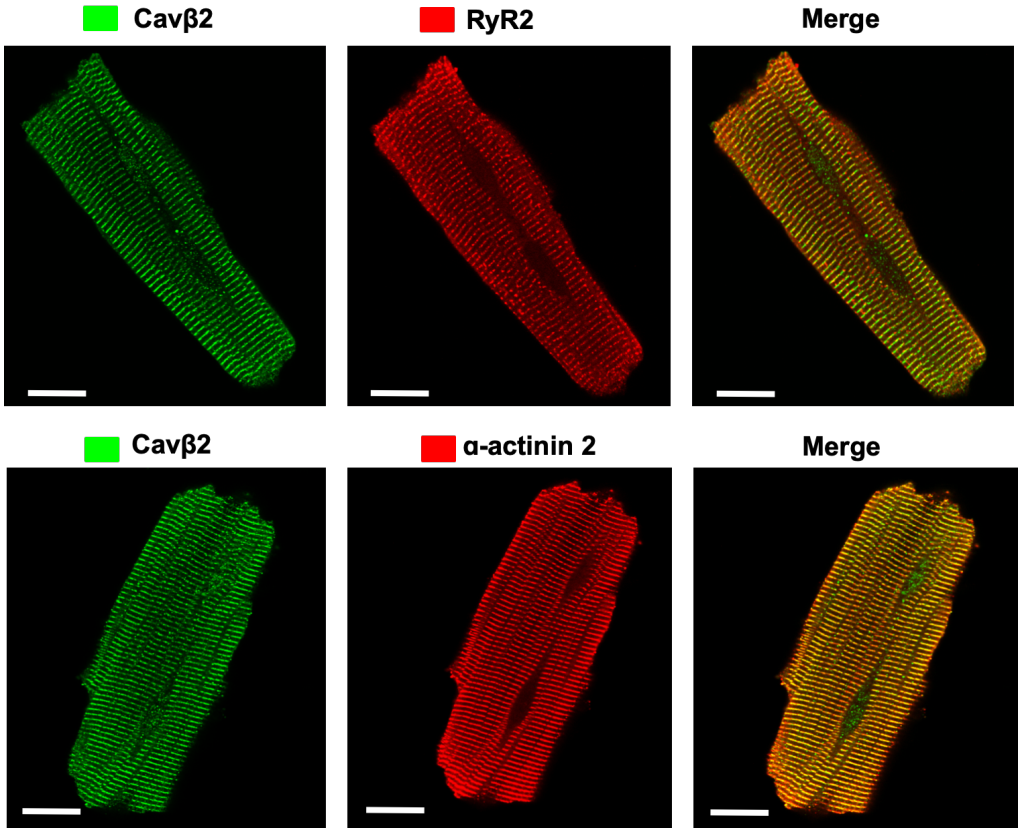

Figure 17. Distribution pattern of Cavβ2, the RyR2 and α-actinin 2 in adult rat cardiomyocytes. Confocal fluorescence microscopy images from ARC after labeling with anti-Cavβ2 antibody (in green) and specific antibodies for either the RyR2 or anti-α-actinin 2 (both in red). Visualization was done using FITC-conjugated secondary antibodies. Scale bar represents 40 μm. ARC: adult rat cardiomyocyte; RyR2: ryanodine receptor 2.

Since, the resolution of the confocal microscope is insufficient to identify the physical apposition of two molecules by comparing the distribution of their fluorescence microscopy images (Dunn KW *et al*, 2011), therefore, this technique is rather used to determine whether two molecules associate with the same structures like, for example, T-tubules, nucleus or microtubules.

4.5 Coimmunoprecipitation of Cavβ2b with the RyR2

Among the potential Cavβ2b interactors identified in this work we selected the RyR2 for validation purposes, since it was one of the proteins detected with the highest accuracy by MS. In total, 77 peptides from this protein were detected by LC-MS/MS (Table S1, supplementary information). The potential interaction between Cavβ2b and the RyR2 was assessed using coimmunoprecipitation. A polyclonal anti-Cavβ2b antibody targeting the N-terminal domain of Cavβ2b was incubated with mouse heart lysates and the complex Cavβ2b-RyR2 was captured using a protein G matrix. Then, the complex was eluted and

the RyR2 detected by western blot with a specific antibody (Figure 18A). A total heart lysate was used as positive control for the detection of the RyR2 (molecular weight: 565 kDa). Figures 18B and S7 (supplementary information) show that the RyR2 was detected only in the sample where Cavβ2b was incubated with the whole heart extract and not in the negative controls, confirming the interaction of Cavβ2b with the RyR2.

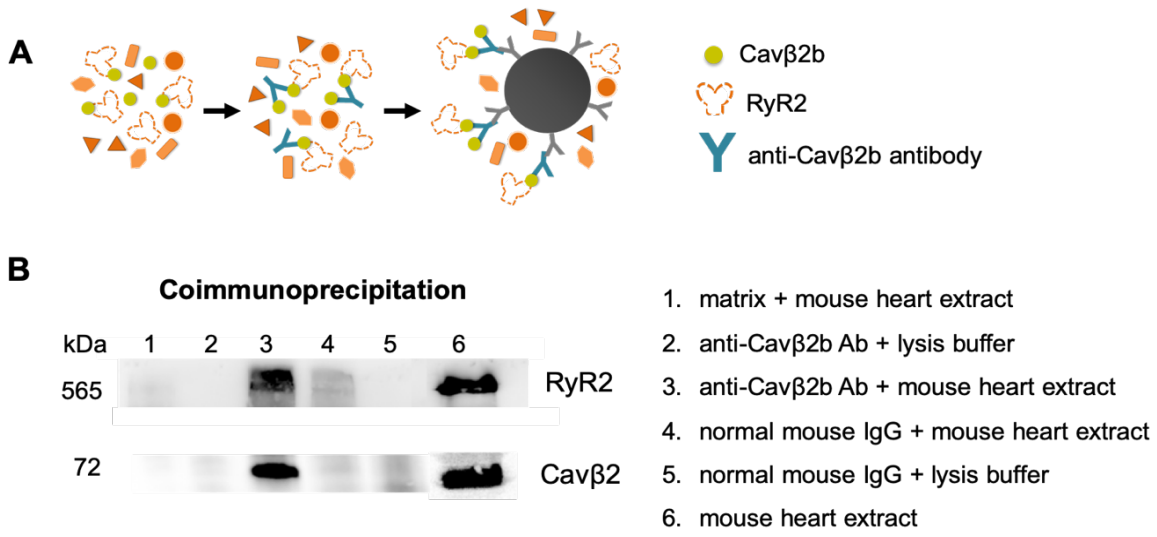

Figure 18. Coimmunoprecipitation of the RyR2 with Cavβ2b in mouse heart lysates. (A) Schematic representation of the coimmunoprecipitation. Cavβ2b was immunoprecipitated by an anti-Cavβ2b antibody (homemade) and the coprecipitated RyR2 was analyzed by western blot (6% SDS-PAGE gel). (B) Western blot using anti-RyR2 (top) and anti-Cavβ2 (bottom) antibodies (commercial sources). Normal mouse IgG was used as negative control. The lysis buffer contained 20 mM Tris pH 7.5, 150 mM NaCl and 1% [v/v] NP-40. Ab: antibody; RyR2: ryanodine receptor 2.

4.5.1 The SH3 domain of Cavβ2b interacts with the RyR2

Cavβ2b has conserved SH3 and GK domains flanked by the non-conserved HOOK domain and the N- and C-termini (Figure 19A). To find out which region of Cavβ2b mediates the interaction with the RyR2, we created recombinant proteins with the GST-Twin-strep-tag genetically linked to the N-terminus of the full-length Cavβ2b and each of its individual domains. The purified fusion proteins were resolved by SDS-PAGE and their purity assessed by staining the gel with Coomassie Blue (Figure 19B). Then, each recombinant protein was incubated with mouse heart lysates. The only exception was the GST-strep-GK recombinant protein, which aggregated after expression in *E. coli*. With an estimated molecular weight of around 53 kDa, this fusion protein underwent premature elution in the void volume during the size exclusion chromatography. Since aggregated proteins lose their three-dimensional structure and are unable to properly interact with other proteins, we excluded the GK domain from the analysis.

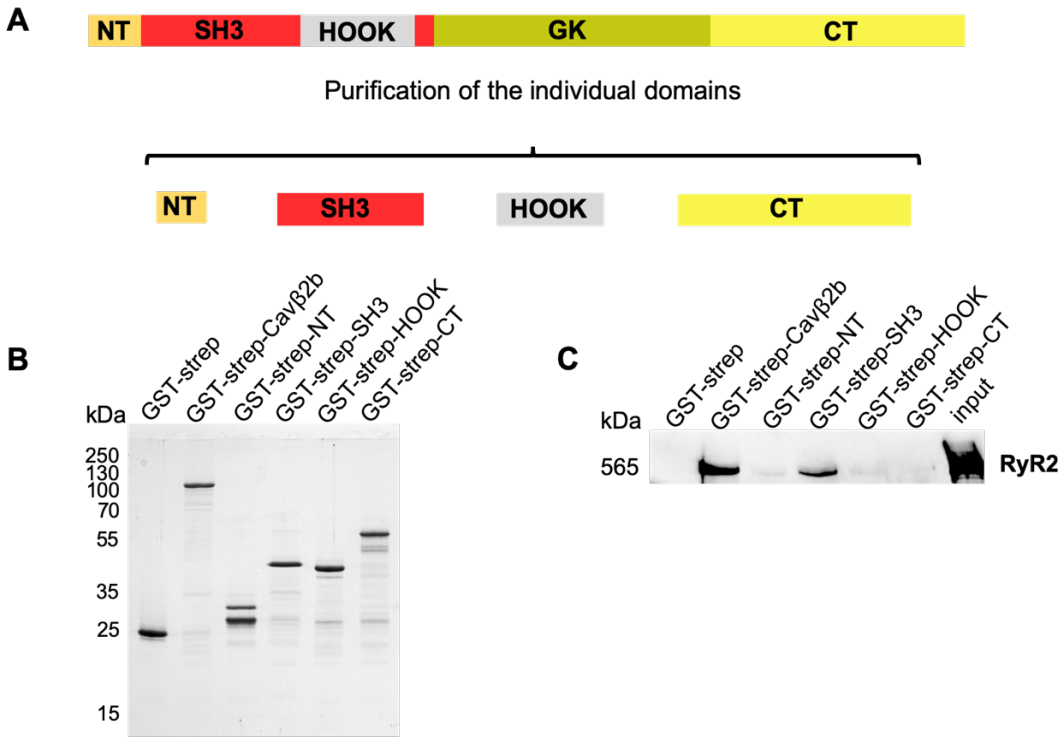

Figure 19. Mapping of the RyR2-interacting region of Cavβ2b. (A) Schematic diagram of Cavβ2b domains: NT (N-terminus), SH3 (Src-3 homology), HOOK (linker region), GK (guanylate kinase), CT (C-terminus). (B) Assessment of the purity of the Cavβ2b domains (1 µg per lane) by Coomassie Blue-stained 12% SDS-PAGE gel. (C) Strep-tag pull-down of the RyR2 with the recombinant GST-strep-Cavβ2b and its individual domains. The purified Cavβ2b and its fragments were incubated with mouse heart lysates and the eluates were analyzed by western blot using an anti-RyR2 antibody. The data shown are representative of three independent experiments (Figure S6, supplementary information). GST: glutathione S-transferase; RyR2: ryanodine receptor 2; strep: Twin-strep-tag.

Equimolar samples of the purified full-length Cavβ2b and the Cavβ2b fragments were immobilized onto Strep-Tactin beads through the Twin-strep-tag inserted in their sequences. Mouse heart lysates were then applied to each matrix and after extensive washing the eluates from the pull-down were resolved by SDS-PAGE and probed with an anti-RyR2 antibody. The analysis by western blot revealed that the full-length Cavβ2b and its SH3 domain bind strongly to the RyR2, suggesting that the interaction between Cavβ2b and the RyR2 is mediated by the SH3 domain (Figure 19C). Replicates of these experiments including quantification of the immunoblots are shown in figure S6, supplementary information.

4.5.2 Functional characterization of the interaction of Cavβ2b with the RyR2

To assess the role of the interaction between Cavβ2b and the RyR2 in cardiomyocytes, we expressed the SH3 domain of Cavβ2b (Cavβ2b-SH3) in ARC and evaluated its effect on L-type Ca^{2+} currents and Ca^{2+} transients. We hypothesized that if the Cavβ2b-RyR2

interaction has a physiological role in linking LTCC and RyR2 in cardiomyocytes, the overexpression of the Cavβ2b-SH3 domain, which does not interact with Cav1.2 (Chen YH *et al.*, 2004; Opatowsky Y *et al.*, 2004; Van Petegem F *et al.*, 2004; Findeisen F *et al.*, 2017), could disrupt endogenous LTCC-RyR2 complexes and therefore affect the CICR in these cells. The Cavβ2b-SH3 domain containing a V5 tag at the C-terminus was transduced in ARC using an adenovirus system. Twenty-four hours after transduction, the expression of the Cavβ2b-SH3 domain, which appeared at the expected molecular weight of 16 kDa, was confirmed by western blot using an anti-V5 antibody (Figure 20). In parallel, we evaluated the effect of the recombinant Cavβ2b-SH3 domain on the expression of Cavβ2, SERCA2a, Cav1.2 and the RyR2. No changes were detected on the expression of Cavβ2, SERCA2a and the RyR2 after overexpression of the Cavβ2b-SH3 domain in ARC. However, an increase in the expression of Cav1.2 was detected in cardiomyocytes overexpressing the Cavβ2b-SH3 domain compared to the negative control (Figure 20).

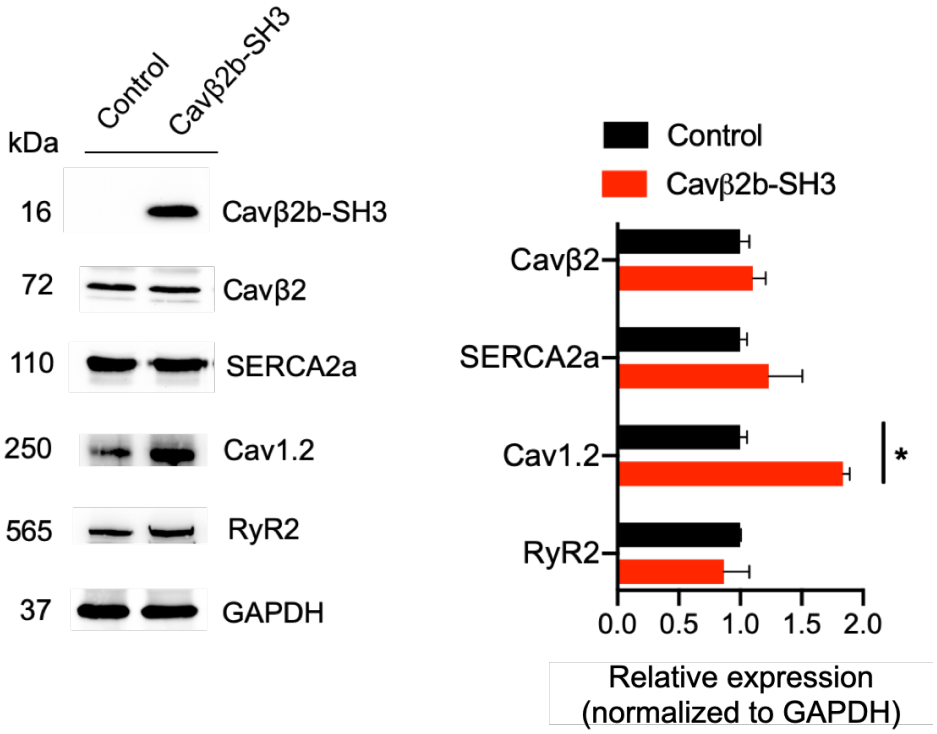

Figure 20. Effect of the overexpression of the Cavβ2b-SH3 domain in adult rat cardiomyocytes. ARC were infected with a Cavβ2b-SH3-coding virus or with a virus containing an empty vector lacking the region coding for the Cavβ2b-SH3 domain (control). After 24h, cell lysates were prepared from the ARC and analyzed by western blot. Left panel: western blot analysis of the expression of Cavβ2, SERCA2a, Cav1.2, RyR2 and GAPDH after Cavβ2b-SH3 domain overexpression. Right panel: bar plots (mean ± SEM) of the densitometric measurements of protein levels (normalized to the GAPDH loading control). ARC: adult rat cardiomyocytes; GAPDH: glyceraldehyde-3-phosphate dehydrogenase; RyR2: ryanodine receptor 2; SERCA2a: sarcoplasmic/endoplasmic reticulum Ca^{2+} ATPase 2a.

The effects of the Cavβ2b-SH3 domain on L-type Ca^{2+} currents were assessed by whole-cell patch-clamp analysis. Overexpression of the Cavβ2b-SH3 domain did not affect L-type Ca^{2+} currents in ARC under our recording conditions (Figure 21A and B). Similar to the negative control ARC, infected with adenovirus containing an empty vector, the Cavβ2b-SH3-overexpressing ARC showed high-density Ca^{2+} currents and a peak current between 0 and +10 mV, characteristic of L-type Ca^{2+} channels (Zhou Z and January CT, 1998; Yang *et al.*, 2019). Moreover, incubation with 30 nM isoprenaline produced a 1.8-fold increase in the Ca^{2+} current at 0 mV in Cavβ2b-SH3-overexpressing cells, which was not significantly different from the 1.6-fold increment in the negative control cells (Figure 21B and C).

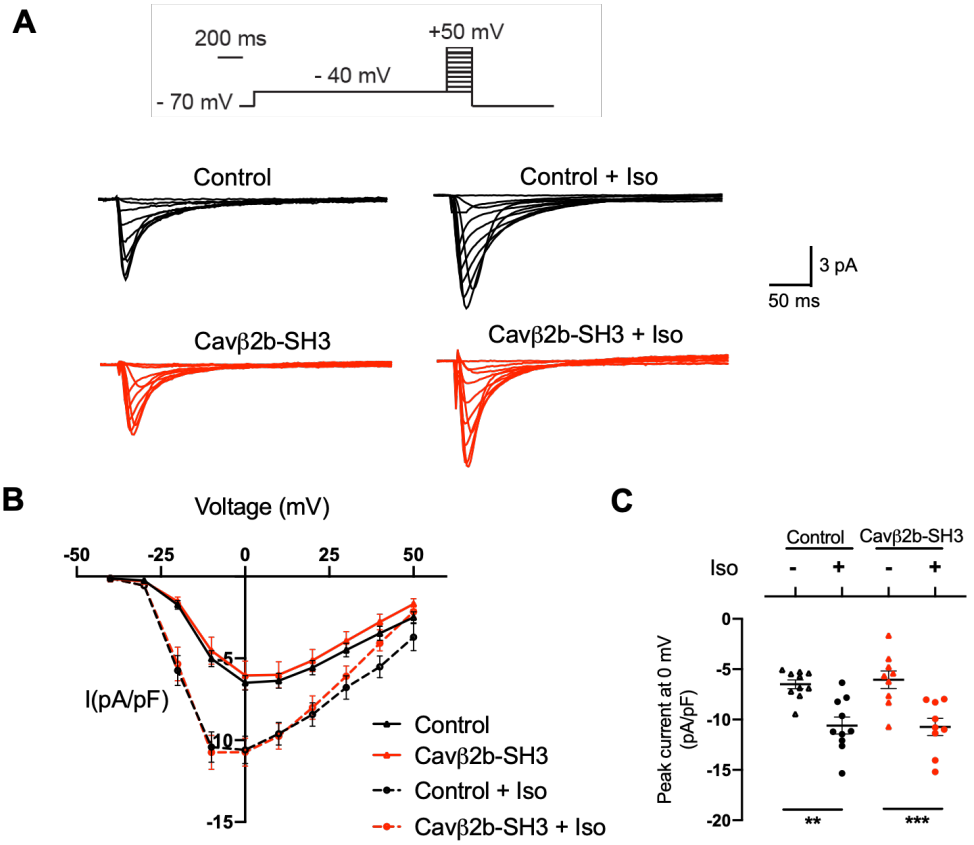

Figure 21. Endogenous L-type Ca^{2+} currents from adult rat cardiomyocytes overexpressing the Cavβ2b-SH3 domain. (A) Voltage step protocol and representative whole-cell endogenous L-type Ca^{2+} current traces measured in the absence or presence of 30 nM Iso using ARC infected with a virus containing an empty vector lacking the region coding for the Cavβ2b-SH3 domain (control, black traces) or with the Cavβ2b-SH3-coding virus (red traces). Currents were elicited using a voltage step protocol ranging from -40 mV to +50 mV with 10-mV increments and with a holding potential set up at -70 mV. (B) Voltage dependence of Ca^{2+} current density curves measured in ARC infected with the indicated adenovirus and in the absence or presence of 30 nM Iso. (C) Scatter plot showing peak Ca^{2+} current plots at 0 mV in ARC infected with the indicated adenovirus and in the absence or presence of 30 nM Iso. Data are presented as mean ± SEM; **p < 0.01, ***p < 0.001 by one or two-way ANOVA/multiple comparison; n = 10 control cells, n = 9 Cavβ2b-SH3-overexpressing cells. ARC: adult rat cardiomyocytes; Iso: isoprenaline.

To evaluate the effect of Cavβ2b-SH3 domain expression on CICR, intracellular Ca^{2+} transients were measured using the fluorescent calcium-sensitive dye Fluo-4AM at different pacing frequencies. Figure 22A illustrates fast-time-base recordings of mean Ca^{2+} transients in ARC overexpressing the Cavβ2b-SH3 domain and in the negative control cells at stimulation frequencies between 0.5 and 4.0 Hz.

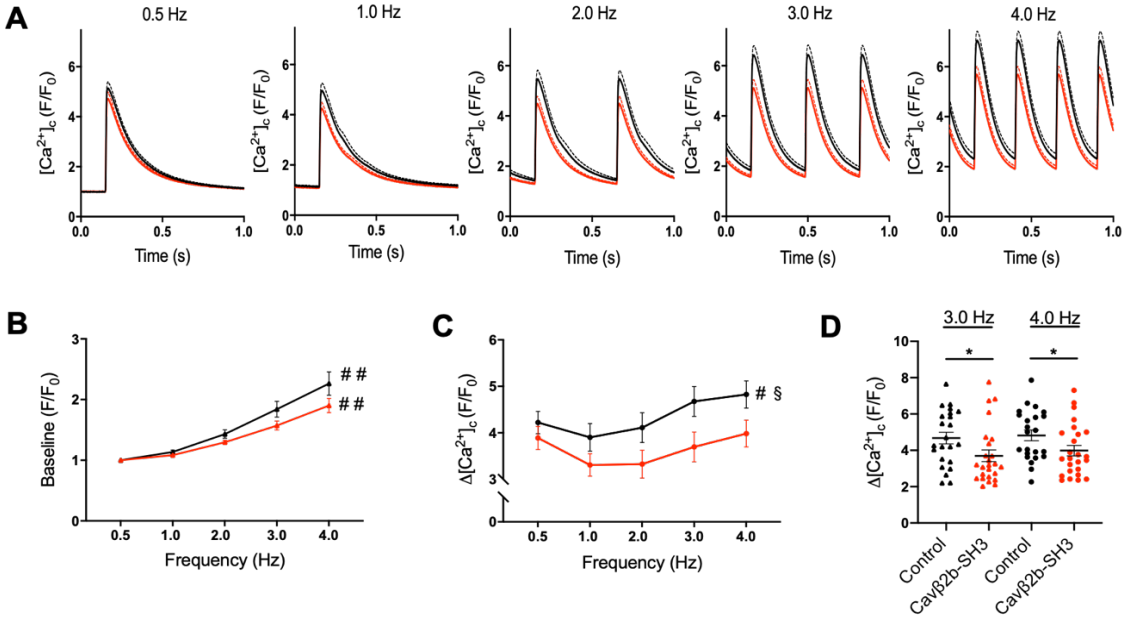

Figure 22. Ca^{2+} transient amplitude at different pacing frequencies in cardiomyocytes overexpressing the Cavβ2b-SH3 domain. Fluorescence of calcium-bound Fluo4-AM was recorded at stimulation frequencies of 0.5, 1.0, 2.0, 3.0 and 4.0 Hz from ARC infected with a virus containing an empty vector lacking the region coding for the Cavβ2b-SH3 domain (control, in black) or with a Cavβ2b-SH3-coding virus (in red). (A) Mean trace of Ca^{2+} transients. (B) Diastolic (baseline) Ca^{2+} concentration at the different pacing frequencies. (C) Ca^{2+} transient amplitude after baseline subtraction at the different pacing frequencies. (D) Scatter plot showing the Ca^{2+} transient amplitudes for each cell after baseline subtraction at 3.0 and 4.0 Hz pacing frequencies. Data are presented as mean ± SEM; $^{\#}p < 0.05$ between frequencies (one-way ANOVA), $^{\#\#}p < 0.01$ between frequencies (one-way ANOVA), $^{\S}p < 0.05$ between control and Cavβ2b-SH3-overexpressing cells (two-way ANOVA), *p < 0.05 between control and Cavβ2b-SH3-overexpressing cells (unpaired *t*-test); n = 23 control cells, n = 25 Cavβ2b-SH3-overexpressing cells. ARC: adult rat cardiomyocytes.

A rise in the diastolic (baseline) Ca^{2+} levels was observed in control and Cavβ2b-SH3-expressing cardiomyocytes when the stimulation frequencies increased, but no significant differences were observed between the two groups (Figure 22B). This indicates that the overexpression of the Cavβ2b-SH3 domain had no significant effect on the diastolic Ca^{2+} concentration in the cytosol at the stimulation frequencies used. A pacing frequency-dependent increase in the amplitude of the Ca^{2+} transients was observed in control cells (Figure 22C), an effect that was completely absent in Cavβ2b-SH3-expressing cardiomyocytes (Figure 22C). Additionally, the amplitudes of the Ca^{2+}

transients measured at low pacing frequencies (0.5-2.0 Hz) were similar in control and Cavβ2b-SH3-expressing cardiomyocytes. However, the cardiomyocytes overexpressing the Cavβ2b-SH3 domain exhibited significantly lower Ca^{2+} transient amplitudes than the negative control cells at both 3.0 Hz (3.70 ± 0.32 vs 4.68 ± 0.32, p = 0.0365) and 4.0 Hz (3.99 ± 0.29 vs 4.83 ± 0.29, p = 0.0459) (Figure 22D).

Caffeine is an agonist of the RyR2 (Kong H *et al.*, 2008) that triggers near total SR Ca^{2+} release and the resulting cytosolic Ca^{2+} increase serves as an estimate of the SR Ca^{2+} content. Therefore, Ca^{2+} transients were recorded before and immediately after caffeine application (Figure 23A).

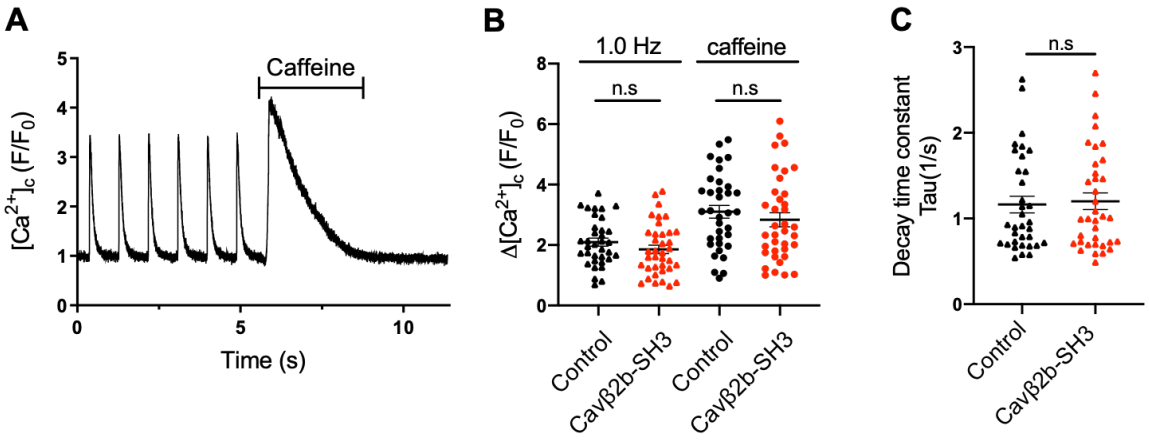

Figure 23. Sarcoplasmic reticulum Ca^{2+} content and cytosolic Ca^{2+} removal in cardiomyocytes overexpressing the Cavβ2b-SH3 domain. ARC were paced at 1.0 Hz for 1 min to establish steady-state contractions. Then, the pacing was paused and the release of the total SR Ca^{2+} content was induced by fast perfusion with normal Tyrode's solution supplemented with 1.8 mM Ca^{2+} and 10 mM caffeine. (A) Representative fluorescence tracing during the 1.0-Hz pacing and Ca^{2+} release induced by application of caffeine. (B) Ca^{2+} transient amplitude at 1.0 Hz and SR Ca^{2+} content assessed by caffeine-induced Ca^{2+} release; n = 35 control cells, n = 37 Cavβ2b-SH3-overexpressing cells. (C) Decay time constant (Tau); n = 34 control cells, n = 36 Cavβ2b-SH3-overexpressing cells. Data are presented as mean ± SEM. Statistical analysis were preformed using the unpaired *t*-test. ARC infected with a virus containing an empty vector lacking the region coding for the Cavβ2b-SH3 domain were used as control. ARC: adult rat cardiomyocytes; n.s: not significant; SR: sarcoplasmic reticulum.

ARC were pre-loaded with Fluo-4 AM and SR Ca^{2+} release was induced by fast perfusion with normal Tyrode's solution supplemented with 1.8 mM Ca^{2+}, followed by addition of 10 mM caffeine. As shown in the scatter plots (Figure 23B), caffeine caused a similarly strong transient in both the Cavβ2b-SH3-overexpressing and the negative control cardiomyocytes (p = 0.745), indicating that RyR2-dependent SR Ca^{2+} release was fully functional.

We also determined the rate constant of cytoplasmic calcium removal through the SERCA2a and the Na^+/Ca^{2+} exchanger to assess whether these proteins were functioning properly. No significant differences ($p = 0.780$) in the time constant of calcium decay (Tau) calculated for the caffeine-induced transient were observed between the Caβ2b-SH3-overexpressing and the negative control cells, as shown in the scattered plots in figure 23C.

5. DISCUSSION

LTCC are heteromultimeric membrane proteins that allow Ca^{2+} entry upon plasma membrane depolarization. Among all the auxiliary subunits of LTCC, the cytosolic β subunit has been shown to interact with the AID in the pore-forming α1 subunit and to regulate the trafficking and biophysical properties of these channels. However, Cavβ is now known to interact with many other proteins, which has led to considering this subunit as rather a multifunctional protein. Interestingly, several recent studies highlight new Cavβ functions that are independent of its role in the regulation of the LTCC (Rima M *et al.*, 2016). Of the four Cavβ isoforms, Cavβ2 is predominantly expressed in cardiomyocytes, specifically the splice variant Cavβ2b (Link S *et al.*, 2009). This subunit is known to associate with diverse proteins besides LTCC, such as ahnak, dynamin and actin, but the molecular composition of the Cavβ2b nanoenvironments in cardiomyocytes is yet unresolved.

In this work, we mapped the protein interaction network of Cavβ2b using a proteomic strategy that exploits the extreme affinity (Kd 10^{-14} M) of streptavidin for biotin (Haugland RP and You WW, 2008). The strategy was based on the labeling of proteins in living cells using APEX, an engineered ascorbate peroxidase. Since APEX oxidizes biotin-phenol to phenoxyl radicals in the presence of H_2O_2, proteins within a radius of around 20 nm were expected to be covalently labeled with the biotin group, enabling their enrichment using streptavidin-coated beads and their identification by MS (Rhee HW *et al.*, 2013; Hung V *et al.*, 2014). Given its stability and small size, the biotin tag rarely affects the function of labeled molecules. Additionally, biotin labeling has the main advantage that it is performed in living cells, preserving their architectural integrity and allowing for pull-down-associated false positives to be discarded. A mutation introduced in the original enzyme led to the development of the more catalytically active APEX2, which enables superior enrichment of proteins for proteomic studies (Lam S *et al.*, 2015).

5.1 Subcellular localization of the endogenous Cavβ2b and the recombinant protein Cavβ2b-V5-APEX2

In our work, Cavβ2b was fused to APEX2 and expressed in ARC by means of an adenoviral system. Then, we checked the expression levels and the subcellular localization of endogenous Cavβ2b and recombinant Cavβ2b-V5-APEX2. We found the endogenous Cavβ2b to be mainly associated to the membrane, but it was also detected in the cytosolic and nuclear fractions. As previously mentioned, Cavβ2 is predominantly localized at the dyadic junction, associated with Cav1.2 along the T-tubules (Gao T *et al.*,

1997). Our observation is in agreement with a previous work using membrane fractionation, which provided evidence of the differential subcellular distribution of the endogenous Cavβ2 subunit in canine ventricular cardiomyocytes. In this study, the authors analyzed by western blot a membrane homogenate and three sucrose density gradient fractions enriched in surface sarcolemma, T-tubular sarcolemma, and junctional complexes. Their results showed that the Cavβ2 isoform was preferentially localized in the T-tubular sarcolemma, with a weaker presence in the surface sarcolemma and junctional complexes (Foell JD *et al.*, 2004).

The Subcellular Protein Fractionation kit from Thermo Fisher Scientific used in our work enables the separation of a membrane fraction that comprises plasma, mitochondria and ER/Golgi apparatus membranes. Therefore, the Cavβ2b molecules found in this membrane fraction could be associated to Cav1.2 at the dyadic junction, or at the ER/Golgi apparatus when transporting this protein to the plasma membrane.

On the other hand, Cavβ2b is classified as a cytosolic protein based both on primary sequence analysis and on its subcellular localization when expressed in the absence of Cav1.2. In the presence of Cav1.2, Cavβ2 switches its localization from cytosolic to membrane-bound (Perez-Reyes E *et al.*, 1992; Buraei Z and Yang J, 2013). Although the detection of Cavβ2b in the cytosolic fraction suggests the existence of a pool of this protein that is not bound to the channel, the fact that this fraction was contaminated with membrane-associated proteins refutes this suggestion.

Additionally, we observed Cavβ2 also in the nuclear fraction. Our group recently provided the first evidence of a nuclear pool of Cavβ2 in primary isolated adult mouse and neonatal rat cardiomyocytes (unpublished data), as previously described for the cardiac HL-1 cell line (Rusconi F *et al.*, 2016). However, the mechanism whereby Cavβ2 translocates to the nucleus in cardiomyocytes is still unclear. Its relatively high molecular weight (72 kDa) makes it impossible for Cavβ2 to passively diffuse through the nuclear pores (Timney BL *et al.*, 2016). Therefore, the nuclear translocation of Cavβ2 would require the presence of a nuclear localization signal within its amino acid sequence or its interaction with a nucleus-targeted protein. The latter suggestion is supported by *in silico* predictions performed by our group in which no NLS could be identified within the sequence of Cavβ2 (unpublished data).

The recombinant Cavβ2b-V5-APEX2 protein was also detected in the three fractions analyzed, but with a more homogenous distribution than the endogenous Cavβ2b (Figure 9C). This difference in distribution does not pose a problem for the proteomic strategy

used in this work, since detectable levels of Cavβ2b-V5-APEX2 in each subcellular location are enough for the identification of proteins residing in the nanoenvironments of Cavβ2b. However, for the identification of the nanoenvironments of Cavβ2b the cardiomyocytes were lysed with NP-40, a detergent that does not lyse the nucleus. Therefore, the scope of this study excludes the identification of interactions between Cavβ2b and nearby proteins in the nucleus.

5.2 Identification of proteins in the Cavβ2b nanoenvironments using proximity labeling biotinylation

Proximity labeling biotinylation provides a means to capture the nanoenvironment of a protein as it exists *in situ*. Accordingly, we expected the Cavβ2b-V5-APEX2 fusion strategy to label not only interacting partners, but also other proteins in the vicinity of Cavβ2b. Such proteins, referred to as bystanders, comprise compartment-specific proteins residing in the local environment of the protein of interest, but not physically interacting nor directly participating in its function.

Sixty-one proteins were annotated as components of the Cavβ2b nanoenvironments in ARC. Importantly, 56 of these proteins were simultaneously identified by proximity labeling biotinylation as components of a Cav1.2 macromolecular complex (Liu G *et al.*, 2020). In that study, the authors generated transgenic mice with doxycycline-inducible, cardiomyocyte-specific expression of Cavα1 or Cavβ2b fused to APEX2. With this method the overexpression of the fusion proteins (Cavα1-APEX2 or Cavβ2b-APEX2) occurs *in vivo*, avoiding the use of adenovirus as expression system. The fact that 92% of the proteins identified in our study as constituents of the Cavβ2b nanoenvironments were commonly detected by another research group using a different strategy is a significant validation of our results and of the strategy and analytical tools used in our work. The remaining five proteins cannot be ruled out as part of the Cavβ2b nanoenvironments only because they were not identified by Liu G and coworkers, since they may have been missed by their detection strategy. Alternatively, these proteins may have been only randomly labeled by Cavβ2b-V5-APEX2 while accidentally interacting with the recombinant protein in a crowded molecular environment or when passing close to it.

Among the proteins of the Cavβ2b nanoenvironments identified in our study, ahnak had previously been reported as a Cavβ interacting partner (Haase H *et al.*, 1999). The interaction of Cavβ2 with ahnak was detected by coimmunoprecipitation using cardiomyocytes isolated from rodent or human hearts (Haase H *et al.*, 1999). It has been suggested that the phosphorylation of Cavβ2 and ahnak by PKA weakens the interaction

between the two proteins and upregulates L-type Ca^{2+} currents (Haase H *et al.*, 2005, 2007). The previously reported Cavβ2 interactors CAMKII and actin (Grueter CE *et al.*, 2008; Stölting G *et al.*, 2015) were also identified in our study, but were not included in the final list as constituents of the Cavβ2b nanoenvironments because they did not meet the cutoff criteria from the proteomic analysis. The cutoff we used for the classification of proteins as interactors separates enriched proteins from background binders by accepting only the proteins identified in all the replicates and enriched more than one standard deviation above the population mean while meeting statistical significance ($p < 0.01$). A stringent cutoff leads to a low false positive rate, but may miss weaker or more transient interactors, such as CAMKII and actin. Alternatively, a permissive cutoff would include these, but at the cost of increasing false positives. In our study, the stringent cutoff excluded the VDAC1 channel as a constituent of Cavβ2b nanoenvironments. Pull-down assays followed by western blot using an anti-VDAC1 antibody confirmed that the recombinant protein GST-strep-Cavβ2b does not interact with this channel and therefore that VDAC1 is not an interacting partner of Cavβ2b (Figure 16B).

As the main binding partner of Cavβ2 in cardiomyocytes, Cav1.2 was expected to be identified by our proteomics approach. However, no peptide from this protein was detected by MS. Cav1.2 is a transmembrane protein containing four homologous repeats (I-IV), each with six transmembrane segments (S1-S6) (Figure 2A). The low abundance, limited solubility and restricted enzyme accessibility are major factors that make the analysis of transmembrane proteins more difficult than for common soluble proteins. The combination of SDS-PAGE, in gel-digestion and LC-MS/MS has been applied to transmembrane protein analyses, but the remaining problems of protein insolubility and the low recovery of hydrophobic peptides from in-gel digestion still hinder protein identification (Lu B *et al.*, 2008; Schey K *et al.*, 2013; Zhan LP *et al.*, 2018).

In contrast to our results, Liu G *et al.* (2020) identified Cav1.2 by MS as an interacting partner of Cavβ2b. Differences in the sample preparation method could explain these different outcomes. For example, while they added trypsin to digest the complexes captured on the beads (on-bead digestion), we used an in-gel digestion method, where Cavβ2b-V5-APEX2 and its interacting proteins were eluted from the beads and an SDS-PAGE step was performed before trypsin digestion. The addition of further steps could reduce the recovery of the peptides and make the identification of less abundant proteins more difficult. However, although we could not identify Cav1.2 using MS, western blot analysis after the streptavidin enrichment of biotinylated proteins revealed a robust

biotinylation of Cav1.2 by Cavβ2b-V5-APEX2 (Figure 10B), which supports the validity of the proximity labeling biotinylation strategy used in our work.

The results of our database search indicated that the proposed constituents of the Cavβ2b nanoenvironments are present in distinct cellular compartments (Figure 12A). Among these potential interactors, 35% are localized in the cytosol, whereas 19% of the identified proteins, shown in figure 12A as nuclear proteins, can be found both in the nucleus and the cytosol. Since the cell lysis buffer used in this experiment contained only the NP-40 detergent, which does not lyse the nucleus, none of the proteins classified as nuclear could have been biotinylated in this organelle but had to be biotinylated in the cytosol.

Cytoskeletal proteins accounted for 19% of the final candidates identified in our study (Figure 12A), including proteins that interact selectively and non-covalently with actin filaments. One of the cytoskeletal proteins identified was α-actinin 2, whose primary function is to crosslink filamentous actin molecules and titin molecules from adjoining sarcomeres at Z-discs (Beggs AH *et al.*, 1992; Grison M *et al.*, 2017). Of the four members of the α-actinin family, only the isoforms α-actinin 2 and α-actinin 3 localize at the Z-discs, with α-actinin 2 as the major isoform in cardiomyocytes (Sjoblom B *et al.*, 2008). Aside from their interactions with actin filaments, the α-actinin family members interact with many cytoskeletal and regulatory proteins (Otey C and Carpen O, 2004). It has been reported that α-actinin 1 binds to the proximal C-terminus of Cav1.2, thereby enhancing not only the surface localization but also the activity of the channel in neurons (Hall D *et al.*, 2013; Tseng P *et al.*, 2017; Turner M *et al.*, 2020). However, no such physical interaction of α-actinin 2 with Cav1.2 or the Cavβ2b subunit has been described to occur in cardiomyoyctes. The results of our strep-tag pull-down and confocal microscopy studies indicate that there could be a close association between Cavβ2b and α-actinin 2 in these cells (Figure 16A and 17), as previously suggested by Gao T *et al.* (1997). However, it remains to be determined whether these two molecules actually interact in cardiomyoyctes or if there is an indirect interaction between them that could be mediated by Cav1.2 or other proteins of the cytoskeleton such as actin.

We also identified the filamin-C (FLN-C) isoform as a potential interacting partner of Cavβ2b. This protein is expressed primarily in adult cardiac tissue and localizes in the Z-discs, sarcolemma and intercalated discs (Thompson TG *et al.*, 2000; van der Ven PF *et al.*, 2000; Dalkilic I *et al.*, 2006). FLN-C has been shown to interact with many proteins, but its specific functions are not clear. Filamin family members are actin cross-linkers and serve as scaffolds for many other proteins, including channels, receptors, intracellular signaling molecules, and transcription factors (Nakamura F *et al*., 2011). On the other

hand, vinculin, another protein identified in our study, is an actin-binding protein that is essential for embryogenesis and participates in cardiomyocyte adhesion and contraction. It was recently demonstrated that the recruitment of vinculin is required to couple the cardiomyocyte adherent junctions to the contractile actin, and this stabilizes the adherent junctions-actin interface under mechanical load (Merkel CD *et al.*, 2019). We did not identify actin among the potential binding partners of Cavβ2b. Stölting G *et al*. (2015) had previously demonstrated that Cavβ2 interacts with actin filaments and suggested that the latter provide the tracks for transporting the channels to the cell surface in the HL-1 cardiac muscle cell line. However, this hypothesis has been challenged by the results of Liu G *et al.* (2020), which suggest that the Cavβ2 subunit is not necessary for the trafficking of the channel in cardiomyocytes.

JPH2 is another protein identified in the nanoenvironments of Cavβ2b by MS. This result was confirmed by western blot analyses after proximity labeling biotinylation with Cavβ2b-V5-APEX2 (Figure 14) and after strep-tag pull-down with the recombinant protein His-strep-Cavβ2b (Figure 15B). JPH2 is a membrane-binding protein that provides a structural bridge between T-tubules and the SR and is required for normal EC coupling in cardiomyocytes (Takeshima H *et al.*, 2000). JPH2 contributes significantly to the overall structure of the dyad. When JPH2 levels are reduced in mice, T-tubules either do not form or remain in an immature longitudinal configuration (Jones P *et al.*, 2018). Since the dyadic anchor JPH2 has been shown to interact with LTCC and RyR2 (Jiang M *et al.*, 2016; Munro ML *et al.*, 2016), it might work together with Cavβ2b to maintain LTCC and the RyR2 as part of a dyadic protein complex (Lucia L *et al.*, 2011), especially in embryonic hearts, where both Cavβ2b and JPH2 are essential (Takeshima H *et al.*, 2000; Weissgerber P *et al.*, 2006).

The proteins identified in the nanoenviroments of Cavβ2b are involved in diverse biological processes (Figure 12B and Figure 13). However, this does not mean that Cavβ2b is involved in all these processes. Moreover, as previously mentioned, some of these proteins are only bystanders in relation to Cavβ2b and neither interact physically with it nor directly participate in its function. The evidence available so far is still insufficient to establish a link between Cavβ2b and most of the biological process in which the proteins identified in its nanoenvironments might participate.

5.3 Interaction of Cavβ2b with the RyR2 through the Cavβ2b-SH3 domain

Among the potential Cavβ2b interactors identified in this work, we focused on the RyR2, since it was one of the proteins detected with the highest accuracy by MS. This protein is the predominant isoform of the RyR in cardiac muscle (Nakai J *et al.*, 1990; Otsu K *et al.*, 1990), localizes in the SR membrane and mediates the release of Ca^{2+} from the SR during EC coupling. Another RyR isoform, RyR1, is primarily expressed in skeletal muscle (Takeshima H *et al.*, 1989; Zorzato F *et al.*, 1990) and has been demonstrated to interact with Cavβ1a, the skeletal muscle isoform of Cavβ (Cheng W *et al.*, 2005; Rebbeck RT *et al.*, 2011; Hernández-Ochoa EO *et al.*, 2014). Cavβ1a mediates the translocation of Cav1.1 to the triad and its assembly into tetrads that are closely aligned with the RyR1 in the SR, thereby facilitating the Cav1.1-RyR1 interaction. Indeed, a cry-electron microscopy study of Cav1.1 pointed to the role of Cavβ as an anchor that helps the flexible II-III loop of Cavα1 to interact with the RyR1 (Hu H *et al.*, 2015).

In our study, we demonstrated for the first time the interaction between the cardiac muscle isoform Cavβ2b and the RyR2, as evidenced by the results from biotinylation experiments with Cavβ2b-V5-APEX2 (Figure 14), *in vitro* pull-down with the recombinant protein strep-Cavβ2b (Figures 15 and 19) and coimmunoprecipitation (Figure 18). Additionally, we demonstrated that the SH3 domain of Cavβ2b is involved in the binding of this protein to the RyR2 (Figure 19). This is not surprising, since diverse SH3 domains participate in many protein-protein interactions by binding to polyproline-rich motifs in target proteins (Mayer BJ, 2001). Most of the previously validated partners of Cavβ have been proposed to interact with its SH3 domain. For example, the binding of Cavβ and bestrophin-1 is mediated by the interaction between the SH3 domain of Cavβ and PxxP motifs on the C-terminus of bestrophin-1 (Reichhart N *et al.*, 2010; Milenkovic VM *et al.*, 2011). The pore-forming subunit of the BKCa channel interacts with Cavβ1 through a non-canonical SH3-binding motif (Zou S *et al.*, 2008), while dynamin interacts *in vitro* with the SH3 domain of Cavβ2 and this interaction seems to facilitate the recruitment of dynamin to the plasma membrane (Gonzalez-Gutierrez G *et al.*, 2007). Additionally, the interaction of Cavβ2 with actin filaments seems to occur through the SH3 and GK domains of Cavβ2 (Stölting G *et al.*, 2015). Moreover, although the region of Cavβ2 responsible for its interaction with ahnak is unknown, it is probably located in the conserved GK or SH3 domains, since ahnak coimmunoprecipitates with Cavβ1b, Cavβ2, Cavβ3 and Cavβ4b (Haase H *et al.*, 1999; Hohaus A *et al.*, 2002; Alvarez J *et al.*, 2004; Shao Y *et al.*, 2009; Jin J *et al.*, 2019).

Crystallography studies of Cavβ show that the SH3 domain is exposed to the cytosol. However, the PxxP-binding site is occluded by the HOOK region and a loop linking two

consecutive β-sheets in SH3 (Chen YH *et al.*, 2004; Opatowsky Y *et al.*, 2004; Van Petegem F *et al.*, 2004). Simulated docking predictions indicate that canonical binding residues in the SH3 domain are unlikely to interact with PxxP motifs. Several authors propose that the interaction may occur through non-canonical binding residues or require a structural rearrangement that would likely expose the PxxP-binding site on the SH3 domain to enable the binding of Cavβ to other proteins (Chen YH *et al.*, 2004; Gonzalez-Gutierrez G *et al.*, 2007).

In our experiments we could not assess whether the GK domain of Cavβ2b is involved in the interaction with the RyR2, since we failed to purify this protein fragment. However, the GK domain strongly interacts with Cav1.2, functioning as a regulator of the channel activity, and it is therefore unlikely that it also interacts with the RyR2 (Pragnell M *et al.*, 1994; De Waard M *et al.*, 1995; Gonzalez-Gutierrez G *et al.*, 2008).

According to studies using Cavβ1a/Cavβ2a chimeras and truncation mutants, some distinctive elements in the C-terminus of the Cavβ1a subunit are critical for its binding to the RyR1 and their deletion leads to the loss of EC coupling in skeletal muscle cells (Beurg M *et al.*, 1999; Sheridan DC *et al.*, 2003; Cheng W *et al.*, 2005; Rebbeck RT *et al.*, 2011; Eltit JM *et al*., 2014; Hernández-Ochoa EO *et al.*, 2014). However, the C-terminal region of Cavβ2b is 115 amino acids longer than that of Cavβ1a, is predicted to be more hydrophilic and seems not to be involved in the interaction with the RyR2 (Figure 19C).

The Cavβ2b-binding site in the RyR2 is still unknown. Looking for canonical or non-canonical SH3-binding motifs in the RyR2 (accession number B0LPN4), we used the **L**inear **M**otif **D**omain **I**nteraction **Pred**iction (LMDIPred) web server, an online resource for sequence-based prediction of binding sites for SH3, WW or PDZ domains (Sarkar D *et al*., 2018). The predicted motifs were a canonical SH3-binding sequence (^{1574}**P**QC**PP**R^{1579}) in the SPRY3 domain of the RyR2 and a non-canonical sequence (^{4672}KK**P**KKD^{4677}) in its S2S3 domain (Peng W *et al.*, 2016) (Figure 24A).

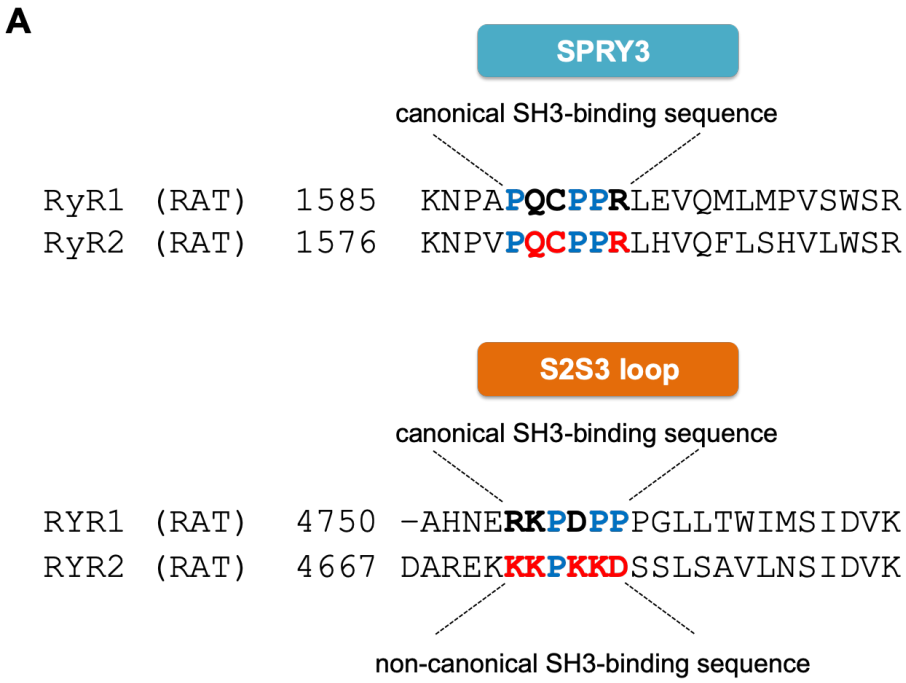

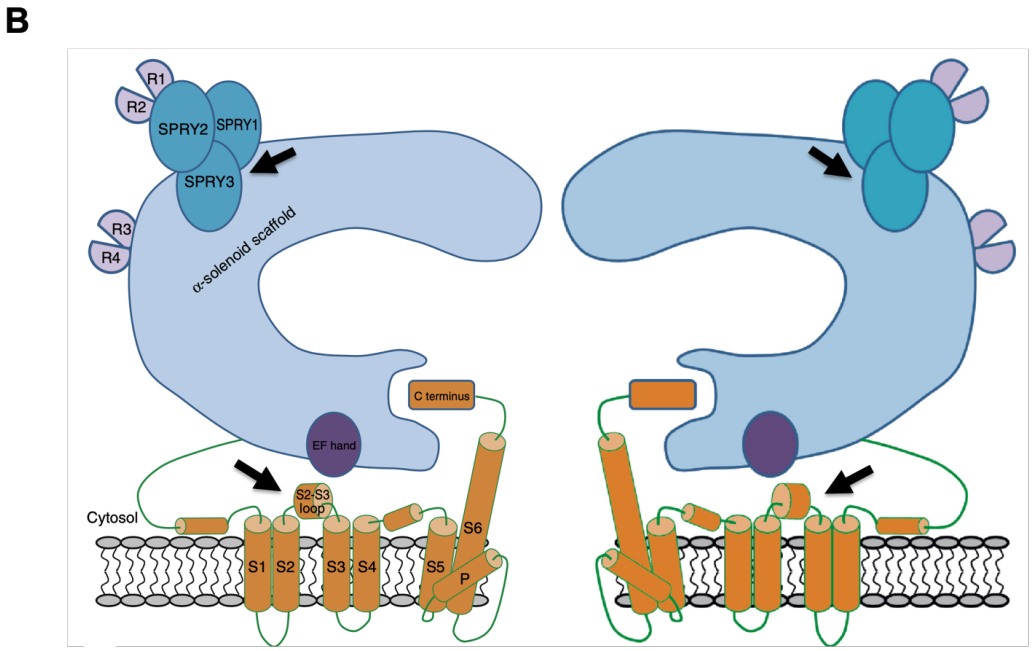

Figure 24. Predicted canonical and non-canonical SH3-binding sites in the RyR. (A) Sequence fragments containing predicted canonical and non-canonical SH3-binding sites in the SPRY3 domain and the S2S3 domain of rat RyR1 and RyR2. The SPRY3 and S2S3 domains are shown by black arrows in the figure (B). (B) Representation of two subunits of the RyR channel, taken from Liu B *et al*. (2018).

SPRY domains are often involved in protein-protein interactions (Wang D *et al.*, 2002, 2005). In the RyR, SPRY1 forms a binding site for FKBP12 (12-kDa FK506-binding protein) together with the Handle domain (Yan Z *et al.*, 2015). SPRY2 has been suggested to participate in the interaction with the cytosolic loop connecting the

transmembrane repeats II and III of Cav1.1, and to have a functional role in EC coupling in skeletal muscle (Cui Y *et al.*, 2009; Tae HS *et al.*, 2009, 2011). However, recent work negates the SPRY2 domain of the RyR1 as the major link with Cav1.1 (Lau K and Van Petegem F, 2014). SPRY3 has also been suggested to participate in the direct coupling mechanism in skeletal muscle (Perez CF *et al*., 2003; Bai XC *et al*., 2016). This region contains the LZ2 motif that mediates the binding of PP2A to the RyR2 (Marx SO *et al.*, 2001; Meissner G, 2017). It also includes a long disordered loop that corresponds to divergent region 2 (DR2) and represents one of the most prominent differences among the three RyR isoforms (Willegems K and Efremov RG, 2017). DR2 is present in both RyR1 (amino acids 1342-1403) and RyR2 (amino acids 1316-1400), but is almost completely absent in RyR3 (Sorrentino V and Volpe P, 1993). Deletion of DR2 from the RyR1 selectively abolished depolarization-evoked Ca^{2+} transients (Perez CF *et al*., 2003). Since SPYR3 is positioned on the upper surface of the RyR (Figure 24B), facing the plasma membrane, it might be involved in interactions with proteins located in the terminal junctions, like Cavβ2b. In the future, interaction experiments combining site-directed mutagenesis should be performed to elucidate the specific binding site on the RyR2 that is important for its interaction with Cavβ2b.

Considering that the canonical SH3-binding sequence **P**QC**PP**R is conserved in the RyR1 and the RyR2, the SH3 domain of the skeletal isoform Cavβ1a could, in addition to the C-terminus, provide a binding site for the interaction of Cavβ1a with the RyR1. However, although the role of the SH3 domain in this interaction cannot be ruled out, it is worth noting that the SH3 domain of Cavβ1a has the highest sequence variation between the Cavβ isoforms. Specifically, as opposed to all other Cavβ isoforms, Cavβ1a lacks a salt-bridge between the acidic RT-loop and a conserved basic residue in the α2 helix of its SH3 domain (Norris NC *et al.*, 2017). Other authors have postulated that the SH3 domain of Cavβ1a interacts intramolecularly with a proline-rich region in the C-terminus, and that this interaction is required for Cav1.1 to act as a voltage sensor during EC coupling. According to this hypothesis, such interaction would enable the Cavβ1a subunit to adopt the appropriate conformation necessary to trigger its specific voltage-sensing function (Dayal A *et al.*, 2013).

The S2S3 domain of the RyR1 contains a short linear proline-rich motif, ^{4754}RK**P**D**PP**^{4759} (accession number F1LMY4) that is conserved in different species but differs between RyR isoforms. The location of this motif close to the gating machinery in the core region of the channel suggests that it may play a regulatory role, probably as a potential SH3-binding site (des Georges A *et al.*, 2016). Contrary to the RYR1 and as previously

mentioned, the S2S3 domain in the RyR2 contains the non-canonical motif ^{4672}KK**P**KKD^{4677} as an SH3-binding site (Figure 24A). However, based on the structural model proposed for the Cav1.1-RyR1 interaction complex (Bai XC *et al*., 2016), we think that it is unlikely for this motif to interact with Cavβ2b when linked to Cav1.2, most probably due to distance and steric hindrance factors.

5.4 Functional role of the Cavβ2b-RyR2 interaction in adult rat cardiomyocytes

To investigate the functional role of the interaction between Cavβ2b and the RyR2, we overexpressed the SH3 domain of Cavβ2b and assessed the effects on L-type Ca^{2+} currents and Ca^{2+} transients in ARC of its competition with the full-length Cavβ2b for the binding site on the RyR2. L-type Ca^{2+} currents after overexpression of the Cavβ2b-SH3 domain in ARC were similar in density and voltage dependence to the currents recorded in the negative control cells (Figure 21). Interestingly, an increase in the total expression levels of the Cav1.2 channel was observed in Cavβ2b-SH3-overexpressing cardiomyocytes compared to control cells (Figure 20). A possible explanation for this result can be found in studies reporting that the SH3 domain of Cavβ2 promotes Cav1.2 endocytosis (Gonzalez-Gutierrez G *et al.*, 2007). Accordingly, the overexpression of the Cavβ2b-SH3 domain could increase the amount of internalized LTCC and consequently stimulate the *de novo* synthesis of LTCC as a compensatory mechanism, without affecting the total amount of Cav1.2 in the membrane and thus keeping Cav1.2-mediated Ca^{2+} currents unaltered.

In the majority of species, including humans, increased heart rate increases cardiac contractility (Pieske B *et al.*, 1999). The variation of myocyte contraction strength with increasing pacing frequencies is known as the force-frequency relationship (FFR) and is considered positive or negative depending on whether the contractile strength increases or decreases, respectively. With each heartbeat, cardiomyocytes undergo depolarization and activate the LTCC that, in turn, induce an influx of Ca^{2+}. The Ca^{2+} entering the cell signals the opening of the RyR in the SR, triggering rapid CICR (Bers D, 2002; Eisner D *et al.*, 2017). The release of Ca^{2+} from the intracellular calcium stores provokes an increase in the cytosolic Ca^{2+} concentration, which induces contraction of the myofilaments. This CICR is fundamental to maintaining a positive FFR (Endoh M, 2004). Thus, an increase in the heart pacing frequency enhances CICR and leads to a significant increase in the cardiac muscle contractile force. The ventricular myocardium in humans has a positive FFR (Pieske B *et al.*, 1999), whereas studies of the FFR in rats have provided contradictory results, with negative (Bouchard R and Bose D, 1990) or positive FFR

(Frampton JE *et al*., 1991; Layland J and Kentish J, 1999; Dibb KM *et al.*, 2007) being reported. Central to this contradiction are the conditions under which experiments are performed, especially the pacing frequency, the temperature and the extracellular calcium concentration. Borzak S *et al.* (1991) observed a biphasic FFR in rats that was negative in the range of 0.1-1.0 Hz, flat in the range of 1.0-2.0 Hz and positive between 2.0 and 6.0 Hz. Other authors have later obtained similar results (Gattoni S *et al.*, 2016), but the physiological mechanism behind these findings is not yet well understood.

In our study we evaluated the effect of the overexpression of the Cavβ2b-SH3 domain on Ca^{2+} transients in cardiomyocytes at different stimulation frequencies (0.5, 1.0, 2.0, 3.0, 4.0 Hz). We did not detect differences in the amplitude of the Ca^{2+} transients between control and Cavβ2b-SH3-expressing cardiomyocytes measured at low pacing frequencies (0.5-2.0 Hz) (Figure 22C). This suggests that the Cavβ2b-mediated interaction between LTCC and the RyR2 does not play a critical role in CICR at low myocyte beating rates. However, high pacing frequencies (3.0-4.0 Hz) significantly increased the amplitude of the Ca^{2+} transients in control ARC, a response that was not observed in Cavβ2b-SH3-expressing cardiomyocytes (Figure 22C). Since the Cavβ2b-mediated interaction between LTCC and the RyR2 is probably disrupted in Cavβ2b-SH3-expressing ARC, their unresponsiveness to increased pacing stimuli strongly suggests that this interaction is necessary to upregulate CICR at high pacing frequencies and therefore to enhance contraction.

An increase in pacing frequency induces higher systolic Ca^{2+} transient amplitudes. This effect has been proposed to be mediated by the frequency-dependent activation of calcium/calmodulin-dependent serine/threonine kinase-δ (CaMKIIδ) (Maier LS and Bers DM, 2007), a dodecameric holoenzyme located in the cardiac muscle. At high Ca^{2+} concentrations CaMKIIδ is activated by Ca^{2+}-calmodulin and phosphorylates itself at amino acid Thr287, which enables the enzyme to remain active even when Ca^{2+} levels are low (Miller SG and Kennedy MB, 1986; Hanson PI *et al.*, 1989). It has been hypothesized that the cardiac CaMKIIδ alternates between a phosphorylated active state during cardiac muscle contraction and a dephosphorylated resting state during relaxation. At higher heart beating frequencies, the dephosphorylation rate of CaMKIIδ is not high enough to bring the enzyme back to a resting state before the onset of the next Ca^{2+} transient, which progressively increases the amount of phosphorylated active CaMKIIδ (De Koninck P and Schulman H, 1998). It has been suggested that at high stimulation frequencies the phosphorylation of the RyR2 mediated by the Ca^{2+}/calmodulin kinase-II increases Ca^{2+} transient amplitudes (Kushnir A *et al.*, 2010). However, further elucidation is needed of

how the phosphorylation of the RyR2 combines with the interaction of LTCC and RyR2 through Cavβ2b to upregulate CICR at high pacing frequencies.

In this work, we revealed for the first time a new element of the EC coupling mechanism in cardiomyocytes, namely the interaction between Cavβ2b and the RyR2, which has an important role in CICR at high myocyte beating rates. This finding does not refute the role of the activation of the RyR2 by the Ca^{2+} entering through Cav1.2 as the primary mechanism triggering EC coupling in cardiac cells (Eisner D *et al.*, 2017). Instead, the interaction between Cavβ2b and the RyR2 could serve as a regulatory element that increases Ca^{2+} release by the RyR2 in response to external stimuli requiring an increase in cardiac contraction frequency.

On the other hand, although the physical coupling between Cav1.1 and the RyR1 in skeletal muscle has been clearly demonstrated (Paolini C *et al.*, 2004; Allard B, 2018), it is generally assumed that Cav1.2 and the RyR2 do not directly interact with each other (Franzini-Armstrong C and Protasi F, 1998). However, some authors have suggested a potential interaction between Cav1.2 and the RyR2 (Huang G *et al.*, 2007; Gez LS *et al.*, 2012). A study using Cav1.2 mutants showed that a Ca^{2+}-impermeable Cav1.2 mutant triggered Ca^{2+} transients in neonatal rat cardiomyocytes in the absence of Ca^{2+} influx to the cells (Gez LS *et al.*, 2012). In contrast, a mutation destroying the Ca^{2+}-binding site of the channel abrogated both the spontaneous and the electrically-evoked contraction of the cardiomyocytes. The Ca^{2+} bound to Cav1.2´s selectivity filter seems to provide a signal that activates the RyR2 in response to a conformational change in Cav1.2 during membrane depolarization, but not to the Ca^{2+} ions that enter in the dyadic space (Gez LS *et al.*, 2012).

It has been reported that Homer1 proteins modulate a dynamic interaction between Cav1.2 and the RyR2 in smooth muscle cells, where CICR is also mediated by these two channels. This interaction seems to play an important regulatory role in EC coupling by reducing the responsiveness of the muscle to cell stimulation. The most likely mechanism by which Homer1 affects EC coupling has been suggested to involve the restriction of the interaction between Cav1.2 and RyR2 by restraining the conformational change of these channels required for efficient CICR. A similar mechanism could be relevant for the EC coupling in cardiac muscle cells (Huang G *et al.*, 2007).

The results of our work and previously published evidence suggest that the formation of a complex comprising Cav1.2 and the RyR2 could be an as yet unknown step in the mechanism of EC coupling in cardiomyocytes, where Cavβ2b would conceivably play a more relevant role at high beating rates.

In a previous report, adult mice with cardiomyocyte-specific conditional deletion of the Cavβ2 gene (*Cacnb2*) appeared healthy and did not show any apparent abnormalities or signs of cardiac decompensation under physiological conditions, as determined by their heart rate, the heart, lung and liver weights, as well as the water content of lung and liver (Meissner M *et al.*, 2011). In the cardiomyocytes of these animals, conditional deletion of the *Cacnb2* gene reduced Cavβ2 protein expression by 96%, but caused only a 29% reduction in Ca^{2+} current density at 0 mV. However, neither Ca^{2+} transients nor other parameters related with EC coupling were measured in that study. Therefore, we cannot rule out that, despite the absence of severe impairment of the heart, Ca^{2+} transients and the EC coupling in cardiomyocytes may have been affected by the deletion of the *Cacnb2* gene. This could become apparent during stress exposure, when the FFR is particularly relevant. The measurement of the Ca^{2+} transients at different stimulation frequencies in the Cavβ2-defficient cardiomyocytes isolated from these mice could validate the role of Cavβ2 in CICR at high myocyte beating rates. By using this model, we would expect an increase in the stimulation frequency to reduce the Ca^{2+} transients in Cavβ2-defficient cardiomyocytes as compared to wild-type cardiomyocytes.

On the T-tubule side of the dyad, LTCC are arranged opposite to the RyR clusters. Previous studies indicate that the membrane area occupied by the Cav1.2 clusters is smaller than the one populated by their neighboring RyR2, with the Cav1.2 channels approximately facing the center of these RyR2 clusters (Scriven DRL *et al.*, 2010). The precise mechanism by which individual or grouped LTCC may be anchored and apposed to RyR is unclear, since it is unknown whether Cav1.2 binds directly to the RyR2. It is conceivable that, like in skeletal muscle, the binding of Cavβ2b to the RyR2 is required for an efficient crosstalk between the LTCC and the RyR. This interaction could increase the probability that an entering Ca^{2+} ion may find its binding site on the RyR2, thereby reducing the number of ions required for RyR2 activation.

The cryo-electron microscopy structures of an LTCC complex and the RyR2 were recently published (Wu J *et al.*, 2015; Peng W *et al.*, 2016). According to these reports, the Cavβ subunit in the LTCC complex projects away from the channel by around 7 nm into the intracellular space (Figure 25A) and the big cytosolic domain of the RyR2 protrudes about 15 nm into the cytosol (Figure 25B). Since the gap between the T-tubules and the SR is known to be ~12-20 nm at the dyads (Shaw RM and Colecraft HM, 2013), the Cavβ2 subunit could mediate the docking of LTCC at the RyR2 (Figure 25C) by approaching the two channels and thereby increasing the efficiency of the EC coupling. Alternatively,

Cavβ2b could play a functional role by directly activating the RyR2. These potential roles of the Cavβ2b subunit are not mutually exclusive.

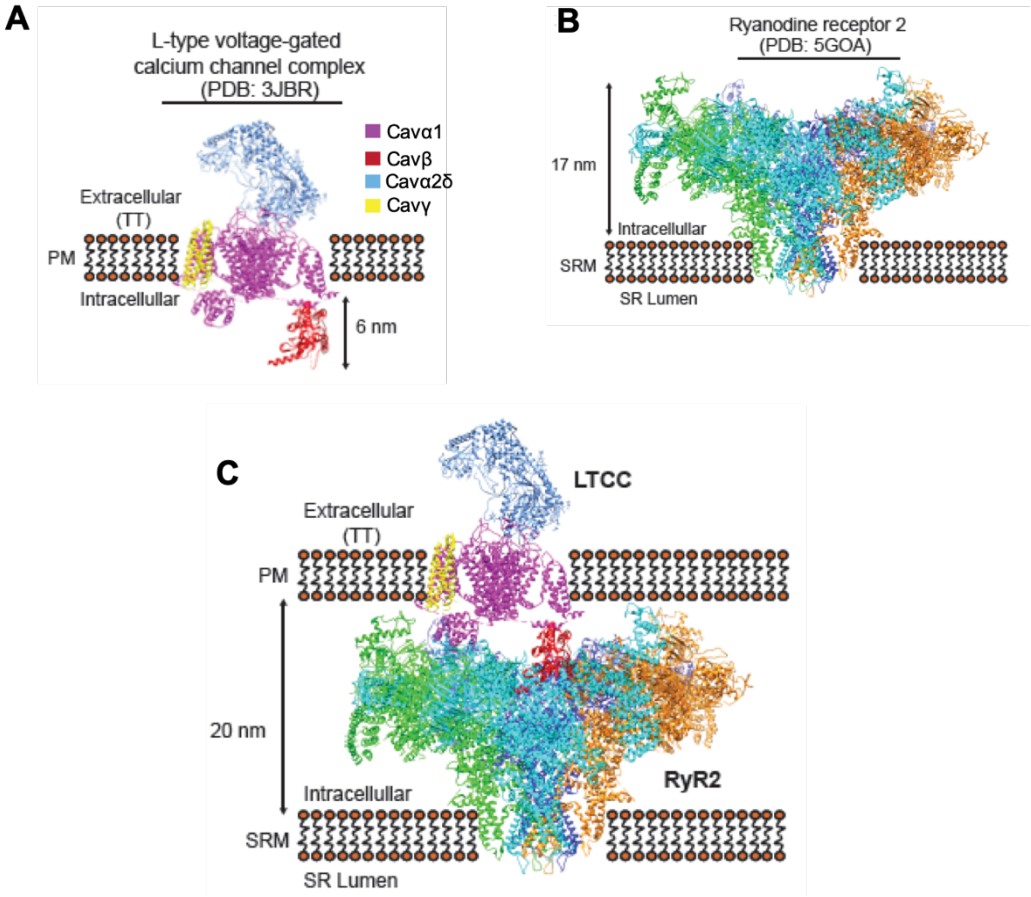

Figure 25. Molecular modeling of the Cavβ2-mediated complex between the LTCC and the RyR2 in adult rat cardiomyocytes. (A) Cryo-EM structure of the LTCC (Protein Data Bank: 3JBR) on the plasma membrane showing the Cavα1 (magenta), Cavβ2 (red), Cavα2δ (blue) and Cavγ (yellow) subunits. (B) Cryo-EM structure of the RyR2 (Protein Data Bank: 5GOA) on the sarcoplasmic reticulum membrane. The four RyR2 subunits are represented in either green, gold, cyan or dark blue. (C) Combination of the structural models from (B) and (C) showing that Cavβ could potentially mediate the interaction between LTCC and RyR2 within the 20-nm distance separating the PM and the SR where both channels are respectively located. LTCC: L-type voltage-gated calcium channel; PDB: Protein Data Bank; PM: plasma membrane; RyR2: ryanodine receptor 2; SR: sarcoplasmic reticulum; SRM: sarcoplasmic reticulum membrane; TT: T-tubules.

5.5 Conclusions, limitations and prospects

Overall, in our work we mapped the protein interaction network of Cavβ2b in rodent hearts and demonstrated that an interaction occurs between this protein and one of its identified partners, the RyR2, mediated by the SH3 domain of Cavβ2b. Further characterization of this interaction will be necessary in order to determine the Cavβ2b-binding site on the RyR2. Interaction studies between the SPRY3 domain of the RyR2 and the SH3 domain of Cavβ2b could support such characterization.

We also took the first steps to study the function of the interaction between Cavβ2b and the RyR2, which seems to have an important role in CICR at high cardiomyocyte beating rates. We assumed that the overexpression of the Cavβ2b-SH3 domain would displace the endogenous Cavβ2b from its interaction with the RyR2. However, this premise was not demonstrated in our work and is its main limitation. Competition studies using cardiomyocytes from transgenic mice overexpressing the Cavβ2b-SH3 domain could extend the knowledge resulting from our current study. Additionally, the measurement of the Ca^{2+} transients at different stimulation frequencies in Cavβ2-defficient cardiomyocytes from the mouse model generated by Meissner M *et al.* (2011) could provide valuable support to our suggestion that Cavβ2b plays a role in CICR.

It is worth mentioning that the use of the Cavβ2b-SH3 domain to displace Cavβ2b from its interaction with the RyR2 could bring about the disruption of the interaction of Cavβ2b with other proteins. So far, only two proteins, dynamin and actin, have been reported to interact with Cavβ2 through its SH3 domain (Gonzalez-Gutierrez G *et al.*, 2007; Stölting G *et al.*, 2015). Dynamin regulates the endocytosis of Cav1.2 and actin seems to participate in the traffic of the channel to the cell surface. Although the displacement of Cavβ2 from its interaction with these two partners would not explain the fact that the changes in calcium transients only occur at high stimulation frequencies, we cannot rule out the possibility that other proteins are affected.

Of the 61 proteins identified as constituents of the Cavβ2b nanoenvironments using an APEX2-catalyzed proximity labeling method, we focused on the RyR2 for the validation of its interaction with Cavβ2b. However, the characterization of the interaction of Cavβ2 with other proteins like JPH2 and α-actinin 2 and the study of the functional role of these interactions could contribute to a better understanding of the role of Cavβ2 in the physiology of cardiomyocytes.

6. REFERENCES

Abiria, S. A. and Colbran, R. J. (2010) 'CaMKII associates with Cav1.2 L-type calcium channels via selected beta subunits to enhance regulatory phosphorylation', *Journal of Neurochemistry*, 112(1), pp. 150-161. doi: 10.1111/j.1471-4159.2009.06436.x.

Alexander, S. P. *et al.* (2017) 'The concise guide to pharmacology: voltage-gated ion channels', *British Journal of Pharmacology*, 174 Suppl, pp. S160-S194. doi: 10.1111/bph.13884.

Allard, B. (2018) 'From excitation to intracellular Ca2+ movements in skeletal muscle: Basic aspects and related clinical disorders', *Neuromuscular Disorders*, 28(5), pp. 394-401. doi: 10.1016/J.NMD.2018.03.004.

Altier, C. *et al.* (2011) 'The Cavβ subunit prevents RFP2-mediated ubiquitination and proteasomal degradation of L-type channels', *Nature Neuroscience*, 14, pp. 173. doi.org/10.1038/nn.2712.

Alvarez, J. *et al.* (2004) 'Calcium current in rat cardiomyocytes is modulated by the carboxyl-terminal Ahnak domain', *Journal of Biological Chemistry*, 279(13), pp. 12456-12461. doi: 10.1074/jbc.M312177200.

Amini, F. *et al.* (2002) 'Protein affinity labeling mediated by genetically encoded peptide tags', *Angewandte Chemie*, 41(2), pp. 356-359. doi: 10.1002/1521-3773(20020118)41:2<356::aid-anie356>3.0.co;2-m.

Baddeley, D. *et al.* (2009) 'Optical single-channel resolution imaging of the ryanodine receptor distribution in rat cardiac myocytes', *Proceedings of the National Academy of Sciences*, 106(52), pp. 22275-22280. doi: 10.1073/pnas.0908971106.

Bai, X. C. *et al.* (2016) 'The central domain of RyR1 is the transducer for long-range allosteric gating of channel opening', *Cell Research*, 26(9), pp. 995-1006. doi: 10.1038/cr.2016.89.

Beggs, A. H. *et al.* (1992) 'Cloning and characterization of two human skeletal muscle alpha-actinin genes located on chromosomes 1 and 11', *The Journal of Biological Chemistry*, 267(13), pp. 9281-9288.

Béguin, P. *et al.* (2001) 'Regulation of Ca2+ channel expression at the cell surface by the small G-protein kir/Gem', *Nature*, 411(6838), pp. 701-706. doi: 10.1038/35079621.

Béguin, P. *et al.* (2007) 'RGK small GTP-binding proteins interact with the nucleotide kinase domain of Ca2+-channel β-subunits via an uncommon effector binding domain', *Journal of Biological Chemistry*, 282(15), pp. 11509-11520. doi: 10.1074/jbc.M606423200.

Béguin, P. *et al.* (2014) 'BARP suppresses voltage-gated calcium channel activity and Ca2+-evoked exocytosis', *The Journal of Cell Biology*, 205(2), pp. 233-249. doi: 10.1083/jcb.201304101.

Beharier, O. *et al.* (2007) 'Crosstalk between L-type calcium channels and ZnT-1, a new player in rate-dependent cardiac electrical remodeling', *Cell Calcium*, 42(1), pp. 71-82. doi: 10.1016/j.ceca.2006.11.007.

Bendayan, M. (2001) 'Worth its weight in gold', *Science*, 291(5507), pp. 1363-1365. doi: 10.1126/science.291.5507.1363.

Bers, D. M. (2002) 'Cardiac excitation-contraction coupling', *Nature*, 415(6868), pp. 198-205. doi: 10.1038/415198a.

Bers, D. M. (2014) 'Sources and sinks of Ca2+ in myocytes: sarcolemma, sarcoplasmic reticulum, mitochondria excitation-contraction coupling', in *Cardiac Electrophysiology: From Cell to Bedside: Sixth Edition*, Elsevier, pp. 161-169. doi: 10.1016/B978-1-4557-2856-5.00016-9.

Bers, D. M. (2017) 'Excitation-Contraction Coupling', in *Cardiac Electrophysiology: From Cell to Bedside: Seventh Edition*, Elsevier, pp. 151-159. doi: 10.1016/B978-0-323-44733-1.00016-X.

Beurg, M. *et al.* (1999) 'Involvement of the carboxy-terminus region of the dihydropyridine receptor β1a subunit in excitation-contraction coupling of skeletal muscle', *Biophysical Journal*, 77(6), pp. 2953-2967. doi: 10.1016/S0006-3495(99)77128-6.

Bhaskar, B. *et al.* (2003) 'A novel heme and peroxide-dependent tryptophan-tyrosine cross-link in a mutant of cytochrome c peroxidase', *Journal of Molecular Biology*, 328(1), pp. 157-166. doi: 10.1016/s0022-2836(03)00179-7.

Bondarenko, P. V *et al*. (2002) 'Identification and relative quantitation of protein mixtures by enzymatic digestion followed by capillary reversed-phase liquid chromatography-tandem mass spectrometry', *Analytical Chemistry*, 74(18), pp. 4741-4749. doi: 10.1021/ac0256991.

Borzak, S. *et al.* (1991) 'Mechanisms of rate staircase in rat ventricular cells', *The American Journal of Physiology*, 260(3 Pt 2), pp. H884-92. doi: 10.1152/ajpheart.1991.260.3.H884.

Bouchard, R. and Bose, D. (1990) 'Analysis of the interval-force relationship in rat and canine ventricular myocardium', *The American Journal of Physiology*, 257, pp. H2036-47. doi: 10.1152/ajpheart.1989.257.6.H2036.

Brandmayr, J. *et al.* (2012) 'Deletion of the C-terminal phosphorylation sites in the cardiac β-subunit does not affect the basic β-adrenergic response of the heart and the Ca(v)1.2 channel', *The Journal of Biological Chemistry*, 287(27), pp. 22584-22592. doi: 10.1074/jbc.M112.366484.

Bünemann, M. *et al.* (1999) 'Functional regulation of L-type calcium channels via protein kinase A-mediated phosphorylation of the β2 subunit', *Journal of Biological Chemistry*, 274(48), pp. 33851-33854. doi: 10.1074/jbc.274.48.33851.

Buraei, Z. and Yang, J. (2010) 'The β subunit of voltage-gated Ca2+ channels', *Physiological Reviews*, 90(4), pp. 1461-1506. doi: 10.1152/physrev.00057.2009.

Buraei, Z. and Yang, J. (2013) 'Structure and function of the β subunit of voltage-gated Ca^{2+} channels', *Biochimica et Biophysica Acta*, 1828(7), pp. 1530-1540. doi: 10.1016/j.bbamem.2012.08.028.

Buraei, Z. *et al.* (2015) 'RGK regulation of voltage-gated calcium channels', *Science China Life Sciences*, 58(1), pp. 28-38. doi: 10.1007/s11427-014-4788-x.

Campiglio, M. and Flucher, B. E. (2015) 'The role of auxiliary subunits for the functional diversity of voltage-gated calcium channels', *Journal of Cellular Physiology*, 230(9), pp. 2019-2031. doi: 10.1002/jcp.24998.

Cantí, C. *et al.* (2005) 'The metal-ion-dependent adhesion site in the Von Willebrand factor-A domain of alpha2delta subunits is key to trafficking voltage-gated Ca2+ channels', *Proceedings of the National Academy of Sciences*, 102(32), pp. 11230-11235. doi: 10.1073/pnas.0504183102.

Cassidy, J. S. *et al.* (2014a) 'Functional exofacially tagged N-type calcium channels elucidate the interaction with auxiliary alpha2delta-1 subunits', *Proceedings of the National Academy of Sciences*, 111(24), pp. 8979-8984. doi: 10.1073/pnas.1403731111.

Castellano, A. *et al.* (1993a) 'Cloning and expression of a neuronal calcium channel β subunit', *Journal of Biological Chemistry*, 268(17), pp. 12359-12366.

Castellano, A. *et al.* (1993b) 'Cloning and expression of a third calcium channel beta subunit', *Journal of Biological Chemistry*, 268(5), pp. 3450-3455.

Catalucci, D. *et al.* (2009) 'Akt regulates L-type Ca2+ channel activity by modulating Cavalpha1 protein stability', *The Journal of Cell Biology*, 184(6), pp. 923-933. doi: 10.1083/jcb.200805063.

Catterall, W. A. (2009) 'Calcium Channels', in *Encyclopedia of Neuroscience*, Elsevier, pp. 543-550. doi: 10.1016/B978-008045046-9.01629-6.

Chapman-Smith, A. and Cronan, J. E. J. (1999) 'Molecular biology of biotin attachment to proteins', *The Journal of Nutrition*, 129(2S Suppl), pp. 477S-484S. doi: 10.1093/jn/129.2.477S.

Chen, X. *et al.* (2018) 'Small-molecule Ca(v)α(1)·Ca(v)β antagonist suppresses neuronal voltage-gated calcium-channel trafficking', *Proceedings of the National Academy of Sciences*, 115(45), pp. E10566-E10575. doi: 10.1073/pnas.1813157115.

Chen, Y. *et al.* (2004) 'Structural basis of the α1-β subunit interaction of voltage-gated Ca2+ channels', *Nature*, 429(6992), pp. 675-680. doi: 10.1038/nature02641.

Cheng, W. *et al.* (2005) 'Interaction between the dihydropyridine receptor Ca2+ channel β -subunit

and ryanodine receptor type 1 strengthens excitation-contraction coupling', *Proceedings of the National Academy of Sciences*, 102(52), pp. 19225-19230. doi: 10.1073/pnas.0504334102.

Chung, C. Y. *et al.* (2017) 'In situ peroxidase labeling and mass-spectrometry connects alpha-synuclein directly to endocytic trafficking and mRNA metabolism in neurons', *Cell Systems*, 4(2), pp. 242-250.e4. doi: 10.1016/j.cels.2017.01.002.

Clément, C. *et al.* (2018) 'High-resolution visualization of H3 variants during replication reveals their controlled recycling', *Nature Communications*, 9(1), p. 3181. doi: 10.1038/s41467-018-05697-1.

Cole, R. L. *et al.* (2005) 'Differential distribution of voltage-gated calcium channel alpha-2 delta (α2δ) subunit mRNA-containing cells in the rat central nervous system and the dorsal root ganglia', *Journal of Comparative Neurology*, 491(3), pp. 246-269. doi: 10.1002/cne.20693.

Colecraft, H. M. *et al.* (2002) 'Novel functional properties of Ca(2+) channel beta subunits revealed by their expression in adult rat heart cells', *The Journal of Physiology*, 541(Pt 2), pp. 435-452. doi: 10.1113/jphysiol.2002.018515.

Cox, J. and Mann, M. (2008) 'MaxQuant enables high peptide identification rates, individualized p.p.b.-range mass accuracies and proteome-wide protein quantification', *Nature Biotechnology*, 26(12), pp. 1367-1372. doi.org/10.1038/nbt.1511.

Cox, J. *et al.* (2014) 'Accurate proteome-wide label-free quantification by delayed normalization and maximal peptide ratio extraction, termed MaxLFQ', *Molecular and Cellular Proteomics*, 13(9), pp. 2513-2526. doi: 10.1074/mcp.M113.031591.

Crowley, P. B. and Golovin, A. (2005) 'Cation-π interactions in protein-protein interfaces', *Proteins: Structure, Function and Genetics*, 59(2), pp. 231-239. doi: 10.1002/prot.20417.

Cui, Y. *et al.* (2009) 'A dihydropyridine receptor α1s loop region critical for skeletal muscle contraction is intrinsically unstructured and binds to a SPRY domain of the type 1 ryanodine receptor', *The International Journal of Biochemistry and Cell Biology*, 41(3), pp. 677-686. doi: 10.1016/j.biocel.2008.08.004.

Dalkilic, I. *et al.* (2006) 'Loss of filamin C (FLNc) results in severe defects in myogenesis and myotube structure', *Molecular and Cellular Biology*, 26(17), pp. 6522-6534. doi: 10.1128/MCB.00243-06.

Dayal, A. et al. (2013) 'Domain cooperativity in the β1a subunit is essential for dihydropyridine receptor voltage sensing in skeletal muscle', Proceedings of the National Academy of Sciences, 110(18), pp. 7488-7493. doi: 10.1073/pnas.1301087110.

Dibb, K. M. et al. (2007) 'Regulation of systolic [Ca2+]i and cellular Ca2+ flux balance in rat ventricular myocytes by SR Ca2+, L-type Ca2+ current and diastolic [Ca2+]i', The Journal of Physiology, 585(Pt 2), pp. 579-592. doi: 10.1113/jphysiol.2007.141473.

Dolphin, A. C. (2013) 'The α2δ subunits of voltage-gated calcium channels', *Biochimica et Biophysica Acta*, 1828(7), pp. 1541-1549. doi: 10.1016/j.bbamem.2012.11.019.

Dolphin, A. C. (2018) 'Voltage-gated calcium channel α2δ subunits: an assessment of proposed novel roles', *F1000Res*, p. 1830. doi: 10.12688/f1000research.16104.1.

Dragicevic, E. *et al.* (2014) 'Cav1.3 channels control D2-autoreceptor responses via NCS-1 in substantia nigra dopamine neurons', *Brain*, 137(8), pp. 2287-2302. doi: 10.1093/brain/awu131.

Dundas, C. M. *et al.* (2013) 'Streptavidin-biotin technology: Improvements and innovations in chemical and biological applications', *Applied Microbiology and Biotechnology*, 97(21), pp. 9343-9353. doi: 10.1007/s00253-013-5232-z.

Dunham, W. H. *et al.* (2012) 'Affinity-purification coupled to mass spectrometry: basic principles and strategies', *Proteomics*, 12(10), pp. 1576-1590. doi: 10.1002/pmic.201100523.

Dunn, K. W. *et al.* (2011) 'A practical guide to evaluating colocalization in biological microscopy', *American Journal of Physiology Cell Physiology*, 300(4), pp. C723-C742. doi: 10.1152/ajpcell.00462.2010.

Dzhura, I. and Neely, A. (2003) 'Differential modulation of cardiac Ca2+ channel gating by beta-

subunits', *Biophysical Journal*, 85(1), pp. 274-289. doi: 10.1016/S0006-3495(03)74473-7.

Eberst, R. *et al.* (1997) 'Identification and functional characterization of a calcium channel γ subunit', *Pflugers Archiv*, 433(5), pp. 633-637. doi: 10.1007/s004240050324.

Eisner, D. A. *et al.* (2017) 'Calcium and excitation-contraction coupling in the heart', *Circulation Research*, 121(2), pp. 181-195. doi: 10.1161/circresaha.117.310230.

Elias, G. M. and Nicoll, R. A. (2007) 'Synaptic trafficking of glutamate receptors by MAGUK scaffolding proteins', *Trends in Cell Biology*, 17(7), pp. 343-352. doi: 10.1016/j.tcb.2007.07.005.

Eltit, J. M. *et al.* (2014) 'Amino acid residues 489-503 of dihydropyridine receptor (DHPR) β1a subunit are critical for structural communication between the skeletal muscle DHPR complex and type 1 Ryanodine Receptor', *Journal of Biological Chemistry*, 289(52), pp. 36116-36124. doi: 10.1074/jbc.m114.615526.

Endoh, M. (2004) 'Force-frequency relationship in intact mammalian ventricular myocardium: physiological and pathophysiological relevance', *European Journal of Pharmacology*, 500(1-3), pp. 73-86. doi: 10.1016/j.ejphar.2004.07.013.

Etemad, S. *et al.* (2014) 'Differential neuronal targeting of a new and two known calcium channel β4 subunit splice variants correlates with their regulation of gene expression', *The Journal of Neuroscience*, 34(4), pp. 1446-1461. doi: 10.1523/jneurosci.3935-13.2014.

Fakler, B. and Adelman, J. P. (2008) 'Control of KCa channels by calcium nano/microdomains', *Neuron*, 59(6), pp. 873-881. doi: 10.1016/j.neuron.2008.09.001.

Fan, M. *et al.* (2010) 'Direct inhibition of P/Q-type voltage-gated Ca2+ channels by Gem does not require a direct Gem/Cavβ interaction', *Proceedings of the National Academy of Sciences*, 107(33), pp. 14887-14892. doi: 10.1073/pnas.1007543107.

Fang, K. and Colecraft, H. M. (2011) 'Mechanism of auxiliary β-subunit-mediated membrane targeting of L-type (Ca(v)1.2) channels', *The Journal of Pysiology*, 589(Pt 18), pp. 4437-4455. doi: 10.1113/jphysiol.2011.214247.

Ferrándiz-Huertas, C. *et al*. (2012) 'Regional expression and subcellular localization of the voltage-gated calcium channel β subunits in the developing mouse brain', *Journal of Neurochemistry*, 122(6), pp. 1095-1107. doi: 10.1111/j.1471-4159.2012.07853.x.

Findeisen, F. *et al.* (2017) 'Stapled voltage-gated calcium channel (Ca(v)) α-interaction domain (AID) peptides act as selective protein-protein interaction inhibitors of Ca(v) function', *Chemical Neuroscience*, 8(6), pp. 1313-1326. doi: 10.1021/acschemneuro.6b00454.

Foell, J. D. *et al.* (2004) 'Molecular heterogeneity of calcium channel beta-subunits in canine and human heart: evidence for differential subcellular localization', *Physiological Genomics*, 17(2), pp. 183-200. doi: 10.1152/physiolgenomics.00207.2003.

Frampton, J. E. *et al.* (1991) 'Diastolic, systolic and sarcoplasmic reticulum [Ca2+] during inotropic interventions in isolated rat myocytes', *The Journal of Physiology*, 437, pp. 351-375. doi: 10.1113/jphysiol.1991.sp018600.

Franzini-Armstrong C, Protasi F, R. V (1998) 'Comparative ultrastructure of Ca2+ release units in skeletal and cardiac muscle', *Annals of the New York Academy of Sciences*, 853, pp. 20-30. doi: 10.1111/j.1749-6632.1998.tb08253.x

Funke, L. *et al.* (2005) 'Membrane-associated guanylate kinases regulate adhesion and plasticity at cell junctions', *Annual Review of Biochemistry*, 74(1), pp. 219-245. doi: 10.1146/annurev.biochem.74.082803.133339.

Gallagher, S. R. (2006) 'One-dimensional SDS gel electrophoresis of proteins', *Current Protocols in Molecular Biology*, 75: 10.2.1-10.2A.37. doi:10.1002/0471142727.mb1002as75.

Gandini, M. A. and Felix, R. (2012) 'Functional interactions between voltage-gated Ca2 + channels and Rab3- interacting molecules (RIMs): New insights into stimulus-secretion coupling', *Biochimica et Biophysica Acta*, 1818(3), pp. 551-558. doi: 10.1016/j.bbamem.2011.12.011.

Ganesan, A. N. *et al.* (2006) 'Beta-adrenergic stimulation of L-type Ca2+ channels in cardiac

myocytes requires the distal carboxyl terminus of alpha1C but not serine 1928', *Circulation Research*, 98(2), pp. e11-e18. doi: 10.1161/01.RES.0000202692.23001.e2.

Gao, T. *et al.* (1997) 'Identification and subcellular localization of the subunits of L-type calcium channels and adenylyl cyclase in cardiac myocytes', *The Journal of Biological Chemistry*, 272(31), pp. 19401-19407. doi: 10.1074/jbc.272.31.19401.

Gattoni, S. *et al.* (2016) 'The calcium-frequency response in the rat ventricular myocyte: an experimental and modelling study', *The Journal of Physiology*, 594(15), pp. 4193-4224. doi: 10.1113/JP272011.

Gavin, A. C. *et al.* (2002) 'Functional organization of the yeast proteome by systematic analysis of protein complexes', *Nature*, 415(6868), pp. 141-147. doi: 10.1038/415141a.

des Georges, A. *et al.* (2016) 'Structural basis for gating and activation of RyR1', *Cell*, 167(1), pp. 145-157.e17. doi: 10.1016/j.cell.2016.08.075.

Gez, L. S. *et al.* (2012) 'Voltage-driven Ca(2+) binding at the L-type Ca(2+) channel triggers cardiac excitation-contraction coupling prior to Ca(2+) influx', *Biochemistry*, 51(48), pp. 9658-9666. doi: 10.1021/bi301124a.

Gonzalez-Gutierrez, G. *et al.* (2007) 'The Src homology 3 domain of the β-subunit of voltage-gated calcium channels promotes endocytosis via dynamin interaction', *Journal of Biological Chemistry*, 282(4), pp. 2156-2162. doi: 10.1074/jbc.M609071200.

Gonzalez-Gutierrez, G. *et al.* (2008) 'The guanylate kinase domain of the beta-subunit of voltage-gated calcium channels suffices to modulate gating', *Proceedings of the National Academy of Sciences*, 105(37), pp. 14198-203. doi: 10.1073/pnas.0806558105.

Greig, C. A. and Jones, D. A. (2016) 'Muscle physiology and contraction', *Surgery*, 34(3), pp. 107-114. doi: 10.1016/j.mpsur.2016.01.004.

Grison, M. *et al.* (2017) 'α-Actinin/titin interaction: A dynamic and mechanically stable cluster of bonds in the muscle Z-disk', *Proceedings of the National Academy of Sciences*, 114(5), pp. 1015-1020. doi: 10.1073/pnas.1612681114.

Grueter, C. E. *et al.* (2008) 'Differential regulated interactions of calcium/calmodulin-dependent protein kinase II with isoforms of voltage-gated calcium channel beta subunits', *Biochemistry*, 47(6), pp. 1760-1767. doi: 10.1021/bi701755q.

Haase, H. *et al.* (1996) 'In-vivo phosphorylation of the cardiac L-type calcium channel beta-subunit in response to catecholamines', *Molecular and Cellular Biochemistry*, 163-164, pp. 99-106. doi: 10.1007/BF00408645.

Haase, H. *et al.* (1999) 'Signaling from β-adrenoceptor to L-type calcium channel: identification of a novel cardiac protein kinase A target possessing similarities to Ahnak', *The FASEB Journal*, 13(15), pp. 2161-2172. doi: 10.1096/fasebj.13.15.2161.

Haase, H. *et al.* (2005) 'Ahnak is critical for cardiac Ca(v)1.2 calcium channel function and its β-adrenergic regulation', *The FASEB Journal*, 19(14), pp. 1969-1977. doi: 10.1096/fj.05-3997com.

Haase, H. (2007) 'Ahnak, a new player in β-adrenergic regulation of the cardiac L-type Ca2+ channel', *Cardiovascular Research*, 73(1), pp. 19-25. doi: 10.1016/j.cardiores.2006.09.001.

Hall, D. D. *et al.* (2013) 'Competition between α-actinin and Ca^{2+}-calmodulin controls surface retention of the L-type Ca^{2+} channel Ca(v)1.2', *Neuron*, 78(3), pp. 483-497. doi: 10.1016/j.neuron.2013.02.032.

Hanson, P. I. *et al.* (1989) 'Expression of a multifunctional Ca2+/calmodulin-dependent protein kinase and mutational analysis of its autoregulation', *Neuron*, 3(1), pp. 59-70. doi: 10.1016/0896-6273(89)90115-3.

Haugland, R. P. and You, W. W. (2008) 'Coupling of antibodies with biotin', *Methods in Molecular Biology*, 418, pp. 13-24. doi: 10.1007/978-1-59745-579-4_2.

Hayashi, T. *et al.* (2009) 'Three-dimensional electron microscopy reveals new details of membrane systems for Ca2+ signaling in the heart', *Journal of Cell Science*, 122(Pt 7), pp. 1005-1013. doi:

10.1242/jcs.028175.

He, M. *et al.* (1997) 'Motif III S5 of L-type calcium channels is involved in the dihydropyridine binding site. A combined radioligand binding and electrophysiological study', *Journal of Biological Chemistry*, 272(5), pp. 2629-2633. doi: 10.1074/jbc.272.5.2629.

He, R. *et al.* (2018) 'New insights into interactions of presynaptic calcium channel subtypes and SNARE proteins in neurotransmitter release', *Frontiers in Molecular Neuroscience*, 11, p. 213. doi: 10.3389/fnmol.2018.00213.

Hein, M. Y. *et al*. (2013) 'Proteomic Analysis of Cellular Systems', in *Handbook of Systems Biology: Concepts and Insights* (Chapter 1), *First Edition*, Academic Press, pp. 3-25. doi.org/10.1016/C2010-0-67190-2.

Helton, T. D. and Horne, W. A. (2002) 'Alternative splicing of the β_4 subunit has α_1 subunit subtype-specific effects on Ca^{2+} channel gating', *The Journal of Neuroscience*, 22(5), pp. 1573-1582. doi: 10.1523/jneurosci.22-05-01573.2002.

Hernández-Ochoa, E. O. *et al.* (2014) 'β1a490-508, a 19-residue peptide from C-terminal tail of Cav1.1 β1a subunit, potentiates voltage-dependent calcium release in adult skeletal muscle fibers', *Biophysical Journal*, 106(3), pp. 535-547. doi: 10.1016/j.bpj.2013.11.4503.

Hibino, H. *et al.* (2003) 'Direct interaction with a nuclear protein and regulation of gene silencing by a variant of the Ca2+-channel beta 4 subunit', *Proceedings of the National Academy of Sciences*, 100(1), pp. 307-312. doi: 10.1073/pnas.0136791100.

Hinshaw, J. E. (2000) 'Dynamin and its role in membrane fission', *Annual Review of Cell and Developmental Biology*, 16(1), pp. 483-519. doi: 10.1146/annurev.cellbio.16.1.483.

Ho, Y. *et al.* (2002) 'Systematic identification of protein complexes in Saccharomyces cerevisiae by mass spectrometry', *Nature*, 415(6868), pp. 180-183. doi: 10.1038/415180a.

Hockerman, G. H. *et al.* (1997) 'Molecular determinants of high affinity phenylalkylamine block of L-type calcium channels in transmembrane segment IIIS6 and the pore region of the α1 subunit', *Journal of Biological Chemistry*, 272(30), pp. 18759-18765. doi: 10.1074/jbc.272.30.18759.

Hohaus, A. *et al.* (2002) ' The carboxyl-terminal region of ahnak provides a link between cardiac L-type Ca 2+ channels and the actin-based cytoskeleton', *The FASEB Journal*, 16(10), pp. 1205-1216. doi: 10.1096/fj.01-0855com.

Hong, T. and Shaw, R. M. (2017) 'Cardiac T-Tubule microanatomy and function', *Physiological Reviews*, 97(1), pp. 227-252. doi: 10.1152/physrev.00037.2015.

Hu, H. *et al.* (2015) 'The molecular architecture of dihydropyrindine receptor/L-type Ca2+ channel complex', *Scientific Reports*, 5, p. 8370. doi: 10.1038/srep08370.

Huang, D. W. *et al*. (2009) 'Systematic and integrative analysis of large gene lists using DAVID bioinformatics resources', *Nature Protocols*, 4(1), pp. 44-57. doi: 10.1038/nprot.2008.211.

Huang, G. *et al.* (2007) 'Ca2+ signaling in microdomains: Homer1 mediates the interaction between RyR2 and Cav1.2 to regulate excitation-contraction coupling', *The Journal of Biological Chemistry*, 282(19), pp. 14283-14290. doi: 10.1074/jbc.M611529200.

Hung, V. *et al.* (2014) 'Proteomic mapping of the human mitochondrial intermembrane space in live cells via ratiometric APEX tagging', *Molecular Cell*, 55(2), pp. 332-341. doi: 10.1016/j.molcel.2014.06.003.

Hung, V. *et al.* (2016) 'Spatially resolved proteomic mapping in living cells with the engineered peroxidase APEX2', *Nature Protocols*, 11(3), pp. 456-475. doi: 10.1038/nprot.2016.018.

James, C. *et al.* (2019) 'Proteomic mapping by rapamycin-dependent targeting of APEX2 identifies binding partners of VAPB at the inner nuclear membrane', *The Journal of Biological Chemistry*, 294(44), pp. 16241-16254. doi: 10.1074/jbc.RA118.007283.

Jay, S. D. *et al.* (1990) 'Primary structure of the gamma subunit of the DHP-sensitive calcium channel from skeletal muscle', *Science*, 248(4954), pp. 490-492. doi: 10.1126/science.2158672.

Jay, S. D. *et al.* (1991) 'Structural characterization of the dihydropyridine-sensitive calcium

channel alpha 2-subunit and the associated delta peptides', *Journal of Biological Chemistry*, 266(5), pp. 3287-3293.

Jayasinghe, I. *et al.* (2018) 'True molecular scale visualization of variable clustering properties of ryanodine receptors', *Cell Reports*, 22(2), pp. 557-567. doi: 10.1016/j.celrep.2017.12.045.

Jiang, L. H. *et al.* (2000) 'Regulation of cloned cardiac L-type calcium channels by cGMP-dependent protein kinase', *Journal of Biological Chemistry*, 275(9), pp. 6135-6143. doi: 10.1074/jbc.275.9.6135.

Jiang, M. *et al.* (2016) 'JPH-2 interacts with Cai-handling proteins and ion channels in dyads: Contribution to premature ventricular contraction-induced cardiomyopathy', *Heart Rhythm*, 13(3), pp. 743-752. doi: 10.1016/j.hrthm.2015.10.037.

Jing, J. *et al.* (2015) 'Proteomic mapping of ER-PM junctions identifies STIMATE as a regulator of Ca(2)(+) influx', *Nature Cell Biology*, 17(10), pp. 1339-1347. doi: 10.1038/ncb3234.

Jin, J. *et al.* (2019) 'Ahnak scaffolds p11/Anxa2 complex and L-type voltage-gated calcium channel and modulates depressive behavior', *Molecular Psychiatry*. doi: 10.1038/s41380-019-0371-y.

Jones, P. P. *et al.* (2018) 'Dyadic plasticity in cardiomyocytes', *Frontiers in Physiology*, 9, p. 1773. doi: 10.3389/fphys.2018.01773.

De Jongh, K. S. *et at.* (1990) 'Subunits of purified calcium channels: Alpha 2 and delta are encoded by the same gene', *Journal of Biological Chemistry*, 265(25), pp. 14738-14741.

Kaeser, P. S. *et al.* (2011) 'RIM proteins tether Ca2+ channels to presynaptic active zones via a direct PDZ-domain interaction', *Cell*, 144(2), pp. 282-295. doi: 10.1016/j.cell.2010.12.029.

Kamijo, S. *et al.* (2018) 'A critical neurodevelopmental role for L-Type voltage-gated calcium channels in neurite extension and radial migration', *The Journal of Neuroscience*, 38(24), pp. 5551-5566. doi: 10.1523/JNEUROSCI.2357-17.2018.

Keilhauer, E. C. *et al.* (2015) 'Accurate protein complex retrieval by affinity enrichment mass spectrometry (AE-MS) rather than affinity purification mass spectrometry (AP-MS)', *Molecular and Cellular Proteomics*, 14(1), pp. 120-135. doi: 10.1074/mcp.M114.041012.

Kiyonaka, S. *et al.* (2007) 'RIM1 confers sustained activity and neurotransmitter vesicle anchoring to presynaptic Ca2+ channels', *Nature Neuroscience*, 10(6), pp. 691-701. doi: 10.1038/nn1904.

Kolstad, T. R. *et al.* (2018) 'Ryanodine receptor dispersion disrupts Ca(2+) release in failing cardiac myocytes', *eLife*, 7, p. e39427. doi: 10.7554/eLife.39427.

Kong, H. *et al.* (2008) 'Caffeine induces Ca2+ release by reducing the threshold for luminal Ca2+ activation of the ryanodine receptor', *The Biochemical Journal*, 414(3), pp. 441-452. doi: 10.1042/BJ20080489.

Kong, Y. *et al.* (2018) 'An FRMD4B variant suppresses dysplastic photoreceptor lesions in models of enhanced S-cone syndrome and of Nrl deficiency', *Human Molecular Genetics*, 27(19), pp. 3340-3352. doi: 10.1093/hmg/ddy238.

De Koninck, P. and Schulman, H. (1998) 'Sensitivity of CaM kinase II to the frequency of Ca2+ oscillations', *Science*, 279(5348), pp. 227-230. doi: 10.1126/science.279.5348.227.

Koval, O. M. *et al.* (2010) 'Cav1.2 beta-subunit coordinates CaMKII-triggered cardiomyocyte death and afterdepolarizations', *Proceedings of the National Academy of Sciences*, 107(11), pp. 4996-5000. doi: 10.1073/pnas.0913760107.

Kumar, R. A. *et al.* (2010) 'A de novo 1p34.2 microdeletion identifies the synaptic vesicle gene RIMS3 as a novel candidate for autism', *Journal of Medical Genetics*, 47(2), pp. 81-90. doi: 10.1136/jmg.2008.065821.

Kushnir, A. *et al.* (2010) 'Role of CaMKIIdelta phosphorylation of the cardiac ryanodine receptor in the force frequency relationship and heart failure', *Proceedings of the National Academy of Sciences*, 107(22), pp. 10274-10279. doi: 10.1073/pnas.1005843107.

Lam, S. S. *et al.* (2015) 'Directed evolution of APEX2 for electron microscopy and proximity labeling', *Nature Methods*, 12(1), pp. 51-54. doi: 10.1038/nmeth.3179.

Lambert, R. C. *et al.* (2014) 'The many faces of T-type calcium channels', *Pflugers Archiv*, 466(3), pp. 451-423. doi: 10.1007/s00424-013-1353-6.

Lanner, J. T. *et al.* (2010) 'Ryanodine receptors: structure, expression, molecular details, and function in calcium release', *Cold Spring Harbor Perspectives in Biology*, 2(11), p. a003996. doi: 10.1101/cshperspect.a003996.

Lau, K. and Van Petegem, F. (2014) 'Crystal structures of wild type and disease mutant forms of the ryanodine receptor SPRY2 domain', *Nature Communications*, 5, pp. 1-11. doi: 10.1038/ncomms6397.

Layland, J. and Kentish, J. C. (1999) 'Positive force- and [Ca2+]i-frequency relationships in rat ventricular trabeculae at physiological frequencies', *The American Journal of Physiology*, 276(1), pp. H9-H18. doi: 10.1152/ajpheart.1999.276.1.H9.

Leckband, D. (2000) 'Measuring the forces that control protein interactions', *Annual Review of Biophysics and Biomolecular Structure*, 29(1), pp. 1-26. doi: 10.1146/annurev.biophys.29.1.1.

Levy, S. *et al.* (2009) 'Molecular basis for zinc transporter 1 action as an endogenous inhibitor of L-type calcium channels', *Journal of Biological Chemistry*, 284(47), pp. 32434-32443. doi: 10.1074/jbc.M109.058842.

Link, S. *et al.* (2009) 'Diversity and developmental expression of L-type calcium channel beta2 proteins and their influence on calcium current in murine heart', *The Journal of Biological Chemistry*, 284(44), pp. 30129-30137. doi: 10.1074/jbc.M109.045583.

Liu, B. *et al.* (2018) 'Structural and molecular bases of sarcoplasmic reticulum ion channel function', in *Cardiac Electrophysiology: From Cell to Bedside: Seventh Edition*, Elsevier, pp. 60-65. doi: 10.1016/B978-0-323-44733-1.00006-7.

Liu, G. *et al.* (2020) 'Mechanism of adrenergic CaV1.2 stimulation revealed by proximity proteomics', *Nature*, 577(7792), pp. 695-700. doi: 10.1038/s41586-020-1947-z.

Lu, B. *et al.* (2008) 'Strategies for shotgun identification of integral membrane proteins by tandem mass spectrometry', *Proteomics*, 8(19), pp. 3947-3955. doi: 10.1002/pmic.200800120.

Luan, C. *et al.* (2019) 'The calcium channel subunit gamma-4 is regulated by MafA and necessary for pancreatic beta-cell specification', *Communications Biology*, 2(1), p. 106. doi: 10.1038/s42003-019-0351-4.

Lucia, G. *et al.* (2011) 'Junctophilin 1 and 2 proteins interact with the L-type ca2+ channel dihydropyridine receptors (DHPRs) in skeletal muscle', *The Journal of Biological Chemistry*, 286, pp. 43717-43725. doi: 10.1074/jbc.M111.292755.

Maerkens, A. *et al.* (2016) 'New insights into the protein aggregation pathology in myotilinopathy by combined proteomic and immunolocalization analyses', *Acta Neuropathologica Communications*, 4, p. 8. doi: 10.1186/s40478-016-0280-0.

Maier, L. S. and Bers, D. M. (2007) 'Role of Ca2+/calmodulin-dependent protein kinase (CaMK) in excitation-contraction coupling in the heart', *Cardiovascular Research*, 73(4), pp. 631-640. doi: 10.1016/j.cardiores.2006.11.005.

Mangoni, M. E. *et al.* (2003) 'Functional role of L-type Cav1.3 Ca2+ channels in cardiac pacemaker activity', *Proceedings of the National Academy of Sciences*, 100(9), pp. 5543-5548. doi: 10.1073/PNAS.0935295100.

Marcantoni, A. *et al.* (2010) 'Loss of Cav1.3 channels reveals the critical role of L-type and BK channel coupling in pacemaking mouse adrenal chromaffin cells', *The Journal of Neuroscience*, 30(2), pp. 491-504. doi: 10.1523/JNEUROSCI.4961-09.2010.

Margas, W. *et al.* (2016) 'Effect of knockout of α2δ-1 on action potentials in mouse sensory neurons', *Philosophical Transactions of the Royal Society B: Biological Sciences*, 371(1700), p. 20150430. doi: 10.1098/rstb.2015.0430.

Marín-García, J. (2014) 'Gene- and Cell-Based Therapy for Cardiovascular Disease', in *Post-Genomic Cardiology* (Chapter 23), *Second Edition*, Academic Press, pp. 783-833. doi.org/10.1016/B978-0-12-404599-6.00023-8.

Marks, A. R. (2013) 'Calcium cycling proteins and heart failure: mechanisms and therapeutics', *The Journal of Clinical Investigation*, 123(1), pp. 46-52. doi: 10.1172/JCI62834.

Martell, J. D. *et al.* (2012) 'Engineered ascorbate peroxidase as a genetically encoded reporter for electron microscopy', *Nature Biotechnology*, 30(11), pp. 1143-1148. doi: 10.1038/nbt.2375.

Marx, S. O. *et al.* (2001) 'Phosphorylation-dependent regulation of ryanodine receptors: a novel role for leucine/isoleucine zippers', *The Journal of Cell Biology*, 153(4), pp. 699-708. doi: 10.1083/jcb.153.4.699.

Matza, D. *et al.* (2008) 'A scaffold protein, Ahnak1, is required for calcium signaling during T cell activation', *Immunity*, 28(1), pp. 64-74. doi: 10.1016/j.immuni.2007.11.020.

Mayer, B. J. (2001) 'SH3 domains: complexity in moderation', *Journal of Cell Science*, 114(7), pp. 1253-1263.

Mayer, G. and Bendayan, M. (1997) 'Biotinyl-tyramide: a novel approach for electron microscopic immunocytochemistry', *Journal of Histochemistry and Cytochemistry*, 45(11), pp. 1449-1454. doi: 10.1177/002215549704501101.

McGee, A. W. *et al.* (2004) 'Calcium channel function regulated by the SH3-GK module in β subunits', *Neuron*, 42(1), pp. 89-99. doi: 10.1016/S0896-6273(04)00149-7.

Meissner, G. (2017) 'The structural basis of ryanodine receptor ion channel function', *The Journal of General Physiology*, 149(12), pp. 1065-1089. doi: 10.1085/jgp.201711878.

Meissner, M. *et al.* (2011) 'Moderate calcium channel dysfunction in adult mice with inducible cardiomyocyte-specific excision of the *Cacnb2* gene', *The Journal of Biological Chemistry*, 286(18), pp. 15875-15882. doi: 10.1074/jbc.M111.227819.

Merkel, C. D. *et al.* (2019) 'Vinculin anchors contractile actin to the cardiomyocyte adherens junction', *Molecular Biology of the Cell*, 30(21), pp. 2639-2650. doi: 10.1091/mbc.E19-04-0216.

Mesirca, P. *et al*. (2014) 'T-type channels in the sino-atrial and atrioventricular pacemaker mechanism', *Pflugers Archiv*, 466(4), pp. 791-799. doi: 10.1007/s00424-014-1482-6.

Mesirca, P. *et al*. (2015) 'Functional role of voltage gated Ca(2+) channels in heart automaticity', *Frontiers in Physiology*, 6, p. 19. doi: 10.3389/fphys.2015.00019.

Meyer, K. and Selbach, M. (2015) 'Quantitative affinity purification mass spectrometry: a versatile technology to study protein-protein interactions', *Frontiers in Genetics*, p. 237. doi: 10.3389/fgene.2015.00237.

Mick, D. U. *et al.* (2015) 'Proteomics of primary cilia by proximity labeling', *Developmental Cell*, 35(4), pp. 497-512. doi: 10.1016/j.devcel.2015.10.015.

Milenkovic, V. M. *et al.* (2011) 'Interaction of bestrophin-1 and Ca2+ channel β-subunits: Identification of new binding domains on the bestrophin-1 C-terminus', *PLoS ONE*, 6(4). doi: 10.1371/journal.pone.0019364.

Miller, S. G. and Kennedy, M. B. (1986) 'Regulation of brain type II Ca2+/calmodulin-dependent protein kinase by autophosphorylation: a Ca2+-triggered molecular switch', *Cell*, 44(6), pp. 861-870. doi: 10.1016/0092-8674(86)90008-5.

Minamihata, K. *et al*. (2011) 'Protein heteroconjugation by the peroxidase-catalyzed tyrosine coupling reaction', *Bioconjugate Chemistry*, 22(11), pp. 2332-2338. doi: 10.1021/bc200420v.

Miranda-Laferte, E. *et al.* (2011) 'Homodimerization of the Src homology 3 domain of the calcium channel β-subunit drives dynamin-dependent endocytosis', *Journal of Biological Chemistry*, 286(25), pp. 22203-22210. doi: 10.1074/jbc.M110.201871.

Mortensen, A. and Skibsted, L. H. (1997) 'Importance of carotenoid structure in radical-scavenging reactions', *Journal of Agricultural and Food Chemistry*, 45(8), pp. 2970-2977. doi: 10.1021/jf970010s.

Muller, M. *et al.* (2020) 'Probing the environment of emerin by enhanced ascorbate peroxidase 2 (APEX2)-mediated proximity labeling', *Cells*, 9(3). doi: 10.3390/cells9030605.

Mulligan, K. A. and Cheyette, B. N. R. (2012) 'Wnt signaling in vertebrate neural development and function', *Journal of Neuroimmune Pharmacology*, 7(4), pp. 774-787. doi: 10.1007/s11481-012-9404-x.

Munro, M. L. *et al.* (2016) 'Junctophilin-2 in the nanoscale organisation and functional signalling of ryanodine receptor clusters in cardiomyocytes', *Journal of Cell Science*, 129(23), pp. 4388-4398. doi: 10.1242/jcs.196873.

Nakai, J. *et al.* (1990) 'Primary structure and functional expression from cDNA of the cardiac ryanodine receptor/calcium release channel', *FEBS letters*, 271(1-2), pp. 169-177. doi: 10.1016/0014-5793(90)80399-4.

Nakamura, F. *et al*. (2011) 'The filamins: organizers of cell structure and function', *Cell Adhesion and Migration*, 5(2), pp. 160-169. doi: 10.4161/cam.5.2.14401.

Nakao, A. *et al.* (2015) 'Comprehensive behavioral analysis of voltage-gated calcium channel beta-anchoring and -regulatory protein knockout mice', *Frontiers in Behavioral Neuroscience*, 9, p. 141. doi: 10.3389/fnbeh.2015.00141.

Neely, A. and Hidalgo, P. (2014) 'Structure-function of proteins interacting with the α1 pore-forming subunit of high-voltage-activated calcium channels', *Frontiers in Physiology*, 5, p. 209. doi: 10.3389/fphys.2014.00209.

Nolte, C. *et al.* (2004) 'ZnT-1 expression in astroglial cells protects against zinc toxicity and slows the accumulation of intracellular zinc', *GLIA*, 48(2), pp. 145-155. doi: 10.1002/glia.20065.

Norris, N. C. *et al.* (2017) 'Structural and biophysical analyses of the skeletal dihydropyridine receptor β subunit β(1a) reveal critical roles of domain interactions for stability', *The Journal of Biological Chemistry*, 292(20), pp. 8401-8411. doi: 10.1074/jbc.M116.763896.

Olsen, O. and Bredt, D. S. (2003) 'Functional analysis of the nucleotide binding domain of membrane-associated guanylate kinases', *Journal of Biological Chemistry*, 278(9), pp. 6873-6878. doi: 10.1074/jbc.M210165200.

Olson, P. A. *et al.* (2005) 'G-protein-coupled receptor modulation of striatal Cav1.3 L-Type Ca2+ channels is dependent on a Shank-binding domain', *The Journal of Neuroscience*, 25(5), pp. 1050-1062. doi: 10.1523/JNEUROSCI.3327-04.2005.

Opatowsky, Y. *et al.* (2004) 'Structural analysis of the voltage-dependent calcium channel β subunit functional core and its complex with the α1 interaction domain', *Neuron*, 42(3), pp. 387-399. doi: 10.1016/S0896-6273(04)00250-8.

Otey, C. A. and Carpen, O. (2004) 'Alpha-actinin revisited: a fresh look at an old player', *Cell Motility and the Cytoskeleton*, 58(2), pp. 104-111. doi: 10.1002/cm.20007.

Otsu, K. *et al.* (1990) 'Molecular cloning of cDNA encoding the Ca2+ release channel (ryanodine receptor) of rabbit cardiac muscle sarcoplasmic reticulum', *The Journal of Biological Chemistry*, 265(23), pp. 13472-13483.

Page, K. M. *et al*. (2016) 'The Cavβ subunit protects the I-II loop of the voltage-gated calcium channel Cav2.2 from proteasomal degradation but not oligoubiquitination', *The Journal of Biological Chemistry*, 291(39), pp. 20402-20416. doi: 10.1074/jbc.M116.737270.

Pankonien, I. *et al.* (2012) 'Ahnak1 interaction is affected by phosphorylation of Ser-296 on Cavβ 2', *Biochemical and Biophysical Research Communications*, 421(2), pp. 184-189. doi: 10.1016/j.bbrc.2012.03.132.

Paolini, C. *et al.* (2004) 'Evidence for conformational coupling between two calcium channels', *Proceedings of the National Academy of Sciences*, 101(34), pp. 12748-12752. doi: 10.1073/pnas.0404836101.

Peng, W. *et al.* (2016) 'Structural basis for the gating mechanism of the type 2 ryanodine receptor RyR2', *Science*, 354(6310). doi: 10.1126/science.aah5324.

Perez-Reyes, E. *et al.* (1992) 'Cloning and expression of a cardiac/brain β subunit of the L-type calcium channel', *Journal of Biological Chemistry*, 267(3), pp. 1792-1797.

Perez, C. F. *et al*. (2003) 'Amino acids 1-1,680 of ryanodine receptor type 1 hold critical determinants of skeletal type for excitation-contraction coupling. Role of divergence domain D2', *Journal of Biological Chemistry*, 278(41), pp. 39644-39652. doi: 10.1074/jbc.M305160200.

Perez de Sevilla Muller, L. *et al.* (2015) 'Expression and cellular localization of the voltage-gated calcium channel alpha2delta3 in the rodent retina', *The Journal of Comparative Neurology*, 523(10), pp. 1443-1460. doi: 10.1002/cne.23751.

Perez White, B. E. *et al.* (2017) 'EphA2 proteomics in human keratinocytes reveals a novel association with afadin and epidermal tight junctions', *Journal of Cell Science*, 130(1), pp. 111-118. doi: 10.1242/jcs.188169.

Van Petegem, F. *et al.* (2004) 'Structure of a complex between a voltage-gated calcium channel β-subunit and an α-subunit domain', *Nature*, 429(6992), pp. 671-675. doi: 10.1038/nature02588.

Pieske, B. *et al.* (1999) 'Ca2+ handling and sarcoplasmic reticulum Ca2+ content in isolated failing and nonfailing human myocardium', *Circulation Research*, 85(1), pp. 38-46. doi: 10.1161/01.res.85.1.38.

Pirone, A. *et al.* (2014) 'α2δ3 is essential for normal structure and function of auditory nerve synapses and is a novel candidate for auditory processing disorders', *The Journal of Neuroscience*, 34(2), pp. 434-445. doi: 10.1523/JNEUROSCI.3085-13.2014.

Platero, J. S. *et al*. (1995) 'Functional analysis of the chromo domain of HP1', *The EMBO Journal*, 14(16), pp. 3977-3986. doi.org/10.1002/j.1460-2075.1995.tb00069.x.

Plum, S. *et al.* (2013) 'Combined enrichment of neuromelanin granules and synaptosomes from human substantia nigra pars compacta tissue for proteomic analysis', *Journal of Proteomics*, 94, pp. 202-206. doi: 10.1016/j.jprot.2013.07.015.

Praefcke, G. J. K. and McMahon, H. T. (2004) 'The dynamin superfamily: universal membrane tubulation and fission molecules?', *Nature Reviews Molecular Cell Biology*, 5(2), pp. 133-147. doi: 10.1038/nrm1313.

Pragnell, M. *et al.* (1991) 'Cloning and tissue-specific expression of the brain calcium channel β-subunit', *FEBS Letters*, 291(2), pp. 253-258. doi: 10.1016/0014-5793(91)81296-K.

Pragnell, M. *et al.* (1994) 'Calcium channel β-subunit binds to a conserved motif in the I-II cytoplasmic linker of the α1-subunit', *Nature*, 368(6466), pp. 67-70. doi: 10.1038/368067a0.

Puri, T. S. *et al.* (1997) 'Differential effects of subunit interactions on protein kinase A- and C-mediated phosphorylation of L-Type calcium channels', *Biochemistry*, 36(31), pp. 9605-9615. doi: 10.1021/bi970500d.

Qin, N. *et al.* (2002) 'Molecular cloning and characterization of the human voltage-gated calcium channel alpha(2)delta-4 subunit', *Molecular Pharmacology*, 62(3), pp. 485-496. doi: 10.1124/mol.62.3.485.

Rajagopal, S. *et al.* (2014) 'Inhibition of protein kinase C (PKC) response of voltage-gated calcium (Cav)2.2 channels expressed in Xenopus oocytes by Cavβ subunits', *Neuroscience*, 280, pp. 1-9. doi: 10.1016/j.neuroscience.2014.08.049.

Rajagopal, S. *et al*. (2014) 'Contribution of protein kinase Cα in the stimulation of insulin by the down-regulation of Cavβ subunits', *Endocrine*, 47(2), pp. 463-471. doi: 10.1007/s12020-013-0149-y.

Ratushny, V. and Golemis, E. (2008) 'Resolving the network of cell signaling pathways using the evolving yeast two-hybrid system', *BioTechniques*, 44(5), pp. 655-662. doi: 10.2144/000112797.

Rebbeck, R. T. *et al.* (2011) 'The β1a subunit of the skeletal DHPR binds to skeletal RyR1 and activates the channel via its 35-residue C-terminal tail', *Biophysical Journal*, 100(4), pp. 922-930. doi: 10.1016/j.bpj.2011.01.022.

Reichhart, N. *et al.* (2010) 'Effect of bestrophin-1 on L-type Ca2+ channel activity depends on the Ca2+ channel beta-subunit', *Experimental Eye Research*, 91(5), pp. 630-639. doi: 10.1016/j.exer.2010.08.001.

Rhee, H. W. *et al.* (2013) 'Proteomic mapping of mitochondria in living cells via spatially restricted enzymatic tagging', *Science*, 339(6125), pp. 1328-1331. doi: 10.1126/science.1230593.

Rima, M. *et al.* (2016) 'Protein partners of the calcium channel beta subunit highlight new cellular functions', *The Biochemical Journal*, 473(13), pp. 1831-1844. doi: 10.1042/BCJ20160125.

Rima, M. *et al.* (2017) 'Down-regulation of the Wnt/β-catenin signaling pathway by *Cacnb4*', *Molecular Biology of the Cell*, 28(25), pp. 3699-3708. doi: 10.1091/mbc.E17-01-0076.

Ríos, E. *et al.* (2019) 'The binding interactions that maintain excitation-contraction coupling junctions in skeletal muscle', *The Journal of General Physiology*, 151(4), pp. 593-605. doi: 10.1085/jgp.201812268.

Ríos, E. and Pizarro, G. (1988) 'Voltage sensors and calcium channels of excitation-contraction coupling', *Physiology*, 3(6), pp. 223-227. doi.org/10.1152/physiologyonline.1988.3.6.223.

Rogers, M. S. *et al.* (2008) 'Cross-link formation of the cysteine 228-tyrosine 272 catalytic cofactor of galactose oxidase does not require dioxygen', *Biochemistry*, 47(39), pp. 10428-10439. doi: 10.1021/bi8010835.

Rosenthal, R. *et al.* (2006) 'Expression of bestrophin-1, the product of the VMD2 gene, modulates voltage-dependent Ca 2+ channels in retinal pigment epithelial cells', *The FASEB Journal*, 20(1), pp. 178-180. doi: 10.1096/fj.05-4495fje.

Roux, K. J. *et al.* (2012) 'A promiscuous biotin ligase fusion protein identifies proximal and interacting proteins in mammalian cells', *The Journal of Cell Biology*, 196(6), pp. 801-810. doi: 10.1083/jcb.201112098.

Rusconi, F. *et al.* (2016) 'Peptidomimetic targeting of cavbeta2 overcomes dysregulation of the l-type calcium channel density and recovers cardiac function', *Circulation*, 134(7), pp. 534-546. doi: 10.1161/CIRCULATIONAHA.116.021347.

Ruth, P. *et al.* (1989) 'Primary structure of the beta subunit of the DHP-sensitive calcium channel from skeletal muscle', *Science*, 245(4922), pp. 1115-1118. doi: 10.1126/science.2549640.

Salkoff, L. *et al.* (2006) 'High-conductance potassium channels of the SLO family', *Nature Reviews Neuroscience*, 7(12), pp. 921-931. doi: 10.1038/nrn1992.

Sarkar, D. *et al*. (2018) 'LMDIPred: A web-server for prediction of linear peptide sequences binding to SH3, WW and PDZ domains', *PLoS ONE*, 13(7), pp. e0200430-e0200430. doi: 10.1371/journal.pone.0200430.

Schey, K. L. *et al*. (2013) 'Mass spectrometry of membrane proteins: a focus on aquaporins', *Biochemistry*, 52(22), pp. 3807-3817. doi: 10.1021/bi301604j.

Schmidt, T. G. M. *et al.* (2013) 'Development of the Twin-Strep-tag(R) and its application for purification of recombinant proteins from cell culture supernatants', *Protein Expression and Purification*, 92(1), pp. 54-61. doi: 10.1016/j.pep.2013.08.021.

Scriven, D. R. L. *et al.* (2010) 'Analysis of Cav1.2 and ryanodine receptor clusters in rat ventricular myocytes', *Biophysical Journal*, 99(12), pp. 3923-3929. doi: 10.1016/j.bpj.2010.11.008.

Segal, D. *et al.* (2004) 'A role for ZnT-1 in regulating cellular cation influx', *Biochemical and Biophysical Research Communications*, 323(4), pp. 1145-1150. doi: 10.1016/j.bbrc.2004.08.211.

Selbach, M. and Mann, M. (2006) 'Protein interaction screening by quantitative immunoprecipitation combined with knockdown (QUICK)', *Nature Methods*, 3(12), pp. 981-983. doi: 10.1038/nmeth972.

Servili, E. *et al.* (2018) 'β-Subunit of the voltage-gated Ca 2+ channel Cav1.2 drives signaling to the nucleus via H-Ras', *Proceedings of the National Academy of Sciences*, 115(37), pp. E8624-E8633. doi: 10.1073/pnas.1805380115.

De Sevilla Müller, L. P. *et al.* (2013) 'Expression of voltage-gated calcium channel α(2)δ(4) subunits in the mouse and rat retina', *The Journal of Comparative Neurology*, 521(11), pp. 2486-2501. doi: 10.1002/cne.23294.

Shao, Y. *et al.* (2009) 'Dynamic interactions between L-type voltage-sensitive calcium channel

Cav1.2 subunits and ahnak in osteoblastic cells', *American Journal of Physiology Cell physiology*, 296(5), pp. C1067-C1078. doi: 10.1152/ajpcell.00427.2008.

Shaw, R. M. and Colecraft, H. M. (2013) 'L-type calcium channel targeting and local signalling in cardiac myocytes', *Cardiovascular Research*, 98(2), pp. 177-186. doi: 10.1093/cvr/cvt021.

Sheridan, D. C. *et al.* (2003) 'Truncation of the carboxyl terminus of the dihydropyridine receptor β1a subunit promotes Ca2+ dependent excitation-contraction coupling in skeletal myotubes', *Biophysical Journal*, 84(1), pp. 220-237. doi: 10.1016/S0006-3495(03)74844-9.

Shusterman, E. *et al.* (2014) 'ZnT-1 extrudes zinc from mammalian cells functioning as a Zn 2+/H+ exchanger', *Metallomics*, 6(9), pp. 1656-1663. doi: 10.1039/c4mt00108g.

Shusterman, E. *et al.* (2017) 'Zinc transport and the inhibition of the L-type calcium channel are two separable functions of ZnT-1', *Metallomics*, 9(3), pp. 228-238. doi: 10.1039/c6mt00296j.

Sjoblom, B. *et al*. (2008) 'Alpha-actinin structure and regulation', *Cellular and Molecular Life Sciences*, 65(17), pp. 2688-2701. doi: 10.1007/s00018-008-8080-8.

Smits, A. H. and Vermeulen, M. (2016) 'Characterizing protein-protein interactions using mass spectrometry: challenges and opportunities', *Trends in Biotechnology*, 34(10), pp. 825-834. doi: 10.1016/j.tibtech.2016.02.014.

Sorrentino, V. and Volpe, P. (1993) 'Ryanodine receptors: how many, where and why?', *Trends in Pharmacological Sciences*, 14(3), pp. 98-103. doi: 10.1016/0165-6147(93)90072-R.

Stern, M. D. *et al*. (1997) 'Local control model of excitation-contraction coupling in skeletal muscle', *The Journal of General Physiology*, 110(4), pp. 415-440. doi: 10.1085/jgp.110.4.415.

Steward, G. F. and Culley, A. (2010) 'Extraction and purification ofnucleic acids from viruses', *Manual of Aquatic Viral Ecology*, pp. 154-165. doi: 10.4319/mave.2010.978-0-9845591-0-7.154.

Stölting, G. *et al.* (2015) 'Direct interaction of Cavβ with actin up-regulates L-type calcium currents in HL-1 cardiomyocytes', *Journal of Biological Chemistry*, 290(8), pp. 4561-4572. doi: 10.1074/jbc.M114.573956.

Tadmouri, A. *et al.* (2012) 'Cacnb4 directly couples electrical activity to gene expression, a process defective in juvenile epilepsy', *The EMBO Journal*, 31(18), pp. 3730-3744. doi: 10.1038/emboj.2012.226.

Tae, H. S. *et al.* (2009) 'Molecular recognition of the disordered dihydropyridine receptor II-III loop by a conserved spry domain of the type 1 ryanodine receptor', *Clinical and Experimental Pharmacology and Physiology*, 36(3), pp. 346-349. doi: 10.1111/j.1440-1681.2008.05130.x.

Tae, H. S. *et al.* (2011) 'Cyclization of the intrinsically disordered α1S dihydropyridine receptor II-III loop enhances secondary structure and in vitro function', *The Journal of Biological Chemistry*, 286(25), pp. 22589-22599. doi: 10.1074/jbc.M110.205476.

Takada, Y. *et al.* (2015) 'Rab3 interacting molecule 3 mutations associated with autism alter regulation of voltage-dependent Ca2+ channels', *Cell Calcium*, pp. 296-306. doi: 10.1016/j.ceca.2015.06.007.

Takeshima, H. *et al.* (1989) 'Primary structure and expression from complementary DNA of skeletal muscle ryanodine receptor', *Nature*, 339(6224), pp. 439-445. doi: 10.1038/339439a0.

Takeshima, H. *et al.* (2000) 'Junctophilins: a novel family of junctional membrane complex proteins', *Molecular Cell*, 6(1), pp. 11-22. doi: 10.1016/s1097-2765(00)00003-4.

Thompson, T. G. *et al.* (2000) 'Filamin 2 (FLN2): A muscle-specific sarcoglycan interacting protein', *The Journal of Cell Biology*, 148(1), pp. 115-126. doi: 10.1083/jcb.148.1.115.

Timney, B. L. *et al.* (2016) 'Simple rules for passive diffusion through the nuclear pore complex', *The Journal of Cell Biology*, 215(1), pp. 57-76. doi: 10.1083/jcb.201601004.

Tran-Van-Minh, A. and Dolphin, A. C. (2010) 'The $\alpha_2\delta$ ligand gabapentin inhibits the Rab11-dependent recycling of the calcium channel subunit $\alpha_2\delta$-2', *The Journal of Neuroscience*, 30(38), pp. 12856-12867. doi: 10.1523/JNEUROSCI.2700-10.2010.

Tristan, C. *et al.* (2011) 'The diverse functions of GAPDH: views from different subcellular compartments', *Cellular Signalling*, 23(2), pp. 317-323. doi: 10.1016/j.cellsig.2010.08.003.

Tseng, P. Y. *et al.* (2017) 'alpha-Actinin promotes surface localization and current density of the Ca(2+) channel Cav1.2 by binding to the IQ region of the alpha1 subunit', *Biochemistry*, 56(28), pp. 3669-3681. doi: 10.1021/acs.biochem.7b00359.

Turner, M. *et al.* (2020) 'alpha-Actinin-1 promotes activity of the L-type Ca(2+) channel Cav1.2', *The EMBO Journal*, 39(5), p. e102622. doi: 10.15252/embj.2019102622.

Uriu, Y. *et al.* (2010) 'Rab3-interacting molecule γ isoforms lacking the rab3-binding domain induce long lasting currents but block neurotransmitter vesicle anchoring in voltage-dependent P/Q-type Ca2+ channels', *Journal of Biological Chemistry*, 285(28), pp. 21750-21767. doi: 10.1074/jbc.M110.101311.

van der Ven, P. F. *et al.* (2000) 'Indications for a novel muscular dystrophy pathway. gamma-filamin, the muscle-specific filamin isoform, interacts with myotilin', *The Journal of Cell Biology*, 151(2), pp. 235-248. doi: 10.1083/jcb.151.2.235.

Vendel, A. C. *et al.* (2006) 'Alternative splicing of the voltage-gated Ca^{2+} channel β_4 subunit creates a uniquely folded N-terminal protein binding domain with cell-specific expression in the cerebellar cortex', *The Journal of Neuroscience*, 26(10), pp. 2635-2644. doi: 10.1523/JNEUROSCI.0067-06.2006.

Vermeulen, M. *et al*. (2008) 'High confidence determination of specific protein-protein interactions using quantitative mass spectrometry', *Current Opinion in Biotechnology*, 19(4), pp. 331-337. doi: 10.1016/j.copbio.2008.06.001.

Viard, P. *et al.* (2004) 'PI3K promotes voltage-dependent calcium channel trafficking to the plasma membrane', *Nature Neuroscience*, 7(9), pp. 939-946. doi: 10.1038/nn1300.

De Waard, M. *et al.* (1995) 'Properties of the α1-β anchoring site in voltage-dependent Ca2+ channels', *Journal of Biological Chemistry*, 270(20), pp. 12056-12064. doi: 10.1074/jbc.270.20.12056.

Waithe, D. *et al.* (2011) 'Beta-subunits promote the expression of Ca(V)2.2 channels by reducing their proteasomal degradation', *The Journal of Biological Chemistry*, 286(11), pp. 9598-9611. doi: 10.1074/jbc.M110.195909.

Wang, D. *et al.* (2002) 'Activation of Ras/Erk pathway by a novel MET-interacting protein RanBPM', *Journal of Biological Chemistry*, 277(39), pp. 36216-36222. doi: 10.1074/jbc.M205111200.

Wang, D. *et al.* (2005) 'The SPRY domain-containing SOCS box protein 1 (SSB-1) interacts with MET and enhances the hepatocyte growth factor-induced Erk-Elk-1-serum response element pathway', *Journal of Biological Chemistry*, 280(16), pp. 16393-16401. doi: 10.1074/JBC.M413897200.

Weiss, S. *et al.* (2013) 'Regulation of cardiac L-Type Ca2+ channel CaV1.2 via the β-adrenergic-cAMP-protein kinase a pathway: Old dogmas, advances, and new uncertainties', *Circulation Research*, 113(5), pp. 617-631. doi: 10.1161/CIRCRESAHA.113.301781.

Weissgerber, P. *et al.* (2006) 'Reduced cardiac L-type Ca2+ current in Cavβ2-/- embryos impairs cardiac development and contraction with secondary defects in vascular maturation', *Circulation Research*, 99(7), pp. 749-757. doi: 10.1161/01.RES.0000243978.15182.c1.

Willegems, K. and Efremov, R. G. (2017) 'Structural details of the ryanodine receptor calcium release channel and its gating mechanism', *Advances in Experimental Medicine and Biology*, 981, pp. 179-204. doi: 10.1007/978-3-319-55858-5_8.

Wong, J. *et al.* (2013) 'Nanoscale distribution of ryanodine receptors and caveolin-3 in mouse ventricular myocytes: dilation of t-tubules near junctions', *Biophysical Journal*, 104(11), pp. L22-4. doi: 10.1016/j.bpj.2013.02.059.

Wu, J. *et al.* (2015) 'Structure of the voltage-gated calcium channel Cav1.1 complex', *Science*, 350(6267), p. aad2395. doi: 10.1126/science.aad2395.

Xu, X. *et al.* (2011) 'The Ca2+ channel beta4c subunit interacts with heterochromatin protein 1 via

a PXVXL binding motif', *The Journal of Biological Chemistry*, 286(11), pp. 9677-9687. doi: 10.1074/jbc.M110.187864.

Xu, X. *et al.* (2015) 'Solution NMR and calorimetric analysis of Rem2 binding to the Ca2+ channel β4 subunit: a low affinity interaction is required for inhibition of Cav2.1 Ca2+ currents', *FASEB Journal*, 29(5), pp. 1794-1804. doi: 10.1096/fj.14-264499.

Yan, Z. *et al.* (2015) 'Structure of the rabbit ryanodine receptor RyR1 at near-atomic resolution', *Nature*, 517(7532), pp. 50-55. doi: 10.1038/nature14063.

Yang, L. *et al.* (2007) 'Protein kinase G phosphorylates Cav1.2 α1c and β2 subunits', *Circulation Research*, 101(5), pp. 465-474. doi: 10.1161/CIRCRESAHA.107.156976.

Yang, L. *et al.* (2011) 'Cardiac L-type calcium channel (Cav1.2) associates with gamma subunits', *FASEB Journal*, 25(3), pp. 928-936. doi: 10.1096/fj.10-172353.

Yang, L. *et al.* (2019) 'Cardiac CaV1.2 channels require β subunits for β-adrenergic-mediated modulation but not trafficking', *The Journal of Clinical Investigation*, 129(2), pp. 647-658. doi: 10.1172/JCI123878.

Yang, T. and Colecraft, H. M. (2013) 'Regulation of voltage-dependent calcium channels by RGK proteins', *Biochimica et Biophysica Acta*, 1828(7), pp. 1644-1654. doi: 10.1016/j.bbamem.2012.10.005.

Yang, T. *et al*. (2012) 'Distinct RGK GTPases differentially use α1- and auxiliary β-binding-dependent mechanisms to inhibit CaV1.2/CaV2.2 channels', *PloS one*, 7(5), pp. e37079-e37079. doi: 10.1371/journal.pone.0037079.

Yin, C. C. *et al*. (2005) 'Physical coupling between ryanodine receptor-calcium release channels', *Journal of Molecular Biology*, 349(3), pp. 538-546. doi: 10.1016/j.jmb.2005.04.002.

Yu, F. H. (2005) 'Overview of molecular relationships in the voltage-gated ion channel superfamily', *Pharmacological Reviews*, 57(4), pp. 387-395. doi: 10.1124/pr.57.4.13.

Yu, K. *et al.* (2008) 'The best disease-linked Cl- channel hBest1 regulates CaV1 (L-type) Ca2+ channels via src-homology-binding domains', *The Journal of Neuroscience*, 28(22), pp. 5660-5670. doi: 10.1523/JNEUROSCI.0065-08.2008.

Zamponi, G. W. *et al.* (2015) 'The physiology, pathology, and pharmacology of voltage-gated calcium channels and their future therapeutic potential', *Pharmacological Reviews*, 67(4), pp. 821-870. doi: 10.1124/pr.114.009654.

Zhan, L. P. *et al*. (2018) 'Mass Spectrometry of Membrane Proteins', in *Membrane Biophysics* (Chapter 10), Springer Nature Singapore, pp. 285-317. doi: 10.1007/978-981-10-6823-2_10.

Zhang, X. *et al.* (2010) 'Pax6 is a human neuroectoderm cell fate determinant', *Cell Stem Cell*, 7(1), pp. 90-100. doi: 10.1016/j.stem.2010.04.017.

Zhou, Z. and January, C. T. (1998) 'Both T- and L-type Ca2+ channels can contribute to excitation-contraction coupling in cardiac Purkinje cells', *Biophysical Journal*, 74(4), pp. 1830-1839. doi: 10.1016/S0006-3495(98)77893-2.

Zorzato, F. *et al.* (1990) 'Molecular cloning of cDNA encoding human and rabbit forms of the Ca2+ release channel (ryanodine receptor) of skeletal muscle sarcoplasmic reticulum', *The Journal of Biological Chemistry*, 265(4), pp. 2244-2256.

Zou, S. *et al.* (2008) 'The β1 subunit of L-type voltage-gated ca2+ channels independently binds to and inhibits the gating of large-conductance Ca2+-activated K+ channels', *Molecular Pharmacology*, 73(2), pp. 369-378. doi: 10.1124/mol.107.040733.

7. SUPPLEMENTARY INFORMATION

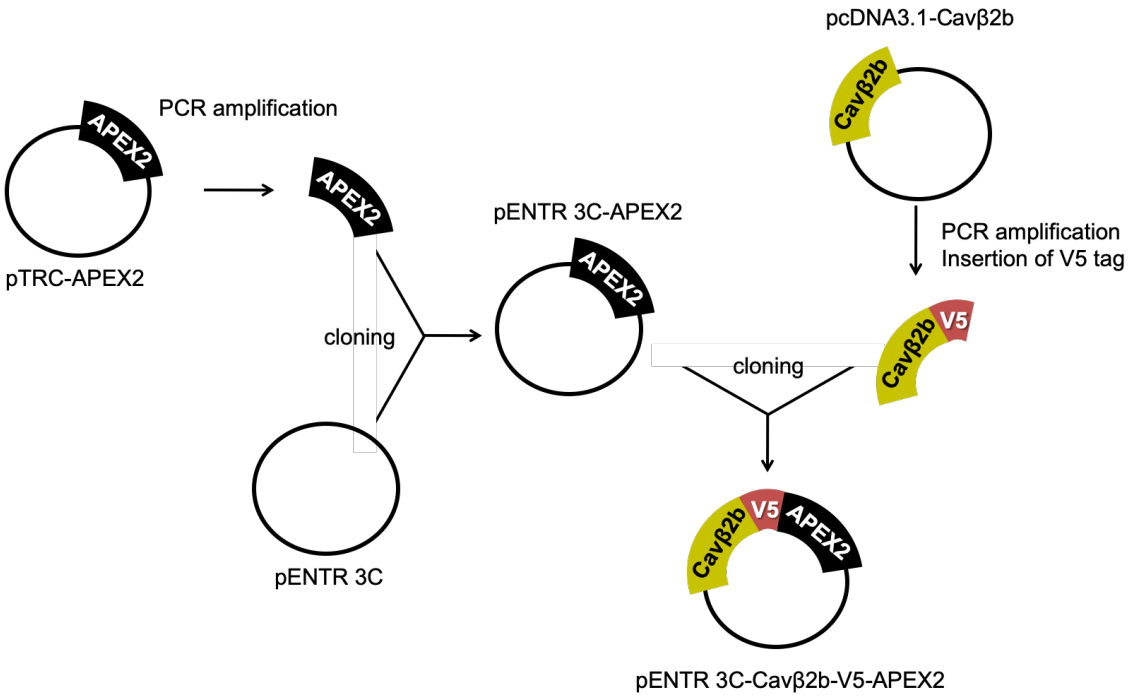

Figure S1. Schematic representation of the construction of the recombinant plasmid pENTR 3C-Cavβ2b-V5-APEX2. The cDNA fragment containing the sequence encoding APEX2 was obtained by PCR amplification from the vector pTRC-APEX2 and cloned into the pENTR 3C vector to produce the pENTR 3C-APEX2 plasmid. To generate the pENTR 3C-Cavβ2b-V5-APEX2 construct, the cDNA encoding the full rat Cavβ2b (accession number Q8VGC3-5) was amplified by PCR from the pcDNA3.1-Cavβ2b vector and inserted in frame upstream of the APEX2 sequence into the pENTR 3C-APEX2 plasmid using standard overlapping PCR methods. The reverse primer used for PCR amplification of the sequence coding for Cavβ2b contained as overhang the cDNA sequence encoding the V5 tag peptide. The plasmid pENTR 3C-Cavβ2b-V5-APEX2 was used for the generation of an adenoviral vector by homologous DNA recombination to express the Cavβ2b-V5-APEX2 protein in adult rat cardiomyocytes.

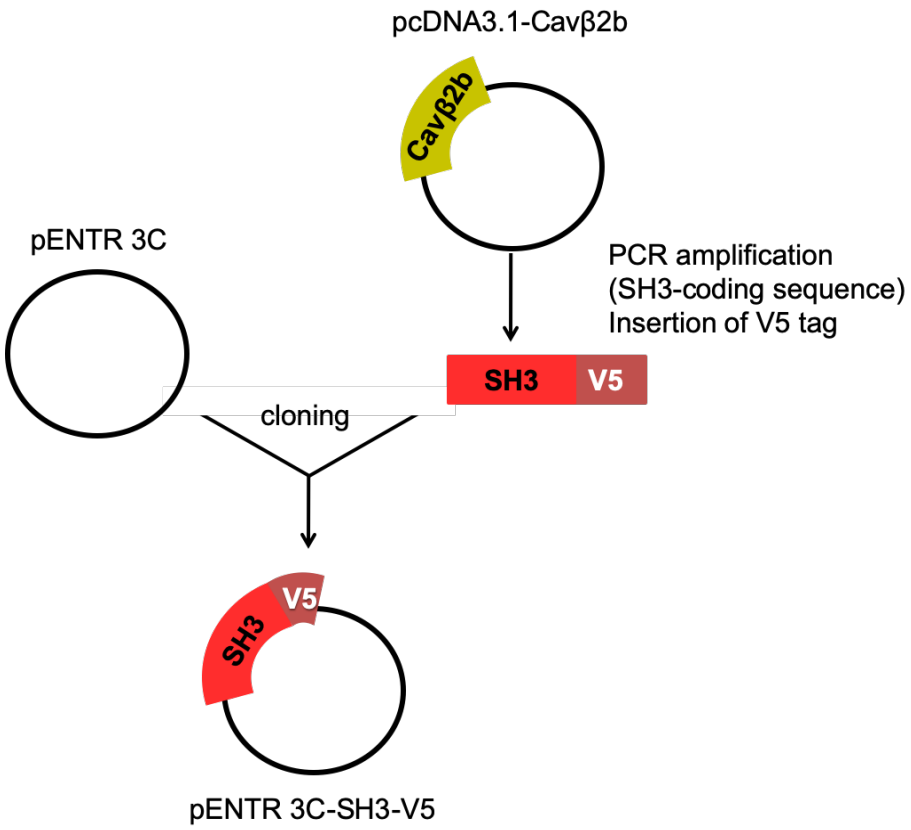

Figure S2. Schematic representation of the construction of the recombinant plasmid pENTR 3C-SH3-V5. The cDNA encoding the SH3 domain of the rat Cavβ2b (amino acids 25-137) was amplified by PCR from the pcDNA3.1-Cavβ2b vector and cloned into the pENTR 3C vector using conventional molecular biology methods. The reverse primer used for PCR amplification of the sequence coding for the SH3 domain contained as overhang the cDNA sequence encoding the V5 tag peptide. The plasmid pENTR 3C-SH3-V5 was used for the generation of an adenoviral vector by homologous DNA recombination to express the Cavβ2b-SH3 domain in adult rat cardiomyocytes. SH3: Src-3 homology domain.

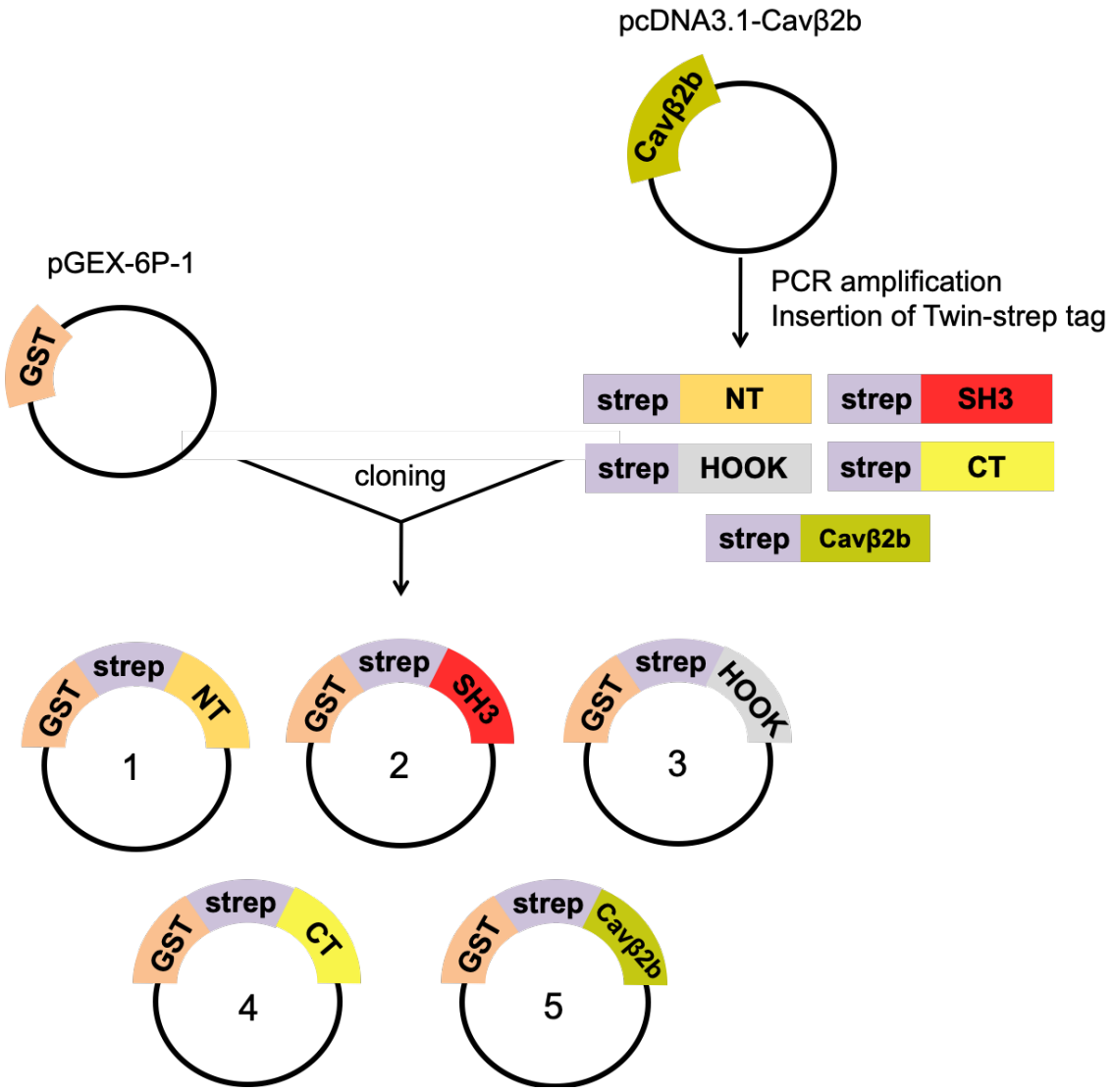

Figure S3. Schematic representation of the construction of the recombinant plasmids used for the expression of GST-fused proteins. The cDNA of the rat Cavβ2b (accession number Q8VGC3-5) and its NT (amino acids 1-24), SH3 (amino acids 25-137), HOOK (amino acids 138-225) and CT (amino acids 424-605) domains were amplified using the pcDNA3.1-Cavβ2b vector. Each specific forward primer contained as overhang the cDNA sequence encoding the Twin-Strep-tag peptide (WSHPQFEKGGGSGGGSGGSAWSHPQFEK). The amplified PCR fragments were cloned in frame into the pGEX-6P-1 vector to fuse a GST moiety at the N-terminus of the resulting proteins. Constructs: 1) pGEX-6P-1-Twin-strep-NT; 2) pGEX-6P-1-Twin-strep-SH3; 3) pGEX-6P-1-Twin-strep-HOOK; 4) pGEX-6P-1-Twin-strep-CT; pGEX-6P-1-Twin-strep-Cavβ2b. CT: C-terminus; GST: glutathione S-transferase; HOOK: linker region; NT: N-terminus; SH3: Src-3 homology domain; strep: Twin-Strep-tag.

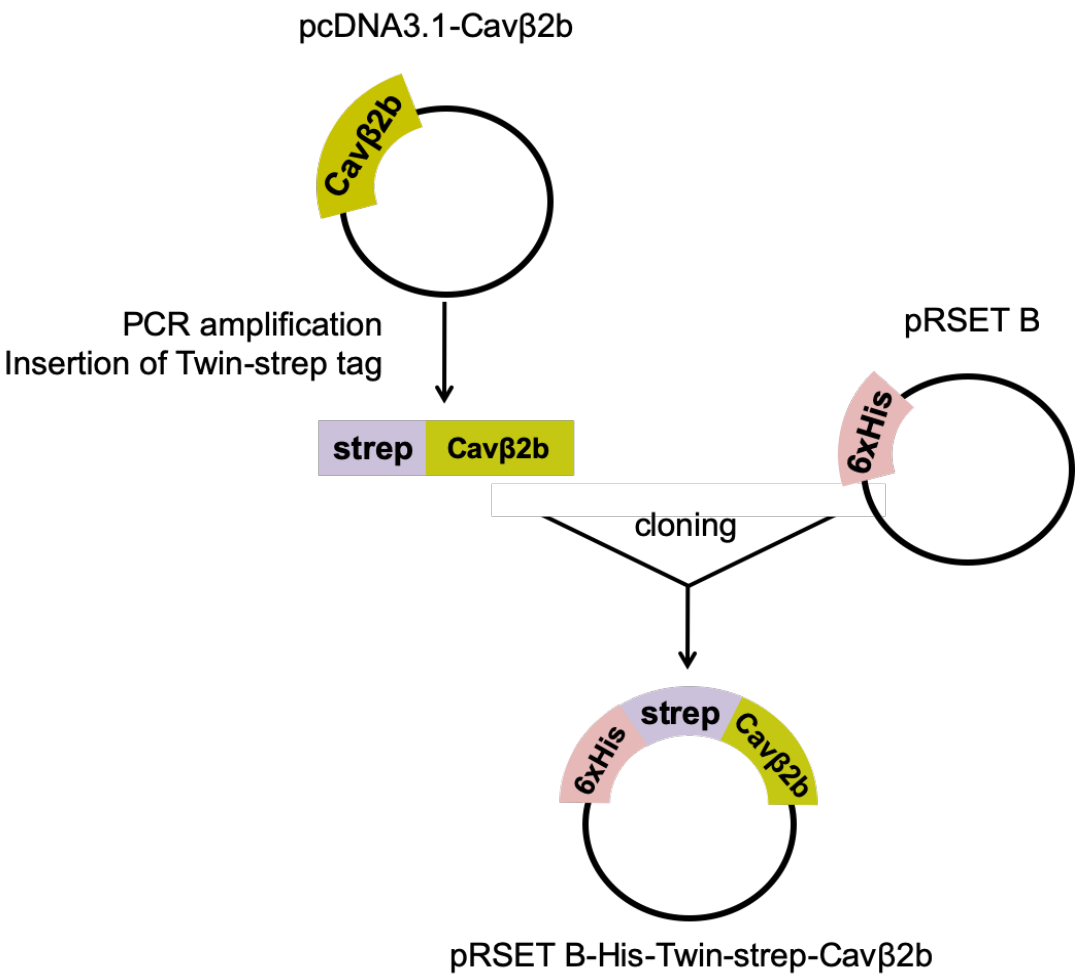

Figure S4. Schematic representation of the construction of the recombinant plasmid used for the expression of the His-Twin-strep-Cavβ2b protein. The cDNA of the rat Cavβ2b (accession number Q8VGC3-5) was amplified using the pcDNA3.1-Cavβ2b vector. The forward primer used for the amplification contained as overhang the cDNA sequence encoding the Twin-strep-tag peptide (WSHPQFEKGGGSGGGSGGSAWSHPQFEK). The amplified PCR fragment was cloned in frame into the pRSET B vector to generate the construct pRSET B-His-Twin-strep-Cavβ2b. This construct carries at its 5' end the sequence coding for a polyhistidine tag (shown in the figure as 6xHis), followed by the Twin-strep-tag (shown in the figure as strep).

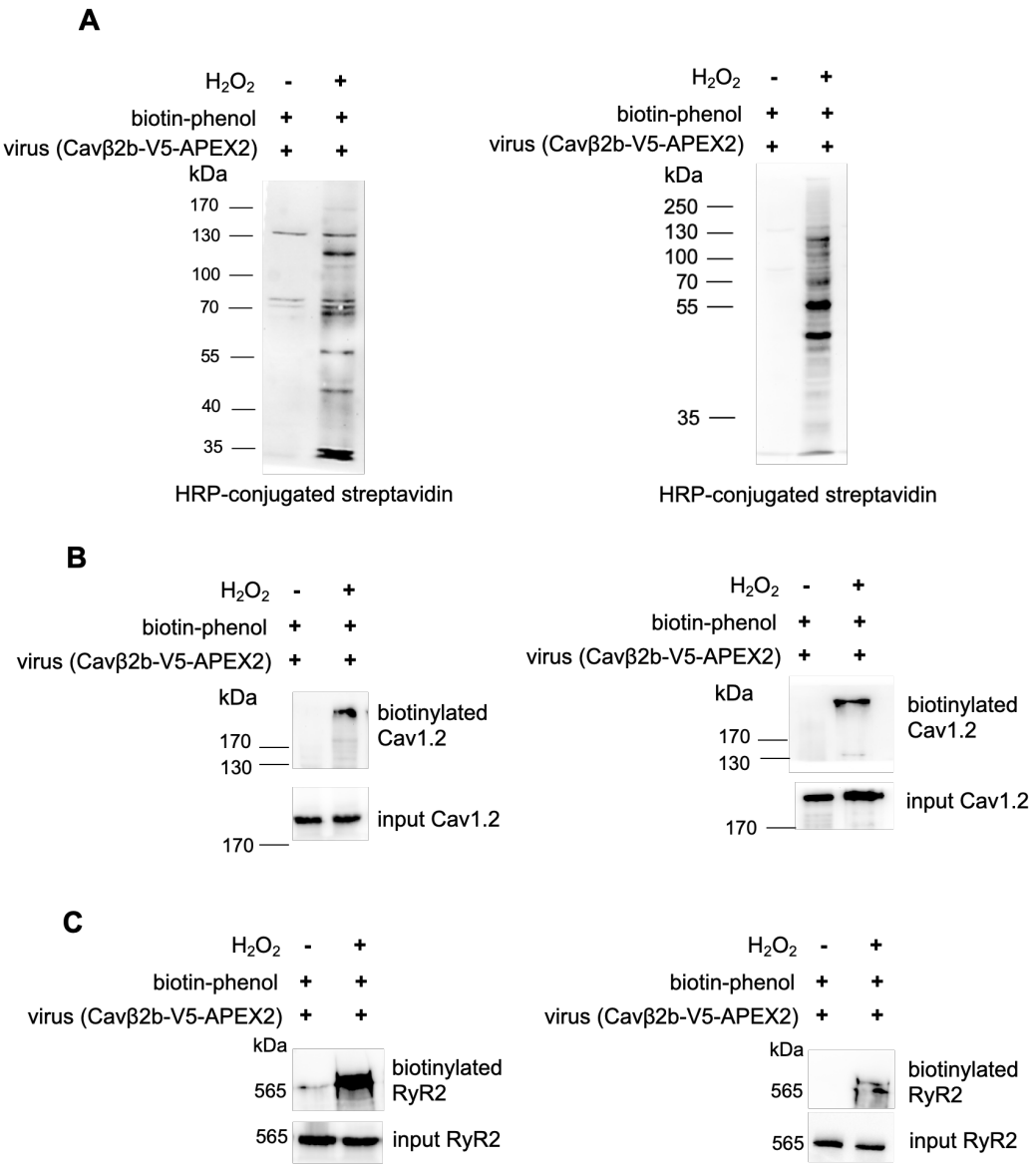

Figure S5. Replicates of the immunoblots of biotin-labeled proteins from adult rat cardiomyocytes transduced with Cavβ2b-V5-APEX2. ARC were infected with adenovirus at a MOI of 75 for the expression of the recombinant protein Cavβ2b-V5-APEX2. Transduced cells were incubated with biotin-phenol for 30 min and then treated with H_2O_2 for 1 min to initiate biotinylation. The cells were lysed and the biotinylated proteins were enriched using streptavidin-coated beads and analyzed by western blot. (A) Streptavidin blot analysis of endogenous proteins biotinylated by Cavβ2b-V5-APEX2. Western blot after streptavidin-mediated enrichment of biotinylated proteins using antibodies against (B) Cav1.2 or (C) RyR2. ARC: adult rat cardiomyocytes; MOI: multiplicity of infection.

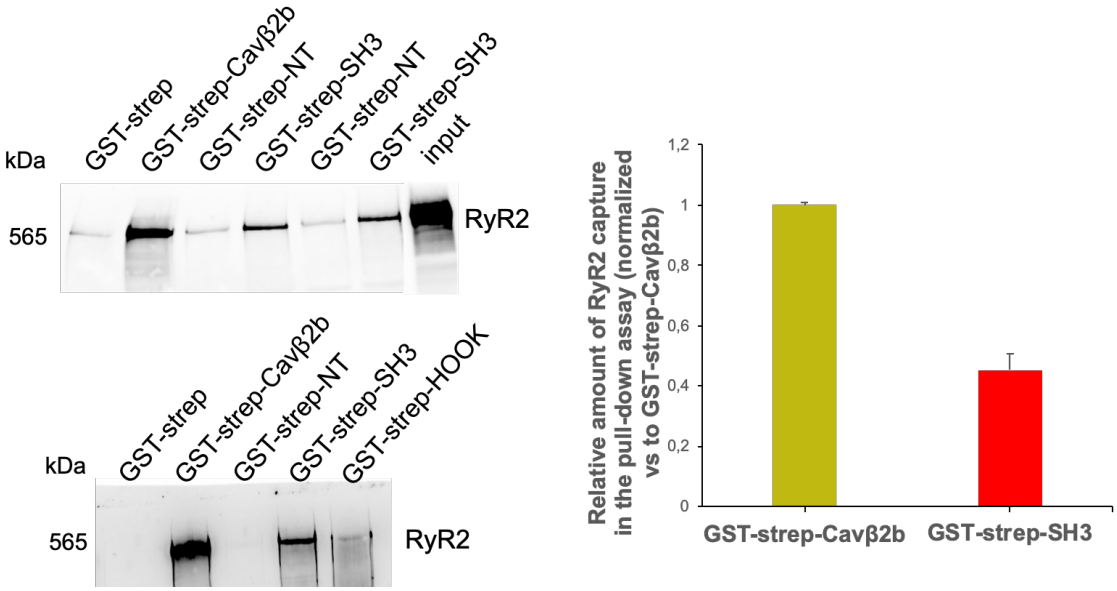

Figure S6. Replicates of the immunoblots of strep-tag pull-down assays. Left panel: the purified GST-strep-Cavβ2b, GST-strep-NT, GST-strep-SH3; GST-strep-HOOK or GST-strep (negative control) were incubated with mouse heart lysates and the eluates were analyzed by western blot using an anti-RyR2 antibody. Right panel: bar plots (mean ± SEM) of densitometric measurements from the western blots showing the relative amount of RyR2 captured in the pull-down assay using GST-strep-SH3. GST: glutathione S-transferase; NT: N-terminus; RyR2: ryanodine receptor 2; SH3: Src-3 homology domain; strep: Twin-strep-tag.

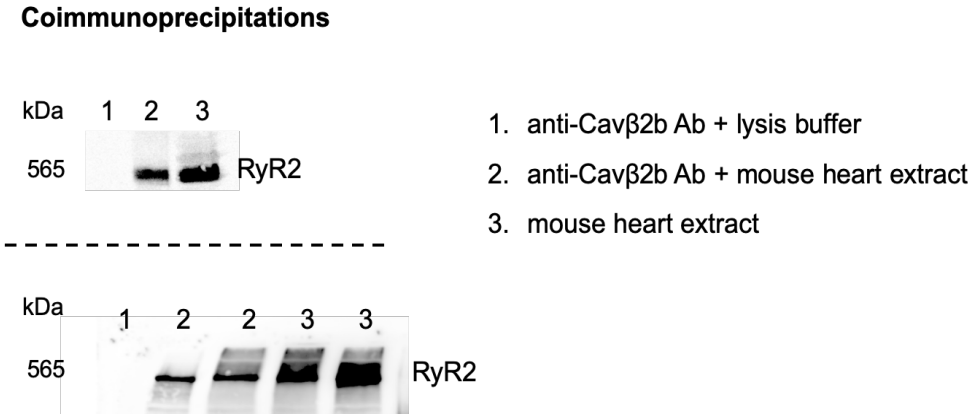

Figure S7. Replicates of the coimmunoprecipitation of the RyR2 with Cavβ2b using mouse heart lysates. Cavβ2b was immunoprecipitated by the anti-Cavβ2b antibody and the coprecipitated RyR2 was analyzed by western blot using anti-RyR2 antibody. The lysis buffer contained 20 mM Tris pH 7.5, 150 mM NaCl and 1% [v/v] NP-40. Ab: antibody; RyR2: ryanodine receptor 2.

Table S1. Proteins in the Cavβ2b nanoenvironments identified by proximity labeling biotinylation.

Protein IDs	Genes	Protein names	Unique peptides	Log_2 (H_2O_2/ no H_2O_2)	-Log_{10} (p value)
A0A096MJ01	*Ldb3*	LIM domain-binding 3	4	3,930	2,367
A0A096MJI9	*Atp1b1*	Na^+/K^+-transporting ATPase subunit beta-1	3	3,651	2,264
A0A0G2JSH9	*Prdx2*	Peroxiredoxin-2	5	4,747	4,060
A0A0G2JSU4	*Ndrg2*	N-myc downstream regulated gene 2	6	4,903	2,551
A0A0G2JU96	*Ahnak*	AHNAK nucleoprotein	17	4,339	3,426
A0A0G2JUC7	*Dctn2*	Dynactin subunit 2	8	3,719	3,423
A0A0G2JWE1*	*Myl6*	Myosin light polypeptide 6	4	4,743	2,051
A0A0G2K1J5	*Plec*	Plectin	21	4,116	3,278
A0A0G2K2T1	*Txlnb*	Taxilin beta	7	3,418	2,775
A0A0G2K5P5	*Myom1*	Myomesin 1	28	4,375	2,836
A0A0G2K6S9*	*Myh11*	Myosin-11	42	5,000	3,368
A0A0G2K7B6	*Dysf*	Dysferlin	38	5,535	3,133
R9PXU6	*Vcl*	Vinculin	23	4,491	2,806
A0A0H2UHR7	*Flnc*	Filamin-C	52	7,414	6,254
A0JPQ4	*Trim72*	Tripartite motif-containing protein 72	9	5,185	2,323
B0LPN4-2	*Ryr2*	Ryanodine receptor 2	77	4,635	2,577
B1PRL5*	*Cavin4*	Caveolae-associated protein 4	4	2,940	2,736
D3Z802	*Nrap*	Nebulin-related-anchoring protein	16	3,022	3,042
D3ZCV0	*Actn2*	Actinin alpha 2	19	4,659	2,367
D4AC36*	*Eif3f*	Eukaryotic translation initiation factor 3 subunit F	6	2,923	3,293
E9PT87	*Mylk3*	Myosin light chain kinase 3	11	3,683	4,352
F1M779	*Cltc*	Clathrin heavy chain	35	6,038	3,029
Q62812*	*Myh9*	Myosin-9	31	4,695	2,918
G3V7K1	*Myom2*	Myomesin 2	37	4,801	3,390

G3V7L6	*Psmc2*	26S protease regulatory subunit 7	12	3,312	4,853
G3V9N0	*Pabpc4*	Polyadenylate-binding protein	8	3,052	2,827
M0R9L0	*Naca*	Nascent polypeptide-associated complex subunit alpha	30	4,794	3,196
M0R9X8	*Dync1h1*	Cytoplasmic dynein 1 heavy chain 1	57	5,576	3,340
O35303	*Dnm1l*	Dynamin-1-like protein	19	4,153	2,662
O35878	*Hspb2*	Heat shock protein beta-2	6	3,429	3,219
P05197	*Eef2*	Elongation factor 2	14	4,221	2,565
P08733	*Myl2*	Myosin regulatory light chain 2	13	3,910	3,618
P09456	*Prkar1a*	cAMP-dependent protein kinase type I-alpha regulatory subunit	9	3,056	2,269
P0DMW1;P0DMW0	*Hspa1b, Hspa1a*	Heat shock 70 kDa protein 1B; Heat shock 70 kDa protein 1A	6	3,018	4,037
P11232	*Txn*	Thioredoxin	2	3,045	2,159
P19804;Q05982	*Nme2, Nme1*	Nucleoside diphosphate kinase B; Nucleoside diphosphate kinase A	6	2,916	2,489
P36201	*Crip2*	Cysteine-rich protein 2	2	3,772	2,795
P46462	*Vcp*	Transitional endoplasmic reticulum ATPase	25	7,527	5,359
P56741	*Mybpc3*	Myosin-binding protein C, cardiac-type	44	5,037	3,181
Q5D059	*Hnrnpk*	Heterogeneous nuclear ribonucleoprotein K	7	3,238	3,531
P61983	*Ywhag*	14-3-3 protein gamma	2	3,182	2,295
P63018	*Hspa8*	Heat shock cognate 71 kDa protein	18	3,242	3,315
Q1JU68	*Eif3a*	Eukaryotic translation initiation factor 3 subunit A	12	3,177	2,194
Q2PQA9	*Kif5b*	Kinesin-1 heavy chain	16	3,322	2,742
Q2PS20	*Jph2*	Junctophilin-2	7	3,188	2,138
Q4FZT9	*Psmd2*	26S proteasome non-ATPase regulatory subunit 2	10	3,646	2,464
Q4G061	*Eif3b*	Eukaryotic translation initiation factor 3 subunit B	8	2,902	2,748

Q4PP99	*Tnnc1*	Cardiac troponin C	8	4,017	2,100
Q5U2U8	*Bag3*	Bcl2-associated athanogene 3	5	3,684	4,435
Q5U300	*Uba1*	Ubiquitin-like modifier-activating enzyme 1	14	3,405	3,276
Q5XI34	*Ppp2r1a*	Protein phosphatase 2 (Formerly 2A), regulatory subunit A (PR 65), alpha isoform, isoform CRA_a	7	4,304	2,856
Q6P6U2	*Psmc3*	26S protease regulatory subunit 6A	12	3,765	2,274
Q68FR6	*Eef1g*	Elongation factor 1-gamma	11	4,308	2,830
Q68FR9	*Eef1d*	Elongation factor 1-delta	5	3,347	2,731
Q68FS2	*Cops4*	COP9 signalosome complex subunit 4	7	2,941	2,186
P48037	*Anxa6*	Annexin A6	23	6,835	5,947
Q6P9V7	*Psme1*	Proteasome activator complex subunit 1	10	3,013	2,170
Q8R3Z7	*Ehd4*	EH-domain-containing 4	12	3,516	2,975
Q9EPX0	*Hspb8*	Heat shock protein beta-8	2	3,361	2,880
Q9Z269	*Vapb*	Vesicle-associated membrane protein-associated protein B	5	4,037	3,617
Q9Z270	*Vapa*	Vesicle-associated membrane protein-associated protein A	4	3,616	2,487

*These proteins were not identified as constituents of the Cav1.2 macromolecular complex by Liu G *et a*l. (2020).

Table S2. Annotation of proteins in the nanoenvironments of Cavβ2b.

Accession number	Protein names	Subcellular localization	Biological processes
A0A096MJ01	LIM domain-binding 3	Cytoskeleton	Sarcomere organization
A0A096MJI9	Na+/K+-transporting ATPase subunit beta-1	Plasma membrane	Ion transport
A0A0G2JSH9	Peroxiredoxin-2	Cytosol	Cellular response to oxidative stress
A0A0G2JSU4	N-myc downstream regulated gene 2	Nucleus	Unknown
A0A0G2JU96	AHNAK nucleoprotein	Cytosol, plasma membrane, nucleus	Excitation- contraction coupling, sarcomere organization, cellular trafficking
A0A0G2JUC7	Dynactin subunit 2	Cytoskeleton	Cellular trafficking
A0A0G2JWE1	Myosin light polypeptide 6	Cytosol	Unknown
A0A0G2K1J5	Plectin	Cytoskeleton	Cell-cell adhesion
A0A0G2K2T1	Taxilin beta	Cytosol	Cellular trafficking
A0A0G2K5P5	Myomesin 1	Cytoskeleton	Muscle contraction
A0A0G2K6S9	Myosin-11	Cytoskeleton	Muscle contraction
A0A0G2K7B6	Dysferlin	Cytoskeleton, plasma membrane	Plasma membrane repair
R9PXU6	Vinculin	Cytoskeleton	Cell-cell adhesion
A0A0H2UHR7	Filamin-C	Cytoskeleton	Unknown
A0JPQ4	Tripartite motif-containing protein 72	Plasma membrane	Plasma membrane repair
B0LPN4	Ryanodine receptor 2	Sarcoplasmic reticulum	Excitation-contraction coupling, ion transport
B1PRL5	Caveolae-associated protein 4	Cytosol, plasma membrane	Sarcomere organization
D3Z802	Nebulin-related-anchoring protein	Cytoskeleton	Sarcomere organization
D3ZCV0	Actinin alpha 2	Cytosol, plasma membrane	Sarcomere organization
D4AC36	Eukaryotic translation initiation factor 3 subunit F	Cytosol	Protein translation
E9PT87	Myosin light chain kinase 3	Cytosol, cytoskeleton	Muscle contraction

F1M779	Clathrin heavy chain	Plasma membrane	Cellular trafficking
Q62812	Myosin-9	Cytoskeleton	Muscle contraction
G3V7K1	Myomesin 2	Cytoskeleton	Muscle contraction
G3V7L6	26S proteasome regulatory subunit 7	Cytosol	Protein degradation
G3V9N0	Polyadenylate-binding protein	Cytosol	Protein translation
M0R9L0	Nascent polypeptide-associated complex subunit alpha	Unknown	Unknown
M0R9X8	Cytoplasmic dynein 1 heavy chain 1	Cytosol, plasma membrane, cytoskeleton	Cellular trafficking
O35303	Dynamin-1-like protein	Membrane, cytosol	Cellular trafficking
O35878	Heat shock protein beta-2	Cytosol, nucleus	Protein folding
P05197	Elongation factor 2	Cytosol, nucleus	Protein translation
P08733	Myosin regulatory light chain 2	Cytoskeleton	Muscle contraction
P09456	cAMP-dependent protein kinase type I-alpha regulatory subunit	Cytosol, plasma membrane	Excitation-contraction coupling, Ca^{2+} signaling
P0DMW1; P0DMW0	Heat shock 70 kDa protein 1B; Heat shock 70 kDa protein 1A	Cytosol, cytoskeleton	Protein folding
P11232	Thioredoxin	Cytosol, nucleus	Cellular response to oxidative stress
P19804; Q05982	Nucleoside diphosphate kinase B; Nucleoside diphosphate kinase A	Cytosol, nucleus	Unknown
P36201	Cysteine-rich protein 2	Cytosol, nucleus	Unknown
P46462	Transitional endoplasmic reticulum ATPase	Cytosol, nucleus, sarcoplasmic reticulum	Protein degradation, cellular trafficking
P56741	Myosin-binding protein C, cardiac-type	Cytoskeleton	Sarcomere organization, muscle contraction, cell-cell adhesion
Q5D059	Heterogeneous nuclear ribonucleoprotein K	Nucleus	Transcription regulator
P61983	14-3-3 protein gamma	Cytosol, plasma membrane	Unknown
P63018	Heat shock cognate 71 kDa protein	Plasma membrane, nucleus	Protein folding
Q1JU68	Eukaryotic translation initiation factor 3 subunit A	Cytosol, nucleus	Protein translation
Q2PQA9	Kinesin-1 heavy chain	Cytoskeleton	Cellular trafficking

Q2PS20	Junctophilin-2	Plasma membrane, sarcoplasmic reticulum	Sarcomere organization, excitation-contraction coupling
Q4FZT9	26S proteasome non-ATPase regulatory subunit 2	Cytosol	Protein degradation
Q4G061	Eukaryotic translation initiation factor 3 subunit B	Cytosol, nucleus	Protein translation
Q4PP99	Cardiac troponin C	Cytoskeleton	Muscle contraction
Q5U2U8	Bcl2-associated athanogene 3	Cytosol	Protein folding
Q5U300	Ubiquitin-like modifier-activating enzyme 1	Cytosol	Protein degradation
Q5XI34	Protein phosphatase 2 (Formerly 2A), regulatory subunit A (PR 65)	Cytosol, nucleus	Excitation-contraction coupling, Ca^{2+} signaling, protein translation
Q6P6U2	26S proteasome regulatory subunit 6A	Cytosol	Protein degradation
Q68FR6	Elongation factor 1-gamma	Cytosol, nucleus	Protein translation
Q68FR9	Elongation factor 1-delta	Cytosol, nucleus	Protein translation
Q68FS2	COP9 signalosome complex subunit 4	Cytosol, nucleus	Protein degradation
P48037	Annexin A6	Plasma membrane, nucleus	Cellular trafficking
Q6P9V7	Proteasome activator subunit 1	Cytosol	Protein degradation
Q8R3Z7	EH-domain-containing 4	Plasma membrane, sarcoplasmic reticulum	Cell-cell adhesion
Q9EPX0	Heat shock protein beta-8	Cytosol, nucleus	Protein folding
Q9Z269	Vesicle-associated membrane protein-associated protein B	Plasma membrane, sarcoplasmic reticulum	Cellular trafficking
Q9Z270	Vesicle-associated membrane protein-associated protein A	Plasma membrane, sarcoplasmic reticulum	Cellular trafficking
P22002[1]	Voltage-dependent L-type calcium channel subunit alpha-1C	Plasma membrane	Excitation- contraction coupling, ion transport

[1]. This protein was identified only by western blot.

8. ACKNOWLEDGMENTS

I would like to express my deep gratitude to everyone who contributed to this work and without whose support this thesis would not have been possible.

First of all, I would like to thank Dr. Erick Miranda Laferte for taking me as his student. I very much enjoyed the wonderful experience of my PhD, during which I have learned countless new things. Thank you for being extremely supportive all along the way and for the very enriching scientific discussions we had.

I am deeply grateful to Prof. Michaela Kuhn for giving me the opportunity to do my research work at the Institute of Physiology and for accepting the supervision of my thesis. This institute has provided me with a great scientific, educational and social environment.

I would also like to thank the members of my thesis committee Prof. Michaela Kuhn and Prof. Thomas Dandekar for the guidance, scientific advice on the project, and all the support throughout these years.

Erick, Simone, Conny, I feel lucky I was part of this small but wonderful team. The time we spent at work and also outside the lab was a lovely experience for me, full of memorable moments. Thank you for everything!

Many scientists made a valuable contribution to this work and I would like to thank especially Prof. Katrin Marcus, Prof. Christoph Maack, Dr. Katalin Barkovits, P.D. Dr. Petra Eder-Negrin, P.D. Dr. Sören Doose, Marvin Jungblut and all the co-authors of this study, for their generous support. One person in particular was a great help: Dr. Michael Kohlhaas. Thank you for all the expertise offered!

Jorge, you have been there for me since the beginning of this journey. Thank you very much for your trust and for always encouraging me to face challenges.

Thanks to all current and former members of the department led by Prof. Michaela Kuhn for the friendly atmosphere at work and your continued help. Thanks to Baerbel Zumkeller for the excellent administrative support.

Thanks to Sandra Bandleon and Antonella Cellini for the hospitality and collaborative spirit in your lab. I also thank Prof. Dr. Viacheslav Nikolaev for his advice with the adenovirus preparations.

And finally, but by no means least, thanks to my mon and my dad for their unconditional guidance in life.

Eidesstattliche Erklärungen nach §7 Abs. 2 Satz 3, 4, 5 der Promotionsordnung der Fakultät für Biologie

Eidesstattliche Erklärung

Hiermit erkläre ich an Eides statt, die Dissertation: **"Interaktom der β2b-Untereinheit von spannungsgesteuerten L-Typ Kalziumkanälen in Kardiomyozyten"**, eigenständig, d. h. insbesondere selbständig und ohne Hilfe eines kommerziellen Promotionsberaters, angefertigt und keine anderen, als die von mir angegebenen Quellen und Hilfsmittel verwendet zu haben.

Ich erkläre außerdem, dass die Dissertation weder in gleicher noch in ähnlicher Form bereits in einem anderen Prüfungsverfahren vorgelegen hat.

Weiterhin erkläre ich, dass bei allen Abbildungen und Texten bei denen die Verwertungsrechte (Copyright) nicht bei mir liegen, diese von den Rechtsinhabern eingeholt wurden und die Textstellen bzw. Abbildungen entsprechend den rechtlichen Vorgaben gekennzeichnet sind sowie bei Abbbildungen, die dem Internet entnommen wurden, der entsprechende Hypertextlink angegeben wurde.

Affidavit

I hereby declare that my thesis entitled: **"Interactome of the β2b subunit of L-type voltage-gated calcium channels in cardiomyocytes"** is the result of my own work. I did not receive any help or support from commercial consultants. All sources and / or materials applied are listed and specified in the thesis.

Furthermore I verify that the thesis has not been submitted as part of another examination process neither in identical nor in similar form.

Besides I declare that if I do not hold the copyright for figures and paragraphs, I obtained it from the rights holder and that paragraphs and figures have been marked according to law or for figures taken from the internet the hyperlink has been added accordingly.

Würzburg, de 14.04.20

_____

Signature PhD-student